1-1-2004

In vitro propagation of some Western Australian seagrasses

Julia Wilson
Edith Cowan University

Edith Cowan University

Copyright Warning

Adaptive applications of Opto-VLSI processors in WDM networks

By

Mehrdad Raisi

A thesis submitted for the degree of

Doctor of Philosophy (Engineering)

at

School of Engineering and Mathematics

Edith Cowan University

Principal Supervisor : Professor Kamran Eshraghian

Co-Supervisor : Professor Kamal Alameh

March 2004

USE OF THESIS

The Use of Thesis statement is not included in this version of the thesis.

DECLARATION

I certify that this thesis does not, to the best of my knowledge and belief:

(i) incorporate without acknowledgement any material previously submitted for a degree or diploma in any institution of higher education;

(ii) contain any material previously published or written by another person except where due reference is made in the text; or

(iii) contain any defamatory material.

Signature *Date* 7/7/05

To My Family

Contents

List of Figures

Abstract

Communication is an inseparable part of human life and its nature continues to evolve and improve. The advent of laser was a herald to the new possibilities in the communication world. In recent years technologies such as Wavelength Division Multiplexing (WDM) and Erbium Doped Fiber Amplifiers (EDFA) have afforded significant boost to the practice of optical communication. At the heart of this brave new world is the need to dynamically/adaptively steer/route beams of light carrying very large amounts of data. In recent years many techniques have been proposed for this purpose by various researchers. In this study we have elected to utilise the beam-steering capabilities of Opto-VLSI processors to investigate band-pass filtering and channel equalisation as two possible and practical applications in WDM networks.

Both optical filtering and channel equalisation play a very significant role in current optical networks and the need for devices capable of performing these functions dynamically and intelligently will only heighten as we adapt a dynamic approach to optical communications. Currently optical filters are used in many parts of existing WDM networks where certain channels need to be selected and processed and as such they play a vital role in channel management. Devices capable of providing spectral equalisation for WDM channels also make immense contributions as they ensure that signal to noise ratio and bit error rate remain within acceptable levels despite the fact that optical amplifiers used to boost signals across large distances invariably introduce unwanted noise and degrade signals.

In this research we report on a novel tunable multi-band band-pass filter which utilises

an Opto-VLSI processor to select an arbitrary number of channels. We experimentally demonstrate the proof-of-principle of a 3-band tunable optical filter having 2 nm bandwidth and more than 8 nm tuning range per band over a 25 nm wavelength span. We provide details on various experimental setups used to test this device and present the results obtained from these experiments confirming the efficacy of Opto-VLSI processors in beam processing.

We also present the results of our research on a novel dynamic WDM channel equaliser. The proof-of-principle of a 4-channel WDM equaliser is experimentally demonstrated. These results confirm that independent power control can be accomplished for each channel by varying the radius and/or peak phase of the circular phase hologram dedicated to that channel allowing theoretical realisation of dynamic WDM equalisation for more than 80 channels. Furthermore we show how both fine and coarse control of channel gain is possible using the radius and phase of holographic phase elements which are generated by the Opto-VLSI processor. Once gain we provide details associated with various experimental setups used to verify our results.

Publications

Refereed Journal Articles

(1) Mehrdad Raisi, Selam Ahderom, Kamal E. Alameh, Kamran Eshraghian,"Opto-VLSI multiband tunable optical filter", IEE Electronic Letters, vol. 39 no. 21, pp. 1533-1535, 2003.

(2) Selam Ahderom, **Mehrdad Raisi**, Kamal E. Alameh, Kamran Eshraghian,"Dynamic WDM equalizer using Opto-VLSI Beam Processor", IEEE Photonics Technology Letters, vol. 15, no. 11, pp. 1603-1605, 2003.

Refereed Conference Papers

(3) Mehrdad Raisi, Selam Ahderom, Kamal E. Alameh, Kamran Eshraghian,"Tunable optical filters employing microphotonics", SPIE International Symposium on Microelectronics, MEMS, and Nanotechnology, Perth, Western Australia, December 2003.

(4) Mehrdad Raisi, Selam Ahderom, Kamal E. Alameh, Kamran Eshraghian,"Dynamic MicroPhotonic WDM Equalizer" Second IEEE International Workshop on Electronic Design, Test and Applications (DELTA), Perth, Western Australia, pp. 59-62, January 2004.

(5) Mehrdad Raisi, Selam Ahderom, Kamal E. Alameh, Kamran Eshraghian, "Multi-band MicroPhotonic Tunable Optical Filter" Second IEEE International Workshop on Electronic Design, Test and Applications (DELTA), Perth, Western Australia, pp. 391-394, January 2004.

(6) Mehrdad Raisi, Selam Ahderom, Kamal E. Alameh, Kamran Eshraghian,"Tunable optical filters employing Opto-VLSI processors", International conference on Computer, Communication and Control technologies (CCCT'03), Vol 2, pp. 29-34, Orlando, USA, 2003.

(7) Ahderom, S., **Raisi, M.**, Lo, K., Alameh, K.E., and Mavaddat, R.,"Applications of liquid crystal spatial light modulators in optical communications", IEEE 5th International Conf. on High-speed Networks and Multimedia Communications, HSNMC'02, Korea, pp. 239-242, July 2002.

(8) Selam Ahderom, **Mehrdad Raisi**, Kamal E. Alameh, Kamran Eshraghian, "Reconfigurable MicroPhotonic Add/Drop Multiplexer Architecture" Second IEEE International Workshop on Electronic Design, Test and Applications (DELTA), Perth, Western Australia, pp. 203-207, January 2004.

(9) Selam Ahderom, **Mehrdad Raisi**, Kamal E. Alameh, Kamran Eshraghian,"Testing and analysis of computer generated holograms for free-space optical communications devices" Second IEEE International Workshop on Electronic Design, Test and Applications (DELTA), Perth, Western Australia, pp. 47-52, January 2004.

(10) Selam Ahderom, **Mehrdad Raisi**, Kamal E. Alameh, Kamran Eshraghian,"High-resolution Dynamic WDM Equalization Using Opto-VLSI Beam Processing", The 7th world multiconference on systemics, cybernetics and informatics (SCI'03), Vol. 10, pp.179-183, Orlando, USA, 2003.

(11) Kamal E. Alameh, Selam Ahderom, **Mehrdad Raisi**, Kamran Eshraghian,"MicroPhotonic Reconfigurable RF Signal Processor" Second IEEE International Workshop on Electronic Design, Test and Applications (DELTA) Perth, Western Australia, pp. 63-67, January 2004.

(12) Kamal E. Alameh, Selam Ahderom, **Mehrdad Raisi**, Kamran Eshraghian,"Opto-VLSI-based Reconfigurable Photonic RF Bandpass Filters" International Conference on Computer, Communication and Control Technologies Vol 2, pp.49-54, Orlando, USA, 2003.

(13) Kamal E. Alameh, Selam Ahderom, **Mehrdad Raisi**, Kamran Eshraghian,"Impact of EDFA Gain Fluctuations on the Response of Opto-VLSI-based Reconfigurable Photonic RF Filters" The 7th world multiconference on systemics, cybernetics and informatics (SCI'03), Vol. 10, pp.184-188, Orlando, USA, 2003.

(14) Kamal E. Alameh, Kamran Eshraghian, Selam Ahderom, **Mehrdad Raisi**, Mike Myung-Ok Lee, Rainer Michalzik,"Integrated MicroPhotonic Broadband Smart Antenna

Beamformer" Second IEEE International Workshop on Electronic Design, Test and Applications (DELTA), Perth, Western Australia, pp. 208-212, January 2004.

(15) K. Alameh, A. Bouzerdoum, S. Ahderom, **M. Raisi**, K. Eshraghian, X. Zhao, R. Zheng, Z. Wang,"Integrated MicroPhotonic Wideband RF Interference Mitigation Filter" Second IEEE International Workshop on Electronic Design, Test and Applications (DELTA), Perth, Western Australia, 387-390, January 2004.

(16) Z. Wang, K. Alameh, S. Ahderom, R. Zheng, **M. Raisi**, K. Eshraghian,"Novel integrated optical router for Microphotonic switching" SPIE International Symposium on Microelectronics, MEMS, and Nanotechnology, Perth, Western Australia, December 2003.

(17) K. Alameh, A. Bouzerdoum, K. Eshraghian, S. Ahderom, **M. Raisi**, X. Zhao, R. Zheng, Z. Wang,"MicroPhotonic Interference mitigation filter for radio astronomy telescopes" SPIE International Symposium on Microelectronics, MEMS, and Nanotechnology, Perth, Western Australia, December 2003.

Other conference Presentations

(18) S. Ahderom, **M. Raisi**, K. Alameh, S. Bouzerdoum, K. Eshraghian, Z. Wang, X. Zhao,"A novel MicroPhotonic processor for adaptive wideband RF interference mitigation" International SKA conference, July 27 - 2 August, Geraldton, Western Australia, 2003.

(19) **Mehrdad Raisi**, Selam Ahderom,"Role of MicroPhotonic processors in future optical networks" The Fourth postgraduate electrical engineering and computing symposium, pp.218-221, Curtin University, Perth, Australia, October 2003.

(20) Selam Ahderom, **Mehrdad Raisi**,"Reconfigurable wavelength equalization using free-space optics" The Fourth postgraduate electrical engineering and computing symposium, pp.192-195, Curtin University, Perth, Australia, October 2003.

Acknowledgements

This work would not have been possible without the help and support of many people. I would like to firstly thank my supervisors Professor Kamran Eshraghian for creating a wonderful environment for research and Associate Professor Kamal Alameh for his unique and invaluable guidance, support and insight. I would like to express my gratitude to professor Rafie Mavaddat for many valuable discussions and help in getting a better understanding of some of theoretical concepts involved in this area. My gratitude and appreciation is also extended to Dr. Daryoush Habibi for his general support and encouragement. I would like to acknowledge contributions from the Univesity of Cambridge and in particular those of Dr. Timothy Wilkinson in the early stages of my research. Furthermore I would like to express my gratitude to the Australian Federal Government for partially funding this research from Australian Research Council grants. I also like to acknowledge the great company and in some cases the assistance provided to me by my colleagues. In no particular order these dear friends are, Kungmeng Lo, Rhong Zheng, Sholeh Eshraghian and Alexander Havstad. A special thank you goes to Selam Ahderom for providing a great deal of assistance with experiments and for being a source of enrichment of my experience during the past few years. I am also indebted to David Lucas for being very generous with his technical expertise and time in assisting us to setup a good optical lab and helping us with some of the various technical challenges which we invariably experienced along the way. I am also grateful for all of those individuals who made my time during the past few years enjoyable. Finally, I would like to thank my family for all the sacrifices they have made and all the love they have bestowed upon me throughout the years.

Chapter 1

Introduction

An ever-advancing trend in technology coupled with an insatiable thirst for varied forms of services means that current optical networks will increasingly need to move from passive to dynamic architectures. The active nature of these architectures will require reconfigurable optical components to meet the level of performance expected of these networks [2]. These sub-systems include tunable optical filters, dynamic gain equalisers, variable optical attenuators, reconfigurable optical add/drop multiplexers, and variable gain amplifiers.

1.1 Background

It is perhaps a well-known fact that the Internet and rapid spread of PCs sparked the communication flame back in the 1980's. Optical revolution however, traces its beginning back to the early 1960's and the discovery of the laser. What has transpired since then has been the driving force behind the optical evolution. Starting in the late 1980's both the Erbium Doped Fiber Amplifier (EDFA) and Wavelength Division Multiplexing have contributed enormously to the advancement of optical communications and partial but continuing fulfillment of its potentials as was dreamed by its early pioneers.

In the late 1980's as the long-haul optical fibers were being deployed the 1310nm wavelength was favored for network operation as it supported higher bit rates relative to 1550

nm. However it was the adoption of Erbium Doped Fiber Amplifier (EDFA) as a preferred mode for amplification that turned the tide towards the use of 1550 nm wavelength in lightwave communications. This is primarily due to the fact that the EDFA gain window is centered around 1550 nm. Use of EDFA in conjunction with Wavelength Division Multiplexing (WDM) has lead to a need for gain equalisation. This is due to the fact that EDFAs do not have a flat gain and as such do not equally amplify all spectral components of signals. WDM systems use many wavelengths within the amplified band and carry multiple channels. For a successful operation each channel should have equal gain. However as a result of this variable gain some channels will end up being dominant while others will be lost in the noise. This phenomenon is more pronounced in long WDM links containing large numbers of cascaded amplifiers.

On another front but somewhat related, new technologies continue to facilitate access to novel and varied services with an ever growing degree of flexibility. This situation has created a strong incentive and an urgent need for reconfigurable components. An urgency that will not subside, as the need for bandwidth intensifies and operators push for higher bit rates.

Computer Generated Holograms (CGH) in concert with Liquid Crystal (LC) technology coupled with Opto-VLSI back-planes offer a great potential for a reconfigurable resolution to these problems. The aim of this research is to investigate, synthesise and characterise suitable architectures based on MicroPhotonic technology for tunable optical filtering and channel equalisation in WDM networks.

1.2 Wavelength Division Multiplexing (WDM)

WDM came about after it was realised that capacity of fiber could be utilised much more efficiently if many channels were multiplexed together and sent across it simultaneously. As a result of advancements in technologies such as tunable lasers and narrowband optical filters, WDM has moved from a lower density or coarse state to what is known today as Dense Wavelength Division Multiplexing (DWDM). The ability to multiplex and transmit

more and more channels across a single fiber is increasing very rapidly. DWDM technology with more than 200 channels has already been demonstrated and at least theoretically it is possible to multiplex over 1000 channels at total bandwidth in Tb/s across a single fiber [3].

1.3 Importance of optical filtering

Tunable optical filters, in particular, play a critical role in wavelength division multiplexed (WDM) optical telecommunication networks, by enabling selective removal of WDM channels. Compared to fixed optical band-pass filters, tunable optical band-pass filters provide more flexibility in fibre optic capacity management. The essential characteristics of next-generation tunable optical filters include low insertion loss, wide tuning range, the capability of providing variable bandwidths, the ability to arbitrarily change the transfer function, high stopband rejection, fast tuning speed, software-driven control, small size, and low cost.

With the emergence of applications such as add/drop multiplexing and gain equalisation, the need for tunable optical filtering gains greater significance. As this figure shows, tunable optical filters can be effectively used for monitoring purposes in these networks. The ability to filter out specific channel/s means that at various stages in the link it is possible to monitor the quality of the data and make necessary adjustments for improvements where necessary.

1.4 Importance of channel equalisation

In an optical network, Erbium Doped Fiber Amplifers (EDFA) are the most common device used for optical amplification of signals. These devices however have a nonlinear gain profile. Lack of flatness of gain of Erbium doped fiber amplifiers amongst other factors causes channel level optical power variation or ripple. This ripple accumulates through the cascaded segments of the transmission system and leaves some channels with lower power and others with higher power as can be seen in figure 1.1 [1]. Lower power channels

can suffer from degradation in Optical Signal to Noise Ratio (OSNR). This penalty in turn limits the reach of the network and requires signal regenerators at short intervals (approximately 500 km). It is in this context that dynamic gain equalisers play a key role for higher capacity, longer reach, more flexible and lower cost in future optical networks.

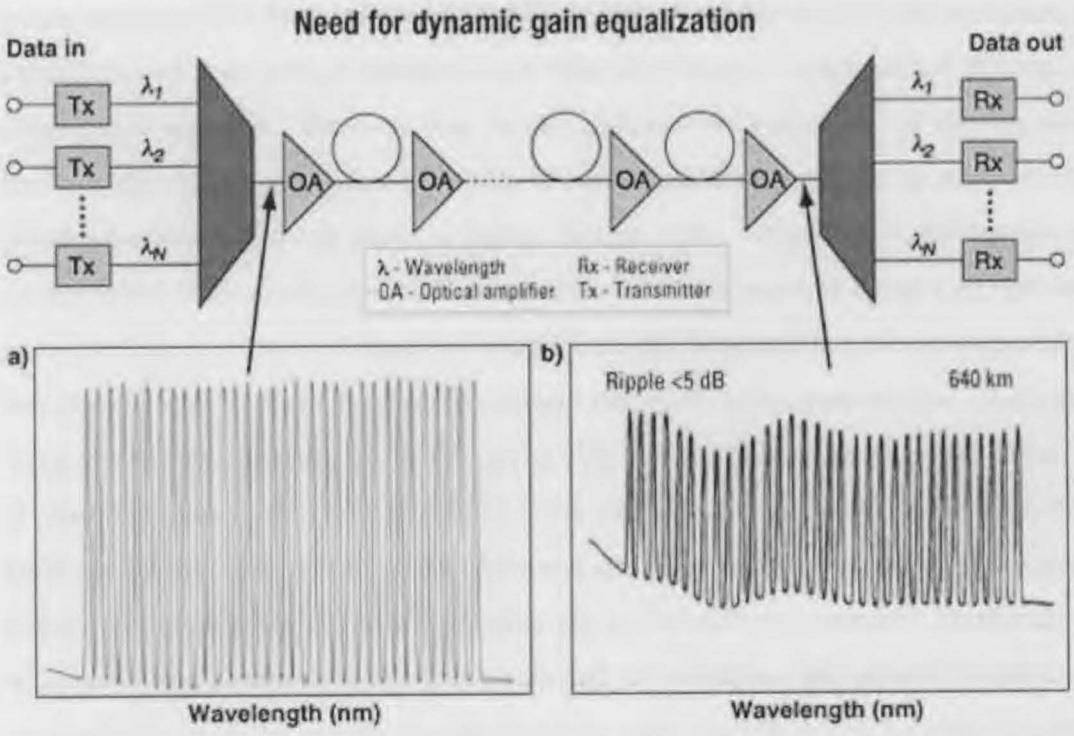

Figure 1.1: The spectrum of channels shown before (a) and after (b) cascaded optical amplifiers - from [1]

1.5 Contributions from this research

In this study, after establishing reconfigurability as a significant and an increasingly pervading approach in dealing with optical networking, we introduce the Opto-VLSI processor as an enabling technology for provision of reconfigurable subsystems for future optical networks. We examine the anatomy and physiology of an Opto-VLSI processor and describe the architecture and dispersive features of such a device that afford it its versatility in

catering for dynamic optical networking. We show using computer simulations and confirm our assertion through experimentation that an Opto-VLSI processor is capable of steering an optical beam falling on its surface. Moreover we reveal the multicasting capability of an Opto-VLSI processor using computer simulation and experiments. We examine at some length, various methods for generation of phase holograms which are the dynamic element used in concert with a VLSI backplane in beam processing. In this context we inspect some of more commonly used algorithms such as simulated annealing and genetic algorithms and draw some conclusions about the effectiveness of each method through a comparative approach. We show that despite each method's strength, all existing and traditionally utilised approaches are either computationally expensive or do not produce phase holograms which can result in highly efficient replay fields. We briefly describe a method which theoretically can produce holograms which can result in replay field that are more predictable in terms of noise distribution and also demonstrate a simple method for reduction of noise in the replay field. We present the results of analysis of phase holograms using one and two dimensional Fourier series. We derive an expression for the efficiency of phase holograms based on a two dimensional model and taking into consideration the finite number of pixels as well as the phase and spatial quantisation involved in the generation and application of phase holograms via an Opto-VLSI processor. Furthermore we examine the results of simulations conducted to investigate the impact of replacing one phase hologram by another and demonstrate how such a task can be achieved with minimum disturbance to the replay field. We demonstrate the results of simulations on the relationship between the number of pixels and the crosstalk as well as power efficiency of a phase hologram. Here we show that within some described frameworks, the effect of number of pixels in both instances is minimised after a certain number of pixels has been used in the generation of the relevant phase hologram. Finally we theoretically demonstrate how phase holograms can be used to modify the profile of an optical beam and for instance change a gaussian profile to one that is spatially circular.

After theoretically establishing and confirming the capability of an Opto-VLSI processor in provision of such dynamic applications as tunable optical filtering and dynamic

WDM channel equalisation, we report on a novel tunable multi-band band-pass filter which utilises an Opto-VLSI processor to select an arbitrary number of channels. We experimentally demonstrate the proof-of-principle of a 3-band tunable optical filter having 2nm bandwidth and more than 8 nm tuning range per band over 25 nm wavelength span. Therefore we confirm that by generating N non-overlapped phase holograms, an N-band optical filter is realised. By selecting holograms which provide the required steering and adjusting the hologram position, filter passbands can independently be tuned over a wavelength span, which is limited by the size of the Opto-VLSI active area and the maximum allowed crosstalk. We provide details on various experimental setups used to test this device and present the results obtained from these experiments confirming the capability of Opto-VLSI processors in dynamic beam processing. We also inspect the results of our research on a novel dynamic WDM channel equaliser. The proof-of-principle of 4-channel WDM equaliser are experimentally demonstrated. These results confirm that independent power control can be accomplished for each channel by varying the radius and/or peak phase of the circular digital hologram dedicated to that channel allowing theoretical realisation of dynamic WDM equalisation for more than 80 channels. Furthermore we show how both fine and coarse control of channel gain is possible using the radius and phase of holographic phase elements which are generated by the Opto-VLSI processor. In this case we have used an input WDM signal that has channel powers ranging from 0 dBm to 6 dBm and attempted to equalise the measured output WDM signal spectrum. Our findings support our assertion and show that by optimising the heights of the pixel block assigned to each channel, the output power levels of the 4 wavelength channels were equalised with less than 0.2 dB ripples. We have also been able to vary the attenuation of any channel without affecting the attenuation of other channels. This demonstrates the channel-by-channel WDM equaliser capability of our proposed structure. Once gain in this case we provide the details associated with various experimental setups used to verify our results. In summary, in this research program, we investigate novel tunable optical filter architectures that can scale to tens of independently controlled passbands while maintaining low loss and high uniformity performance. These architectures are based on a reflective, free-space Opto-VLSI processor, which generates reconfigurable holographic

diffraction gratings to steer/reshape optical beams falling on its surface. We also investigate the capability of an Opto-VLSI processor for dynamic channel equalisation. We experimentally prove that an Opto-VLSI processor is able to provide dynamic channel equalisation for a large number of channels whilst maintaining a very good signal to noise ratio.

1.6 Original contributions to this dissertation

- Investigated and derived a mathematical expression for efficiency of phase holograms taking into consideration phase and spatial quantisation.
- Analysed the effect of pixels on crosstalk and power efficiency using specifically designed scripts.
- Designed and developed programs used to investigate the transient effects associated with switching the holograms
- Derived a mathematical expression for spatial conversion of a gaussian to a circular beam.
- Analysed and evaluated various techniques used for DC balancing an FLC processor.
- Developed scripts for generation of multiphase holograms used as part of the experimental evaluation of tunable optical filter and dynamic WDM equaliser.

1.7 Organisation of chapters

The thrust of this research has been on investigation of architectures which can provide a dynamic/adaptive approach to such important functions as tunable optical filtering and dynamic channel equalisation in WDM networks. In chapter one we provide an introduction and background to this research. We explain the importance of these functions in optical networks and the potential contributions from this research to optical networking.

In Chapter two we present a detailed literature review of various techniques proposed by the research community for tunable optical filtering and channel equalisation. We show

that despite existence of many approaches for tunable optical filtering and gain equalisation, there still exists a real need for a truly dynamic/adaptive solution to optical filtering and channel equalisation.

In Chapter three we introduce the Opto-VLSI processor as an enabling technology and a suitable candidate for provision of reconfigurable sub-systems in dynamic lightwave networks. We first review the history of spatial light modulators and briefly explain the application of various technologies used for purpose of spatial light modulation. We describe the architecture and dispersive features of an Opto-VLSI processor and how it may be used for optical filtering and channel equalisation. We examine the various components that make-up an Opto-VLSI processor. In particular we devote a discussion to the various kinds of liquid crystals which can be used in conjunction with the VLSI back-plane and explain with some degree of detail, the operation of this component of the Opto-VLSI processor.

Results of theoretical analysis for a two dimensional hologram and methods for their generation are presented in chapter four. Additionally in this chapter we present the results of simulations performed to investigate the effect of number of pixels on crosstalk and efficiency as well as the transient effects associated with switching holograms on an Opto-VLSI processor. In this chapter we derive a basic expression for the efficiency of two dimensional phase holograms taking into consideration both the phase and spatial quantisation associated with these objects.

In Chapter five we examine the details associated with our novel reconfigurable tunable optical filter as well as our proposed structures for channel equalisation using an Opto-VLSI processor. In this chapter we present our experimental results for a 3-band tunable optical filter. We experimentally demonstrate the proof-of-principle of a 3-band tunable optical filter having 2 nm bandwidth and more than 8 nm tuning range per band over 25nm wavelength span. We provide details on various experimental setups used to test

this device and present the results obtained from these experiments confirming the capability of Opto-VLSI processors in beam processing. Moreover we present the result of our research on a novel dynamic WDM channel equaliser. The proof-of-principle of 4-channel WDM equaliser are experimentally demonstrated. These results confirm that independent power control can be accomplished for each channel by varying the radius and/or peak phase of the circular digital hologram dedicated to that channel allowing theoretical realisation of dynamic WDM equalisation for more than 80 channels. Furthermore we show how both fine and coarse control of channel gain is possible using the radius and phase of holographic phase elements which are generated by the Opto-VLSI processor. Once again we provide details associated with various experimental setups used to verify our results.

Finally in Chapter six, we conclude with a summary of the findings from this research and suggestions for possible future directions.

Chapter 2

Literature Review

2.1 Techniques for Tunable Optical filtering

Many technologies and methods have been proposed for implementation of tunable optical filters. In this section we will review some of the main technologies which have received significant attention from the research community over the past few years. In the following section we will present a general review of techniques for spectral equalisation.

2.1.1 Fabry-Perot filters

A Fabry-Perot (FP) filter, also called Fabry-Perot interferometer, is an etalon, or a cavity formed by two highly reflective mirrors, which are placed parallel to each other, as shown in the figure 2.1. Light from an input fiber enters the left surface of the cavity normal to the interface. After traversing the cavity, part of the light passes through the right facet and leaves the cavity, whilst a portion of the light is reflected backwards, toward the left facet. After a number of reflections, those wavelengths for which the cavity length is an integral multiple of half the wavelength (so that the round trip through the cavity is an integral multiple of the wavelength) add in phase. These wavelengths, called the resonant wavelengths, propagate through the cavity, while the remaining wavelengths (those with $L = \frac{(2n+1)\lambda}{4}$) destructively interfere. Cavity length and mirror reflectivity are the main elements influencing the transmission spectrum of this type of filter. One of the common measures for characterising a FP filter is Q-factor or finesse which measures

the energy trapped in the cavity relative to the energy loss per cycle. FP filters can be tuned by adjusting the length of the cavity through piezoelectric or electrostatic control or by rotating the filter with respect to the direction of the incident light. Although a wide tuning range and a very narrow bandwidth can be achieved, the shape factor (ratio of -30dB to -3dB bandwidths) of such filters is very large, necessitating large channel spacing to avoid interchannel crosstalk, and hence making them inappropriate for DWDM transmission networks.

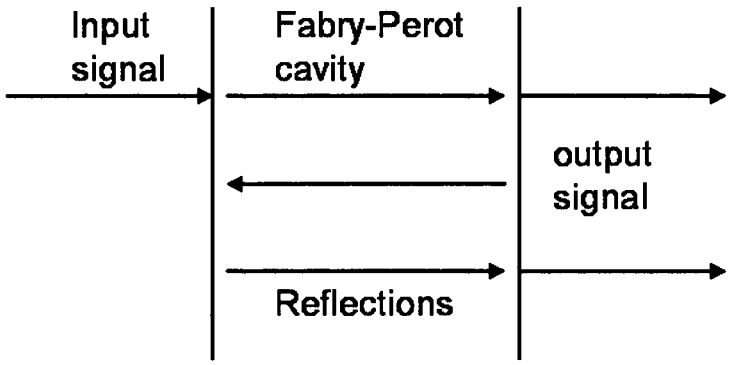

Figure 2.1: Schematic of a Fabry Perot cavity

2.1.2 Fiber Bragg grating

Fiber gratings are written in fibers using the photosensitivity property of the fiber. This is done by exposing the fiber to an interference pattern of ultraviolet (UV) light [4]. In the spots where the UV light waves add in phase, the refractive index of the fiber is permanently raised, and the interference pattern is thereby transformed into a refractive index pattern in the fiber. Tuning the center wavelength (also called Bragg wavelength) of the Bragg grating is achieved by stretching or by heating the Bragg grating so that the refractive index perturbation period is changed [5]. Figure 2.2 visually illustrates the operation of a Fiber Bragg grating. As can be seen from this representation, an input WDM signal containing a number of wavelengths will have one of its wavelengths reflected back by the in-fiber grating whilst the remaining wavelengths pass through the

fiber unhindered. Bragg grating tunable filters can have low insertion loss and more than -25 dB of crosstalk, however, their tuning speed is low (less than 2 ms) and can only have a fixed shape factor.

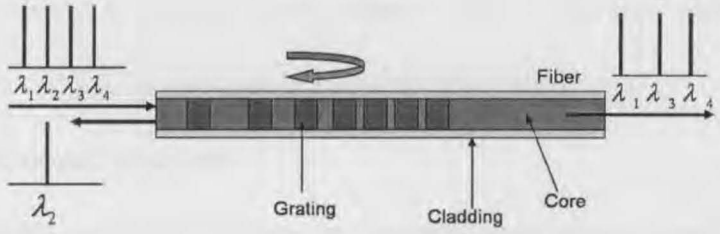

Figure 2.2: Schematic of a fibre bragg grating

2.1.3 Filters based on Ferroelectric liquid crystals

Ferroelectric liquid crystal Fabry-Perot filters contain a Ferroelectric liquid crystal material in their resonant cavity [6, 7]. An electric field is used to change the refractive index of the liquid crystal in the cavity and this in turn affects the optical path traveled by various reflected beams. Once again the peak transmission occurs when the round-trip phase of the light in the resonator equals multiples of 2π. Such filters can provide low bandwidths and a wide tuning range. However, they are polarisation dependent and their shape factor is not adaptable.

Both Warr and Parker have proposed the use of polarisation-insensitive ferroelectric liquid crystal (FLC) spatial light modulators (SLM) in conjunction with a highly wavelength dispersive fixed diffractive grating to realise dynamic digital holography for tunable optical filtering [8,9]. Their approach is based on the superposition of several digital holographic gratings to realise multiple wavelength filtering. However, the main disadvantage of this approach is the high insertion loss, which is proportional to the square of the number of filter passbands. This confines the tunable optical filter to low resolution filtering applications.

Ferroelectric liquid crystal material can also be used in conjunction with Fabry Perot filters as a filler material for the resonant cavity [10]. An electric field is created over this cavity which causes the liquid crystal molecules to change their spatial orientation. This in turns leads to a change of refractive index in the cavity. Maximum transmission occurs when the round-trip phase of the light in the resonator equals multiples of 2π. The change of refractive index of the liquid crystal causes a shift of the filter peak transmittance wavelength.

2.1.4 Directional couplers

Optical directional couplers are devices that transfer the maximum possible optical power from one or more optical devices to another in a selected direction. Single-mode fiber directional couplers use the evanescent property of integrated lightguides on a substrate to couple optical power of a certain wavelength from one guide to another. Figure 2.3 is a schematic representation of a directional coupler. As this illustration shows the device consists of two lightguides of coupling length L separated by distance d. When a voltage V_s is applied, optical power is guided through the same guide but with a phase change. When no voltage is applied, power is transferred through the evanescent separation region to the adjacent guide. In order to achieve maximum power transfer, the two lightguides must be in close proximity and be separated by a distance d which is comparable to the wavelength λ which is to be coupled. The two phase velocities must be in perfect synchronisation and the refractive index must be the same for both guides. Additionally the interaction or coupling length L must precisely equal a coupling length [3].

Vertical directional coupler filters consists of two vertically coupled waveguides of dissimilar dimensions and differing refractive index [11]. The constants for both waveguides will be identical for a designed wavelength. This means that the light launched into one waveguide will completely couple into the second waveguide after traveling the coupling distance. However as the wavelength changes from the designed wavelength, the coupling weakens rapidly due to phase mismatch. InP grating-assisted vertical directional couplers [12] have also been utilised for tunable optical filtering, but they are polarisation-sensitive and can only filter a single wavelength at a time.

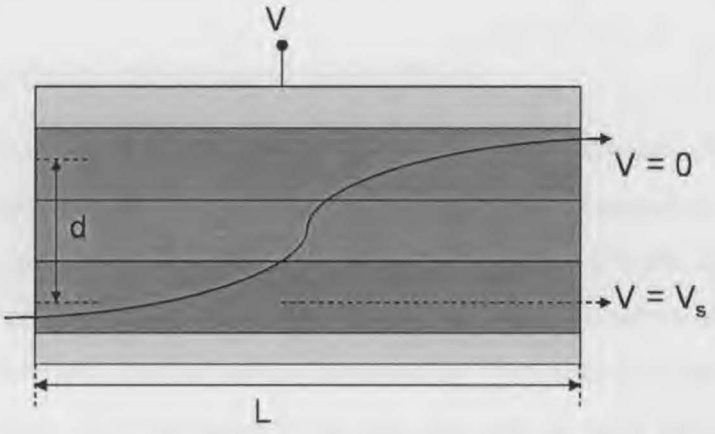

Figure 2.3: Schematic representation of a directional coupler

2.1.5 Acousto-optic filters

The concept of the acousto-optic tunable filter (AOTF) was first introduced in 1969 by S.E. Harris and R.W. Wallace [13]. The interaction between a lightwave and a surface acoustic wave (SAW) over a suitable substrate such as $LiNbO_3$ causes a polarisation shift of the electromagnetic wave only at frequencies that satisfy the following phase-matching condition:

$$|\beta_{TE} - \beta_{TM}| = |k_{ac}|$$

where β_{TE}, β_{TM} and k_{ac} are the wave numbers of the lightwave at TE and TM polarisations, and the SAW, respectively [14]. The acoustic wave as a periodic perturbation is used to convert the mode of the incident light into another mode. With these perturbations only optical waves within a very narrow wavelength range satisfy the mode coupling condition, resulting in highly selective wavelength output. The tuning in these devices is achieved by changing the frequency of the applied SAW with a possible tuning range of 1.3-1.6 μm. Another feature of AOTFs is the ability to simultaneously filter out several channels. Selection of up to five wavelengths separated by 2.2 nm has been demonstrated by Cheung [15]. AOTFs have been used for many applications including EDFA gain equalisation and wavelength demultiplexing [16]. However, AOTFs have many drawbacks, including high insertion loss, polarisation sensitivity, high crosstalk, nonlinearity,

non-standard fabrication requirements, and limited passband [17].

2.1.6 MicroElectroMechanical based filters

MicroElectroMachnical (MEMs) devices came about as an extension of an already developed semiconductor technology. Micro-electro-mechanically-actuated tunable optical filters based on simple cantilever structures have been reported [18–20]. The tuning mechanism is based on displacement of an optical element which is usually achieved by electrostatic force or heating. The architecture proposed by Vail consists of two mirrors making the resonator where one is attached to the substrate and the other suspended on a cantilever. Application of voltage to the device causes an electrostatic force which moves the mirror. The reported tuning range for this device is 70nm in the 900nm band. The bandwidth of this device is reported to be 8nm and increasing with the centre wavelength. The device is reported to have a tuning speed of around 100 μs. The device reported by Tayebati et al. uses quart-wave stack mirrors of wet oxidised AlAs(AlOx)-GaAlAs [20]. The large refractive index difference between the materials produces high reflectivity mirrors. This device has a Full Width at Half Maximum (FWHM) bandwidth of 0.5 nm and a tuning range of 59 nm with reported insertion loss of 0.9dB.

In general, the tuning range for all these MEMs based photonic devices is limited by the actual allowed movement and is limited to only one passband at a time.

2.1.7 Passive diffraction gratings

The term grating is used to describe almost any device whose operation involves interference among multiple optical signals originating from the same source but with different relative phase shifts [21]. The basic operation of a diffraction grating is as follows. Light from a source falls on the surface of the gratings where there are many slits separated by a small space known as the grating pitch. The light travels through these spaces and as a result of diffraction spreads in different directions. The transmitted light from different slits undergoes interference at some distance from the grating plane. At points where

transmitted beams are in phase, constructive interference and an enhancement of light intensity occurs and where beams are out of phase, interference leads to areas with very low intensity of light. This process essentially splits the incoming mixed-wavelength beam of light into its constituent components and therefore can be used to multiplex/demultiplex a WDM signal. The spatial intensity distribution is a function of grating pitch, the wavelength and the angle of incidence. This means that different wavelengths are diffracted at different angles. Furthermore the energy at a single wavelength is distributed over all the discrete angles that satisfy the grating equation [22]. This results in most of the energy to get lost to unwanted orders and in particular the zeroth order. To overcome this problem the gratings are designed so that the light energy is maximum at a particular interference maximum based on the blaze angle [23].

The shortcoming of diffraction gratings for tunable purposes is their passive nature. However these devices can be used in conjunction with programmable gratings to produce effective tunable components [24].

2.1.8 Mach-Zehnder filters

Mach-Zehnder (MZ) modulators resolve different wavelengths by making use of two interfering paths of different lengths. Basically, a MZ device consists of two 3-dB directional couplers with a path length difference between the arms, as shown in figure 2.4 .

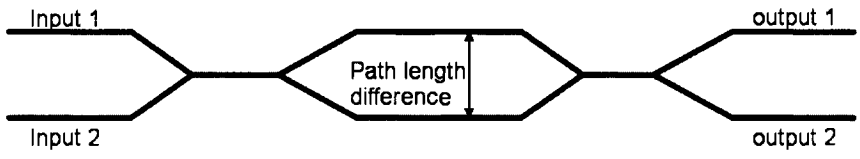

Figure 2.4: Schematic of a Mach-Zehnder Interferometer

An incident beam of light is split in two ways and recombined after a short distance. The combining fields will interfere according to the phase shift difference between them. If the

two paths are of equal length, there will be no phase difference between the two fields and therefore they interfere constructively. However if the two arms of the interferometer are made to be unequal, a periodic frequency dependent phase shift is introduced and the fields combine according to this phase difference.

MZ filters are usually manufactured in $LiNbO_3$ but they can also be made on silica waveguides and fiber devices where the insertion loss is minimized [25]. A device demonstrated by Wooten et al. shows a three-stage cascaded filter that can select one of eight channels with 0.4 nm separation and a switching time of 50 μs [26]. As the transfer characteristic of a MZ modulator is not narrowband, a cascade of several MZ structures is needed to produce a narrowband filter. This increases their insertion loss, and makes them impractical for DWDM systems.

2.2 Gain equalisation

In an optical network, Erbium Doped Fiber Amplifiers (EDFA) are the most common device used for optical amplification of signals. These devices however have a gain profile that is not linear. This variation in the gain of EDFAs amongst other factors causes channel level optical power variation. This variation cascades through the many segments of the transmission system and results in some channels with lower power and others with higher power. Lower power channels can suffer from degradation in signal to noise ratio and increase in Bit Error Rate (BER). This penalty in turn limits the reach of the network and requires signal regenerators at short intervals.

2.2.1 EDFA gain characteristics

There are several phenomena which contribute to lack of uniformity displayed by gain profile of EDFAs. The first factor affecting this lack of uniformity is that the gain profile changes with the total amount of pump power. This phenomenon is known as dynamic gain tilt and is of particular significance in optical add/drop multiplexers where power is distributed per channel. The second fact is the saturable nature of EDFAs. Gain saturation is a nonlinear behaviour where the gain or amplification coefficient is not constant

but is dependent on the power of the input field. If the gain coefficient or the amount of amplification per unit length remains constant then the amount of amplified power is proportional to the input power. But when the gain begins to saturate at increasingly higher-input powers the gain coefficient nonlinearly decreases until stimulated emission depletes the excessive population inversion created by the pump laser. The amplifier produces its maximum output when the gain completely saturates. Any further amplification becomes independent of the input WDM signal power. Time-dependent relaxation oscillations and inhomogeneous broadening effects also contribute to nonlinear gain behaviour of EDFAs. An inhomogeneously broadened gain medium is one created from different sets of ions, atoms or molecules each influencing the shape of the gain curve. These differing influences create an asymmetric gain curve. Temperature and spectral hole-burning also contribute to inhomogeneous broadening. Spectral hole-burning occurs when the lineshape function of a WDM signal saturates the gain around the centre wavelength of a particular channel, creating a hole in the gain profile. This gain is now unavailable or reduced for amplification by other nearby channels. This phenomenon becomes particularly pronounced if only few channels are used as the case may be when using add/drop multiplexers.

2.2.2 Passive gain equalisation

Currently, most EDFA gain-spectrum flattening techniques use a passive optical notch filter (e.g. Bragg grating) whose center wavelength and bandwidth are optimised to flatten the EDFA gain spectrum [27, 28]. However, since the EDFA gain depends on the input WDM signal power, the optimisation of the optical notch filter can only lead to gain-flattening for a limited range of input power levels. Therefore, in order to maintain a high-quality service, dynamic EDFA spectral equalisation is vital. EDFA gain spectrum equalisation is based on cascading several optical equalisers whose center wavelengths and weights are dynamically optimised to minimise the gain ripples over a wide bandwidth.

In a static optical network, existing remedies for gain flattening or ripple reduction include gain flattening filters in each amplifier, variable optical attenuators in the EDFA, clean-up filters and fixed attenuators to trim power prior to multiplexing and launch at the start

of the link.

Static gain filters are normally placed between two Erbium coils in a common dual-stage EDFA design to flatten the gain profile. Current approaches to static gain equalisation include thin film filter [29], fiber Bragg gratings [30] and arrayed wave-guide gratings [31]. In EDFAs, the gain profile changes for different power levels. Therefore, the static filter can only flatten the gain shape at a fixed condition. When operating conditions such as gain, input power, channel count, pump condition and so forth change, the gain profile no longer remains flat. This renders the static approach to gain flattening limited in application. The thin film technology which has been the most successful approach to gain equalisation consists of translucent multilayer structures of materials with different indices of refraction that create interference effects. These effects compensate for the wavelength dependent gain of the EDFA by diminishing transmission for the high gain wavelengths. However this compensation is not completely successful leaving the power of the various channels unequal. Therefore there are typically ripples of about 1dB associated with this technique which can be acceptable for short distance transmissions but once the signal has to traverse through a number of EDFAs the signal to noise levels become intolerable.

2.2.3 Dynamic gain equalisation techniques

The next generation of optical networks will require intelligent dynamic component and sub-systems. There are two general types of dynamic gain equalisation filters: channel based and continuous equalisation [32]. As the name implies, channel based equalisers independently adjust each wavelength channel in the spectrum. This would normally require demultiplexing signals into individual channels, imposing the desired attenuation for each channel and multiplexing the channels back into the transmission line. This method which treats each wavelength individually requires predetermined channel configurations such as wavelength range, channel spacing and bit rate. This fixed channel approach limits scalability and upgradability in rapidly growing systems. Moreover, the multiplexing/demultiplexing process in channel based equalisation can introduce signal distortion as

a result of bandwidth narrowing and additional spectral dispersion, causing power penalties in the transmission system.

Continuous equalising filters utilise a smooth filter function to make the necessary adjustments to the incoming signal. These filters preserve the continuity of the spectrum, without introducing significant bandwidth narrowing or spectral dispersion at any point in the spectrum. The operation of these filters is independent of the channel plan and thus transparent to reconfiguration of channels in the system.

Continuous equalising filters could be built using Fourier or notch filter concepts. In the Fourier method the attenuation profile is the superposition of a series of sinusoidal transmission functions each having different amplitudes and periods. In the case of notch filter the desired spectral profile is achieved by adding the correct attenuation in the desired wavelength band.

The Fourier approach takes a general view of the spectrum and expands the spectral profile over the entire wavelength range. Therefore, when the input spectrum changes, or when wavelength range increases, all basic functions must be adjusted globally. This results in changes across the whole spectrum, even if majority of the spectrum profile does not require any correction. Mach-Zehnder based thermo-optic devices are one class of filters using the Fourier approach. The amplitude from two different channels or wavelengths entering a directional coupler is equally split into two different paths, each having a separate path length. The optical path length is further controlled by changing the temperature of the refractive material in that path. The beams are then combined at a second directional coupler with two different outputs. Each output supports only one of the wavelengths under certain constructive phase conditions, and different wavelengths can be tuned through optical path differences by changing the temperature of the refractive material. These devices generally dissipate a considerable amount of heat into the substrate and are inherently slow.

In contrast, methods using notch filters take a more localised approach, attenuating optical spectrum in smaller bands, without disturbing other parts of the spectrum. This approach allows gain equalisation of new channels without affecting existing channels.

Notch filters can be based on dispersive or non-dispersive methods. With the dispersive approach, broadband optical signals are spatially dispersed into sub-bands, and each band is attenuated selectively to produce the target profile. With the non-dispersive approach, optical signals at selected wavelengths are scattered out of the optical path to achieve the desired attenuation. Dispersive notch filters could be designed via a combination of fixed gratings and dynamically configurable gratings or arrayed waveguide grating (AWG) technology amongst other ways. The non-dispersive notch filters could be based on the all-fiber acousto-optic filter (AOTF) technology.

AOTFs based devices take advantage of the Bragg condition produced when acoustical waves are created in a refractive material in the direction of light propagation. The acoustical waves themselves are created through driving the material with a radio frequency (RF) signal. The acoustical waves set up areas of compression and expansion of the refractive index in the material, which emulates a periodic Bragg structure. The tunable filter passes only those wavelengths that fulfill the Bragg condition. These devices require high power RF signals and carry a significant noise and cost overhead. A dynamic approach to gain flattening has been proposed by Yun et al. [33]

Dynamic spectral equalisation based on LC-SLM technology is another viable approach to channel equalisation. The principle of operation of an LC-based optical dynamic spectral equaliser is as follows. A holographic diffraction grating separates the incoming WDM channels, then a liquid-crystal SLM selectively blocks or attenuates various channels. At the output, another holographic diffraction grating is used to recombine the optical channels into a single fiber. Dynamic spectral equalisers have low polarisation-dependent loss and can achieve channel-blocking isolation as high as 35 dB and up to 15 dB of pass-through channel attenuation.

2.3 Summary

In this chapter we have presented the results of a survey of literature looking at various techniques proposed for optical filtering and spectral equalisation. We have explained the basic functionality of various approaches proposed for dynamic optical filtering and equalisation. We have also presented the main strength and weaknesses of each approach. We have shown that despite the existence of these techniques currently there are no clear solutions for practical dynamic tunable optical filtering and spectral equalisation.

In the following chapter we will introduce the Opto-VLSI processor as an enabling technology and a viable candidate for providing a dynamic solution to optical filtering and spectral equalisation.

Chapter 3

Opto-VLSI Processors

3.1 Introduction

An Opto-VLSI processor is an array of liquid crystal (LC) cells whose optical properties are independently addressed by a Very-Large-Scale-Integrated (VLSI) circuit to create a reconfigurable, reflective, holographic diffraction grating plate. Application of a voltage between the electrodes of the VLSI circuit induces a phase hologram in the LC layer, resulting in optical beam steering and/or beam shaping. Fabricated Opto-VLSI devices are electronically controlled, software-configured, cost effective because of the high-volume manufacturing capability of VLSI as well as the capability of controlling multiple fibre ports in one compact Opto-VLSI module, and very reliable since beam steering is achieved with no mechanically moving parts. These features and the basic capability of an Opto-VLSI processor to spatially modulate light open the way for numerous reconfigurable optical components, such as tunable optical filters and WDM channel equalisers, making the Opto-VLSI technology very attractive for efficiently enabling the network evolution to reconfigurable architectures.

In the following sections, we will first provide a short background on history of devices capable of providing dynamic spatial light modulation and review in some depth the operation of these devices. We will then examine the architecture and operation of an Opto-VLSI processor furnishing some details about the role of liquid crystals used in

these devices.

3.2 A short history of spatial light modulators

A Spatial Light Modulator (SLM) is a real-time reconfigurable device capable of modifying the amplitude, phase or polarisation of an optical wavefront as a function of position across the wavefront. There are two general classes of SLMs based on the way they are addressed. The optically addressed SLMs convert incoherent light to spatial modulation whereas the electrically addressed SLMs convert electrical signals to spatial modulation. An example of an optically addressed SLM is the Hughes liquid crystal light valve [34]. The electrically addressed SLMs can be further divided into transmissive and reflective groups. In general these SLMs utilise the modulation capabilities of either a nematic or ferroelectric liquid crystal. In this section we will briefly describe the operation of all of these SLMs and leave the details associated with liquid crystals to the next section.

3.2.1 Liquid crystal SLMs

As was mentioned previously, SLMs which rely on liquid crystals to provide spatial modulation can be divided into two groups. We will first look at an example of an optically addressed SLM and follow this discussion by providing some explanation and examples for the electrically addressed case.

Probably the best and most commonly used example of an optically addressed SLM is the Hughes liquid crystal light valve [34]. This device consists of a number of thin film layers held between two glass plates. A 5-10 V RMS audio frequency is applied across the two transparent electrodes to provide a field across the device. The device is activated when a writing light beam is made to fall onto a 15 micron thick cadmium sulfide (CdS) photoconductor. A dielectric mirror and a cadmium telluride layer optically isolate the photoconductor from the readout light beam. This enables simultaneous writing and reading operations to take place. However due to the insulating nature of the dielectric mirror, no DC current is able to flow and therefore AC operation is necessary to establish a charge pattern across the liquid crystal. The liquid crystal in this device is used in what

is known as the hybrid field effect mode (no write beam applied) as well as the traditional birefringence effect mode (with write beam applied). The basic operation is as follows: The polarisation of the incident read beam is chosen to be in a direction parallel to the long axis of the aligned liquid crystal molecules. As the light passes through the liquid crystal layer, the direction of polarisation follows the twisted direction of the liquid crystal molecules, arriving at the mirror with a 45^o polarisation rotation. This beam then reflects from the mirror and propagates back through the liquid crystal for a second time. As the direction of the polarisation of the beam is once again aligned with that of liquid crystal molecules the beam undergoes another change bringing it back to its original polarisation state. If there is no write beam, an analyser oriented at 90^o to the direction of incident beam will block it completely resulting in a uniformly dark output image. If a write beam is present, a spatially varying AC electric field is established across the liquid crystal layer and the long axis of the liquid crystal molecules begin to tilt away from the plane of the electrode. If this field was strong enough it would effectively remove the birefringence of the liquid crystal resulting in the device not changing the polarisation state of the reflected beam and therefore it would be again blocked by the analyser. However the fields are only strong enough to cause partial tilting of the molecules. These partially tilted molecules retain some birefringence effect and therefore the linearly polarised input light will be transformed into elliptically polarised light with a degree of ellipticity which is dependent on the strength of the applied field. This field has a component which is parallel to the direction of the output analyser thus allowing some of the reflected light to pass through the analyser unhindered. Optically addressed SLMs in general have variable contrast and sensitivity and a very low yield in manufacturing. They have found some limited application as components in optical correlator devices.

Unlike optically addressed SLMs, the electrically addressed SLMs are pixelated in nature and therefore produce discrete or sampled output images. In general two types of electrically addressed SLMs have been investigated by researchers. In the following we briefly describe the differences between these two variations.

The two general types of liquid crystal based electrically addressed SLMs more commonly used for non-display applications are Ferroelectric Liquid Crystals (FLC) and Nematic Liquid Crystals (NLC). A great deal of research examining optical switching and cross-connect applications has already been conducted on FLC based spatial light modulators with silicon backplane [35–45]. These devices however are bistable in nature and therefore can only work with binary phase holograms. Therefore the optical efficiency of these devices is quite low and furthermore due to the symmetric nature of binary holograms, only half of the replay field can be effectively used. The other challenge associated with these devices is the need to DC balance them. Ensuring DC balancing of FLC-SLMs adds additional processing requirements on the VLSI back-plane. We have investigated and reported in appendix A, some suiteable methods for DC balancing of a FLC-SLM. Use of VLSI circuitry for controlling these devices has meant that these devices could be conveniently fabricated in silicon providing flexibility as well as cost efficiency. In these devices a variety of electronic logic functions and drive electronics can be integrated into each pixel providing a level of intelligence and added usability.

SLMs using Twisted Nematic Liquid Crystals (TNLC) have also been the subject of interest for many researchers for non-display applications [46–50]. More recently the Zero Twist Nematic Liquid Crystal (ZTNLC) is being incorporated with silicon back-plane in order to produce analogue nematic liquid crystal SLMs. These devices whist slower in their response time have the advantage of allowing the use of multi-phase holograms which in turn can improve the optical efficiency of the output. The device we used in this study is a 128×128 pixel zero-twist nematic liquid crystal spatial light modulator with pixel pitch of 40 micron and a silicon backplane.

The liquid crystal SLMs can be further divided into transmissive and reflective in terms of their operation. In case of transmissive SLMs, liquid crystal layer is held between two glass plates with control circuitry added with thin film transistors. Pixels are addressed to change the local electric field across the liquid crystal layer and hence switch the pixels on or off. These devices generally have larger pixel size and smaller fill-factor as well as

not being very flat. They are quite suitable for display applications but not as great a candidate for applications using coherent optics. The SLMs operating in a reflective mode use a liquid crystal layer over a silicon substrate with control voltage supplied to mirrors on the silicon chip. Fig 3.1 schematically illustrates the arrangement of various elements in a reflective silicon back-plane liquid crystal spatial light modulator.

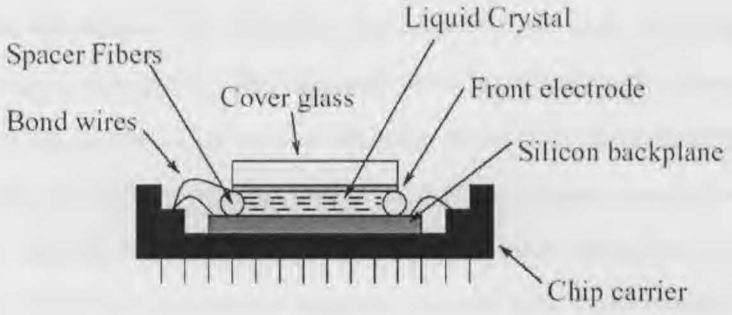

Figure 3.1: Liquid crystal over silicon - from [54]

In this arrangement the silicon back-plane is essentially a memory chip with reflective mirrors. The liquid crystal is switched by addressing the mirrors above it. Through specialised chemical and mechanical polishing it is possible to produce devices which are optically flat with very high reflectivity. These devices have attracted a great deal of interest for applications in coherent optics due to their size, ease of fabrication and optical flatness. Further enhancement of these devices still continues and as such we can expect to see more advanced and efficient versions finding their way to the market in the near future.

3.2.2 Magneto-optic SLMs

Magneto-optic spatial light modulators operate by means of a polarisation rotation under the application of a magnetic field. These SLMs were originally developed by Litton under the name of Light-Mod [51]. This device consists of pixelated crystal of aluminium garnet switched by an array of magnetic coils using magneto-optic effect. The granet mesas are largely transparent to light but when fully magnetised they rotate the polarisation of

incident light as a consequence of the Faraday effect. When the magnetisation direction coincides with the direction of propagation of the light, linearly polarised light will be rotated based on the right hand rule by an angle of $+\theta_f$ that depends on the thickness of the garnet film and when the magnetisation is opposite to the direction of propagation, the rotation of the polarisation is by angle $-\theta f$. The magnetisation directions of the pixels are controlled by a combination of an external magnetic field, supplied by a bias coil and a magnetic field introduced at the corner of each pixel by means of a row and column metallic electrodes. The following sequence of steps need to be followed in order to change the state of a pixel. The bias coil must be driven with current such that it establishes a strong magnetic field in the direction of the desired magnetisation. The next step is to ensure current pulses are present at the row and column electrodes that intersect at the pixel of interest with the direction of those currents being such as to establish a small magnetic field which produces a magnetic domain with magnetisation in the desired direction at the corner of the pixel. Despite the need for high powered drive circuitry and their low efficiency, Magneto-optic spatial light modulators are commonly available and have been used extensively to investigate matched filter correlator applications.

3.2.3 Deformable mirror SLMs

Another technology used in SLMs to modulate the phase of a beam of light is a deformable membrane. Several variations of this technology exist but they all use an electrostatic force for mechanical deformation of a membrane thereby modulating the incident beam of light. Deformable Mirror Device (DMD) is an electronically addressed SLM which combines the VLSI technology with the mechanical motion of pixel-sized elements. These devices were originally developed by Texas Instruments [52]. The original devices were fabricated using a continuous metalised polymer film stretched over a supporting grid structure. Underlying the membrane was an array of transistors. An applied voltage between the metalised membrane and the floating sources of the transistors caused the membrane to deform into the gaps between the membrane and the sources and by selectively applying the voltage to certain pixels, one could independently induce phase shift into selected positions of an incident optical beam. The current DMD devices use torsion elements

which are attached at two opposite ends and undergo deformation via a twisting that is proportional to the voltage on the underlying floating sources. One of the strengths of the DMDs is the ability to work at any wavelength where a good mirror could be made in an integrated form. The main use of these devices has been in display applications however interest in non-display applications of these devices has seen a surge of research activity in this area.

3.2.4 Multiple quantum well SLMs

Multiple Quantum Well (MQW) SLMs consist of alternative thin layers of different semiconductor material. Most commonly GaAs and AlGaAs are the two materials used in construction of these devices. The small thickness of these layers known as quantum wells results in certain quantum-mechanical effects and in particular new absorption peaks associated with structures known as excitons. These structures consist of an electron-hole pair for which the electron and hole are normally separated by a distance that is larger than the thickness of a single layer but which are brought close together by the constraints imposed by the thin layers of the device. Light amplitude modulation in these materials can be achieved by modifying their absorption spectra via an external electric field and phase modulation by exploiting the refractive index change associated with the excitonic peaks. The spectral location of the absorption peak is dependent on an electric field applied normal to the quantum wells. When an electric field is applied across the structure, the exciton resonances move to lower photon energies or longer wavelength. As a consequence if an MQW device is illuminated by light with a properly chosen wavelength, the application of an applied field to the device can change the absorption experienced by that light as it passes through the structure and this can be used to modulate the intensity of the input beam.

3.2.5 Acousto-optic SLMs

Acousto-optic SLMs modulate the properties of optical beams through interaction of acoustic waves with a coherent optical beam. These devices normally consists of a transparent medium into which acoustic waves are launched using a piezoelectric transducer.

The transducer is driven by an RF voltage source and sends a compressional wave into the acoustic medium. The acoustic wave propagates in the medium through small local displacements of molecules. Associated with these changes are small alterations of the local refractive index. This phenomenon is known as acousto-optic and there are two different regimes within which this interaction is utilized. Raman-Nath approach is usually used in cases where a liquid is used as the acousto-optic cell. In this case the optical wavefront is phase modulated by the moving refractive index grating, yielding a complex amplitude of the transmitted signal. For RF frequencies in a higher range (i.e. hundreds of MHz to GHz) and in situations where the acousto-optic medium is crystal, the Bragg regime is the more likely method used for modulation. The main difference between the two methods is that the diffraction efficiency into one first order is generally considerably larger in the Bragg regime than in Raman-Nath and the other orders are generally strongly suppressed by the diffraction process itself. Therefore in both cases an acousto-optic cell acts as a one dimensional spatial light modulator, translating the applied voltage modulation into a spatial wavefront.

3.3 Architecture and operation of Opto-VLSI processors

An Opto-VLSI processor is made-up of a Complimentary Metal Oxide Silicon (CMOS) back-plane containing a rectangular array of square pixels. Each pixel in turn contains a storage element which is permanently electrically connected to a metal mirror on the top surface of the chip above the pixel. This arrangement is illustrated schematically in figure 3.2. At the pixel level, the processor consists of a top glass layer coated with a transparent conductor such as Indium Tin Oxide (ITO) on the inside. The glass plate is bonded to the surface of the chip and a gap of few microns is left for the liquid crystal material.

3.3.1 Pixel design

The pixels can be designed using a dynamic random access memory (DRAM) or static random access memory (SRAM) cell approach. The advantages of the DRAM approach

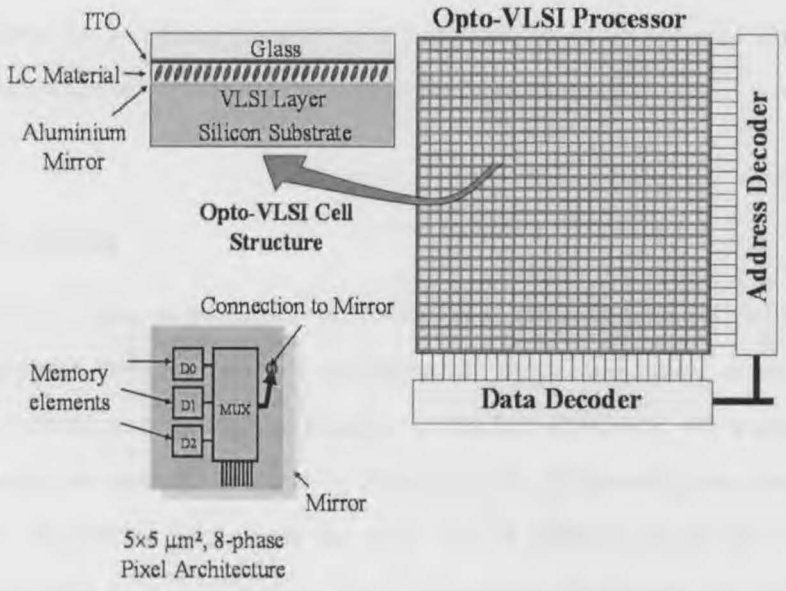

Figure 3.2: Architecture of an Opto-VLSI processor

are small area allowing maximum pixel packing density for a given fabrication process. Simplicity is another advantage of DRAM design methodology. Furthermore pixels designed using DRAM do not contain any complimentary structures. The disadvantages of this approach are loss of drive voltage, insufficient charge storage leading to slow or incomplete switching of LC and charge leakage leading to a phase ripple in processors performing phase modulation and requiring continual refreshing of data in the pixel array. It is worthwhile mentioning that the DRAM approach is inherently an analog approach and as such it is suitable for analog LC materials. The SRAM process is usually preferred if the switching speed, output stability or high optical input power are of greater importance when compared to high pixel packing density. Advantages of this scheme are that the full power rail voltage of the back-plane is available to drive the LC. There is an unlimited amount of charge capacity available for the mirror. The pixel mirror voltage is stable and not subject to reduction as the LC switches. Moreover the voltage is not subject to decay or leakage. On the flip side, the disadvantages of the SRAM process are need for a large area as the SRAM pixels take up a larger space. The complimentary nature of the circuit leaves the pixel vulnerable to a permanent and destructive failure (latch up) which can

be induced by presence of light in the substrate. Finally in the large arrays the transient current produced by switching the state of a large number of SRAM cells simultaneously can cause temporary or permanent damage to the back-plane [53].

3.3.2 Addressing

An opto-VLSI processor is essentially a Spatial Light Modulator (SLM) which is a real-time reconfigurable device capable of modifying the amplitude, phase or polarisation of an optical wavefront as a function of position across the wavefront. For a good review of SLMs the reader can consult the paper by Neff et al. [54]. Addressing the array of LC cells (i.e. applying an electric field across the cell) may be achieved optically or electrically. Electrical addressing is by far the most typical addressing mechanism used in SLMs. In a matrix-addressing scheme, the SLM is organised into linked set of rows and columns, with each row sequentially selected and the data written via the column address line [53,55,56]. Another addressing mechanism that has been proposed is a controlled electron beam in a cathode ray tube applying charge to a surface where a layer of LC is sandwiched. Yet another addressing mechanism is the "traveling wave", where a radio frequency signal is applied at the edges of the SLM to couple charge into a specific row/column of the cell array. In optical addressing, the control signal that determines the cell's electrical field is determined by the optical field arriving at that pixel. Such schemes are generally referred to as "smart pixels" and have great potential in applications where the input and control signals are directly related, as is the case in certain control and signal processing applications [57]. In matrix addressing data is normally written into the pixel array one row at a time. The address circuitry determines whether the array is addressed sequentially or in any chosen order. Data for a row is assembled at the column drivers and transmitted to the column address lines. A pulse is then sent to the gate lines of a row of pixels which switches on the transistors for that row thus allowing the data to flow onto the mirrors.

3.4 Beam processing using Opto-VLSI processors

The basic operation of the processor is as follows. A range of voltages applied between the top mirror and the aluminium metal base causes an incident beam of light to be modulated. The individual pixels are programmed separately whilst the transparent ITO layer is common to all pixels. The modulation can be either phase or amplitude based. Typically in analogue designs for phase modulation, the phase level changes with the level of applied voltage. The circuitry that surrounds the pixels on the back-plane, allows the $M \times N$ array of pixels to be addressed as required. Thus the row address circuit typically consists of a $M \times 1$ bit shift register or decoder used to activate the rows one by one so that data may be written into them. The column address circuit involves demultiplexing to allow the data which is to be transmitted into a given row of pixels to be assembled from a manageable number of bonding pads (about 64) and subsequently transmitted onto the column bus lines [58].

One of the main advantages that an Opto-VLSI processor has over its rivals is its ability to offer both steering as well as multicasting capabilities. This feature certainly sets this device apart from many of the other techniques offered for beam processing and can be utilised in fields such as adaptive signal processing [59] as part of a reconfigurable beam splitter fabric. As can be seen from figure 3.3 by selecting the appropriate phase hologram we can steer an input optical beam to a desired location within the replay field (essentially the Fourier Transform of the hologram) or split this beam into N output beam in a multicast arrangement. The steering angle θ is define by the wavelength (λ), Number of phase levels (M) and the pixel size (d). In the absence of a phase hologram the processor acts as a mirror reflecting the incoming beam with an angle which is equal to that of incident as described by Snell's law [23]. In the case where a phase hologram is present the processor will imprint a phase variation on the wavefront thereby steering it with an angle θ that is determined by the wavelength of the incoming beam as well as the hologram period which consists of number of pixels used in a period and the pixel pitch of the hologram.

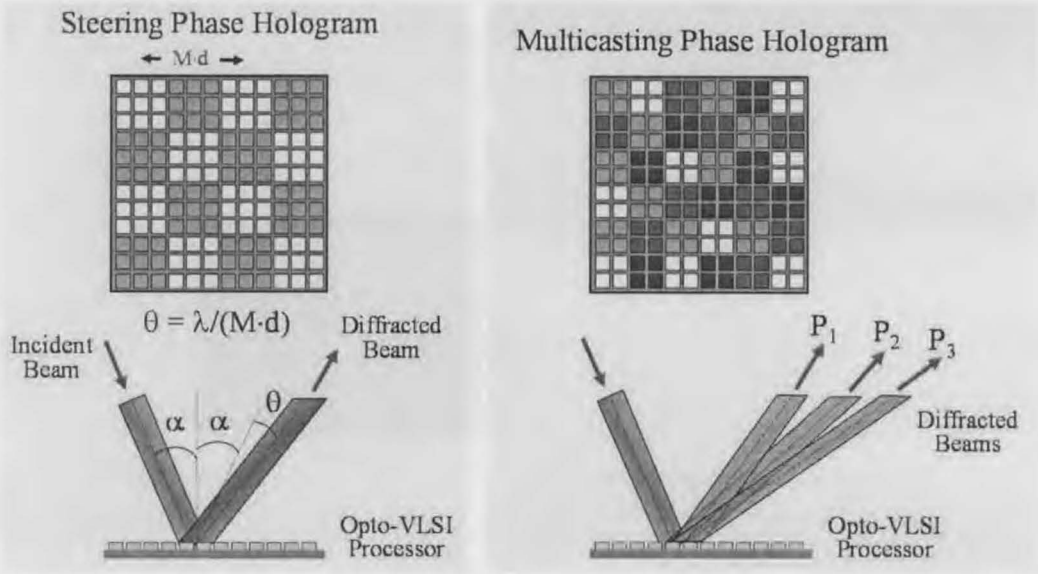

Figure 3.3: Beam steering and multicasting capability of Opto-VLSI processors

Figure 3.5 schematically represents the beam steering capability of an Opto-VLSI processor. In this case it can be seen that by modifying the phase hologram the incident beam can be sent to various locations in the replay field. We can target one or more positions in the replay field and using our algorithms generate the necessary hologram to direct the incident light to the selected spots in the replay field. A phase hologram can be thought of as a programmable grating and therefore by reprogramming the grating and thereby changing its slope we are able to steer the incoming beam to various locations. For a more detailed discussion on generation of phase holograms please refer to chapter 4. Figure 3.8 represents the experimental results confirming the capability of an Opto-VLSI processor in beam-steering.

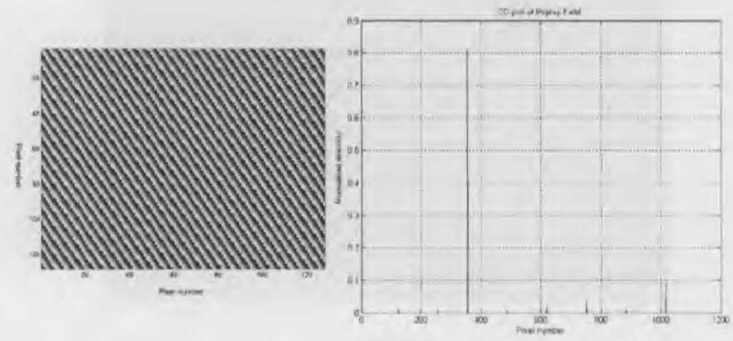

Figure 3.4: Beam steering capability of an Opto-VLSI processor - first position

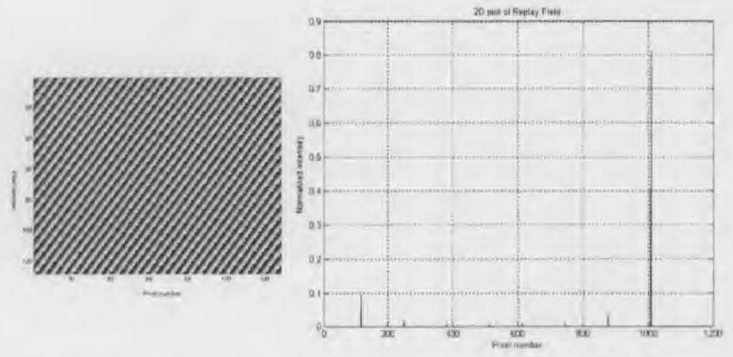

Figure 3.5: Beam steering capability of an Opto-VLSI processor - second position

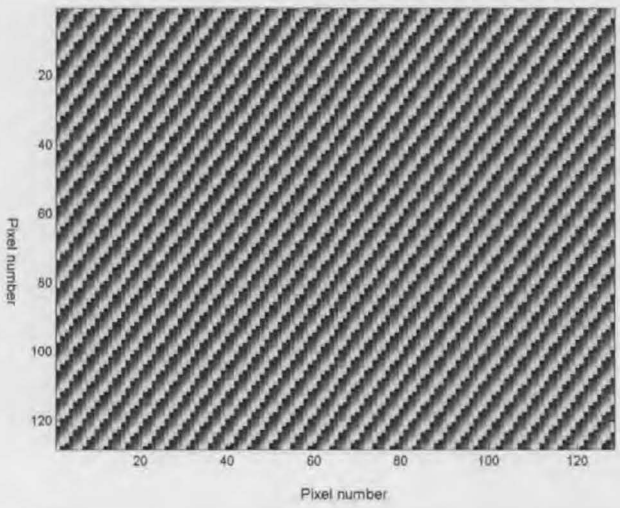

Figure 3.6: A hologram used to represent the beam steering capability of an Opto-VLSI processor

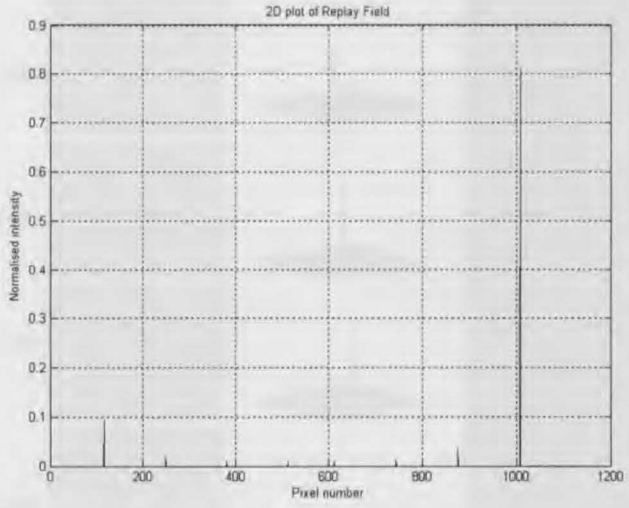

Figure 3.7: The replay field resulting from the previous hologram

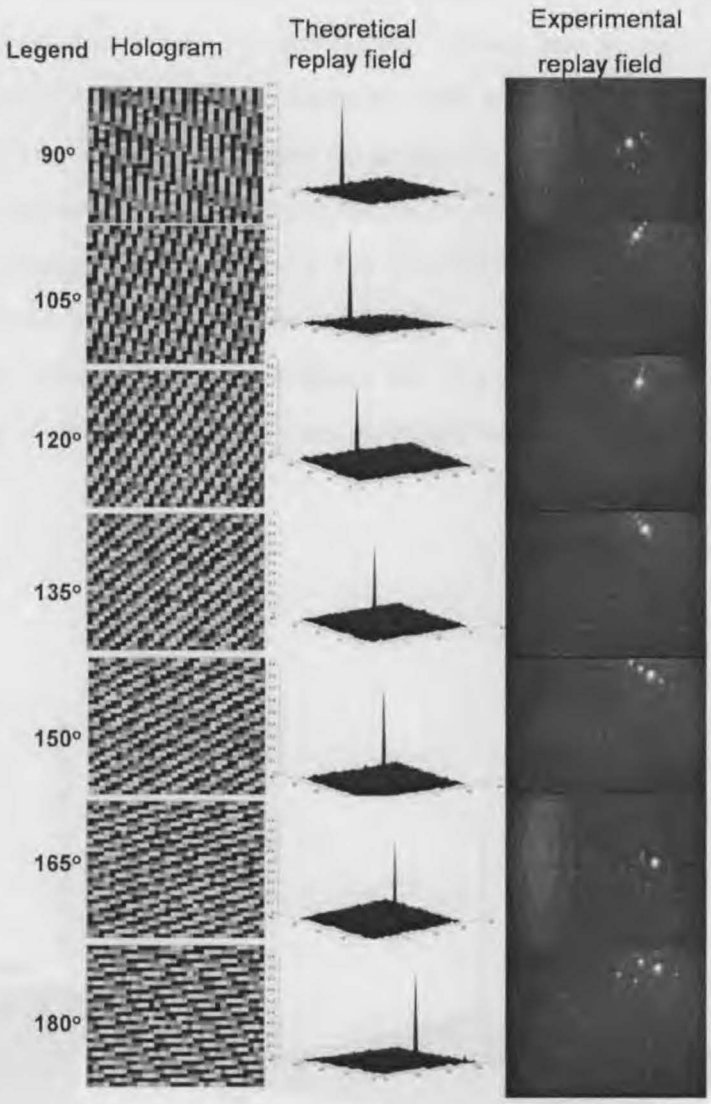

Figure 3.8: Experimental results confirming the beam steering capability of an Opto-VLSI processor

The following figures represent the multicasting capability of Opto-VLSI processor. Figure 3.9 shows the simulation results for multicasting. In this case we have used an 8 phase hologram and set different intensity weights for each pair of output beam. Figure 3.10 shows the holograms and their associated replay field for a 1×8 splitter. Figures 3.11 and 3.12 show that by designing and applying the appropriate phase hologram we have been able to experimentally prove the ability of the Opto-VLSI processor to split one incoming beam into 8 output beams. The additional set of beams present are due to the periodic nature of pixels. In figure 3.10 we have shown that it is possible to arbitrarily control the intensity of any of the beams using an appropriately designed phase hologram.

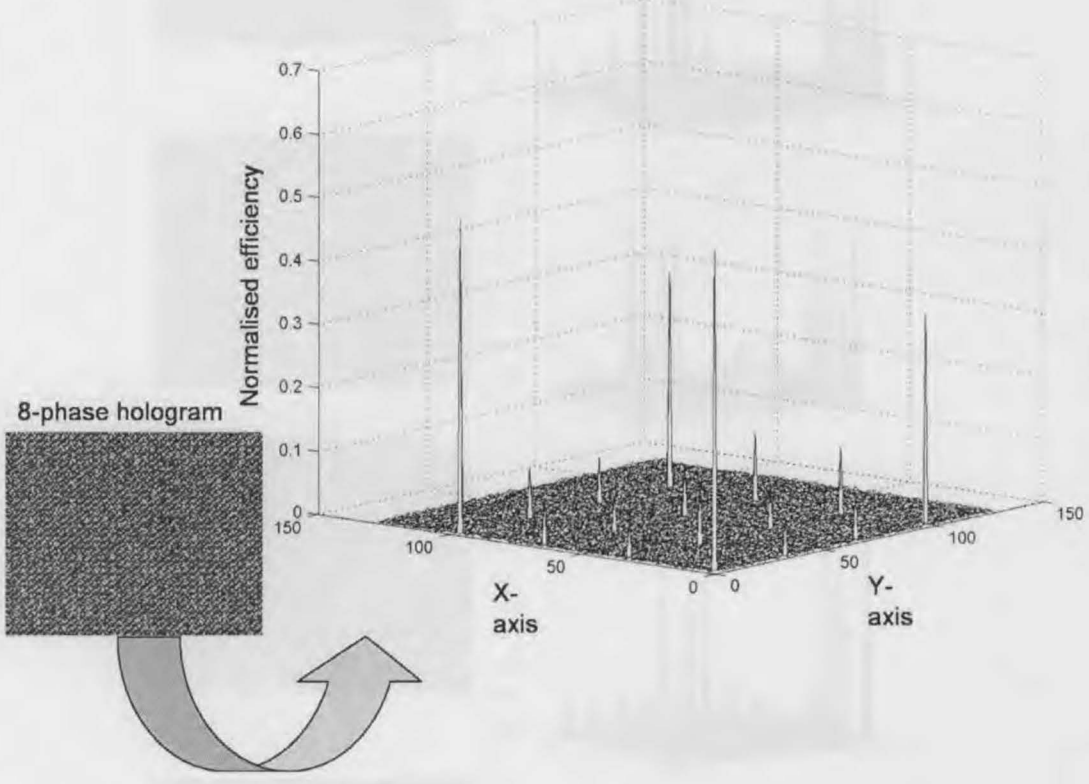

Figure 3.9: Simulation results showing the multicasting capability of the Opto-VLSI processor

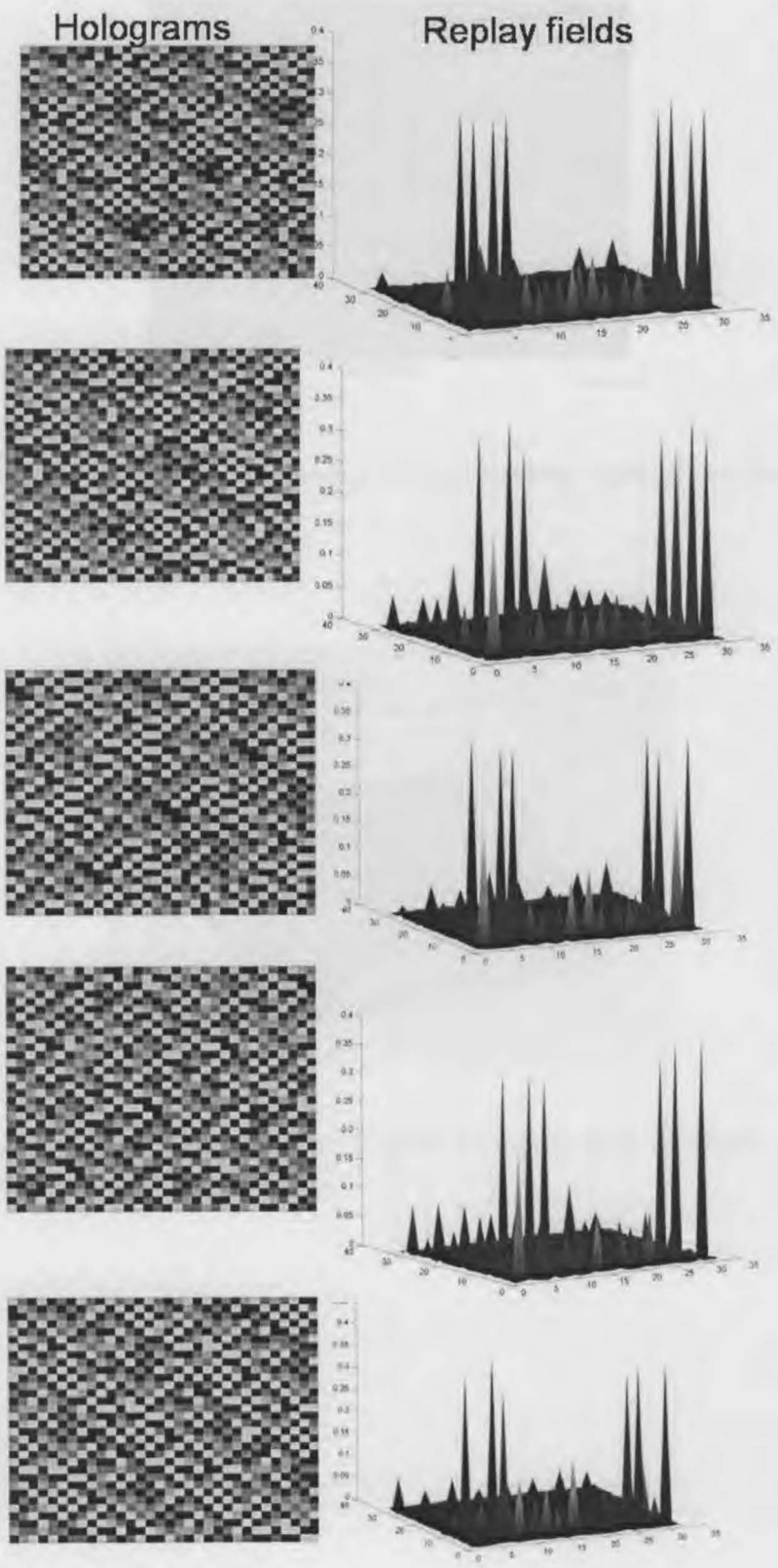

Figure 3.10: Hologram and replay fields illustrating the multicasting capability of Opto-VLSI processor

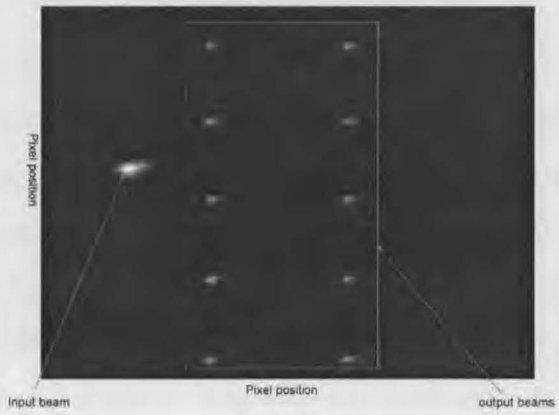

Figure 3.11: Experimental results showing the multicasting capability of the Opto-VLSI processor

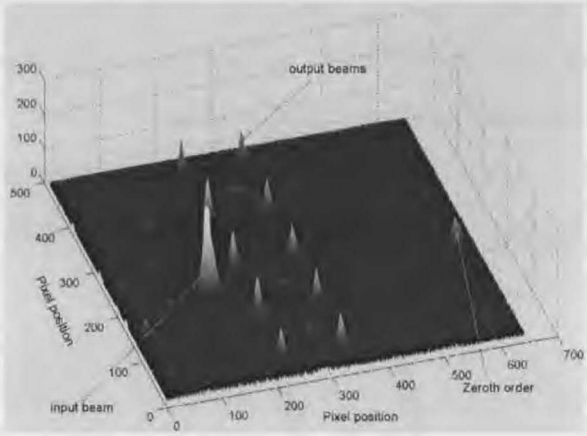

Figure 3.12: Experimental results showing in 2D the multicasting capability of the Opto-VLSI processor

3.4.1 Liquid cyrstals

As was mentioned in the previous section an Opto-VLSI processor consists of an array of liquid crystal cells supported by a VLSI back-plane. Liquid crystals (LC) are commonly found in a meta-state. This means that their molecules lack the rigid structure of solids and free-floating disposition displayed by liquids and only assume some degree of spatial ordering. There are three different general classes (or phases) of liquid crystals that are of interest in optics: (1)Nematic (2) Smectic (3)Cholesteric. These classes are differentiated by the different molecular orders or organisational constraints. In case of nematic liquid crystals, the molecules throughout the entire volume of the material favour a parallel orientation pointing on average in one direction as defined by the director $\hat{a}$, with randomly located centres within that volume. In smectic liquid crystals the molecules again favour parallel alignment but their centres lie in parallel layers with randomness of location only within a layer. Here the molecules lie essentially randomly ordered within planes with $\hat{a}$ perpendicular (in case of smectic A phase) or tiltled (for smectic C phase) at some angle θ to the layer normal. Finally, a cholesteric liquid crystal is a nematic phase with chirality that undergoes helical rotation. In case of chiral liquid crystals the director $\hat{a}$ precesses around layer normal in some well defined way.

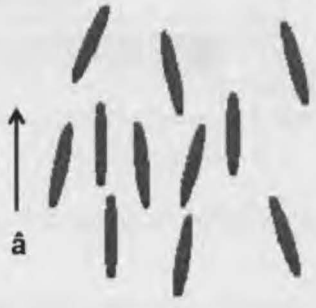

Figure 3.13: Molecular arrangment for a Nematic liquid crystal

The anisotropic molecular property of liquid crystals provides the key to usefulness of LCs by allowing LC molecules to be controlled by external factors such as electric fields. This gives LCs very useful electro-optical characteristics such as the ability to be used for phase modulation. The important anisotropic properties are (1) refractive index n, in which the

birefringence Δn is given by $n|| - n\perp$ and (2) the electric permittivity ϵ in which the dielectric anisotropy $\Delta\epsilon$ is given by $\epsilon|| - \epsilon\perp$. Here the subscripts refer to the values of n or ϵ parallel and perpendicular to the director $\hat{a}$, and typical values of Δn and $\Delta\epsilon$ are ≈ 0.15 and 30 respectively. In the absence of an external electric field the liquid crystals may be preferentially ordered by surface aligning agents or topography [60]. Two important arrangements are possible. In the planar alignment case the molecules are constrained to lie in the plane of the surface with $\hat{a}$ pointing in the one direction. In the homeotropic case the surface treatment causes the molecules to be aligned with $\hat{a}$ perpendicular to the surface. Application of an external field $\underline{E}$ changes the energy of the system and generally causes a realignment of the liquid crystal such that $\hat{a}$ aligns parallel to $\underline{E}$ for $\Delta\epsilon > 0$ or perpendicular to $\underline{E}$ for $\Delta\epsilon < 0$. The orientational process and dynamics which may be monitored through changes in the refractive index are controlled by the elastic constants $(k_{ii}, i = 1, 2, 3, 4)$, the viscosity coefficient (n_i) and the applied voltage. The basis for an electro-optic device is therefore a thin layer of liquid crystal (thickness d)constrained between two aligning surfaces and across which an external field may be applied as shown in figure below.

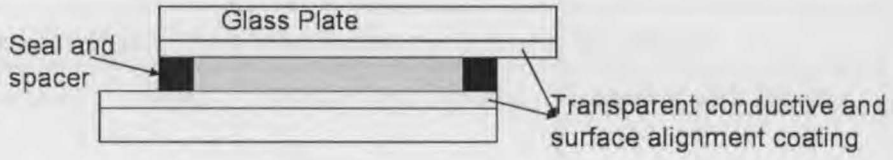

Figure 3.14: Schematic of liquid crystal construction

On removal of the field the induced order will normally relax back to the original surface induced alignment state. In typical liquid crystal devices sample thicknesses are of the order of $2 - 20\mu m$ and fields of $\approx 0.1 - 10V/\mu m$ are used. Thus the applied voltages are relatively low and since the devices are non conducting, power requirements are minimal. A typical cell of a reflective SLM is shown in Figure 3.15.

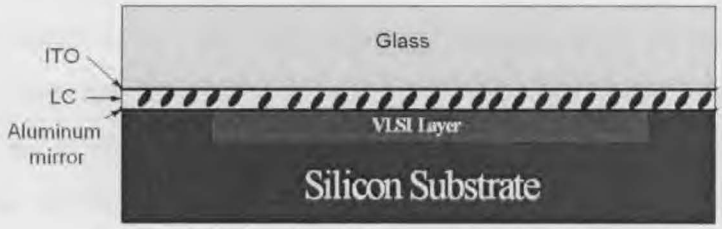

Figure 3.15: Typical cell of a reflective SLM

In terms of phase modulation LCs can be divided into two groups, Ferroelectric and Nematic [61]. In this study nematic liquid crystals are used as the modulating material. The table below shows some of the salient properties of ferroelectric and nematic liquid crystals [62].

	Nematic LCs	Ferroelectric LCs
Achievable phase shift	0 to typically 10 waves	Up to 1 wave
Control	Continuous	mostly Binary
Speed	depends on phase shift $\approx$ 5ms for $\frac{\lambda}{2}$ $\approx$ 1s for several λ	in μs commercial SLMs have frame rates in KHz
wavelength range	0.4-2.2 μm	0.4-2.2 μm
polarisation dependence	operates with linearly polarised light	operates with linearly polarised light
Transmittance	up to 95%	up to 95%
Operating voltage	$\approx$ 10V AC	$\approx$ 5V

The birefringent nature of LCs means that as polarised light enters the LC layer, the material performs two basic functions; wave division and retardation. That is, the liquid crystal divides a single wave, which is linearly polarised, into two orthogonally polarised waves and induces a time delay between these waves. This time delay occurs because the anisotropic structure of the LC material is such that the index of refraction is not the same

in all directions. If a polariser is placed after the device, the two waves are forced to interfere. If the two waves are in phase, light is strongly transmitted. If the two waves are out of phase, destructive interference occurs and light is dissipated at the polariser. Whether the two waves are in phase depends primarily on three things: (1) the birefringence of the LC material (or the difference in the index of refraction of the two paths), (2) the thickness of the LC layer, and (3) the wavelength of the input light. As an electric field is applied to a nematic LC layer, there is a corresponding reduction in the birefringence of the LC material. The birefringence change induces a phase-only modulation of the input light.

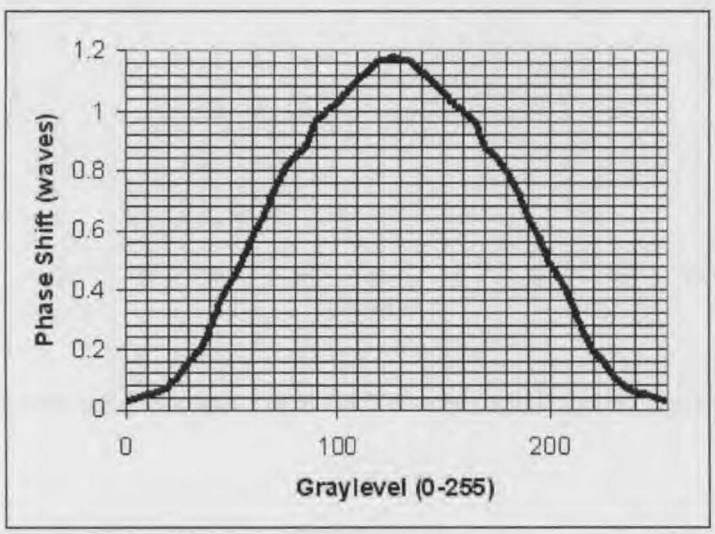

Figure 3.16: Typical response curve for a nematic liquid crystal

Figure 3.16 shows the typical response curve for a nematic LC-SLM. It is worth noting that unless nematic liquid crystals are driven with AC voltage they will degrade. The pixels in this SLM (which is the device we used in our experiments) can be programmed to 256 (8-bit) gray-levels or voltage steps between 0-5 V. The cover glass electrode is set to the mid-range of 2.5 V. The symmetric nature of the curve above is due to the fact that nematic LC responds only to the strength of the electric field, not the sign. For example, a gray-level of 51 would result in a voltage of ((51/256)*5V) or 1.0 V. The difference between the pixel voltage (1.0V) and the cover glass (2.5V) results in a 1.5V field. Likewise,

a gray-level of 205 results in a pixel voltage of 4.0 V, and a field of +1.5V. Since the LC only responds to the field strength, the same phase response is seen for gray scale 51 and 205. Therefore, despite 8-bits of pixel voltage addressing, only 7-bits of phase response is achieved. figure 3.17 illustrates the experimental response curve we have obtained for the Nematic liquid crystal processor we used in this study.

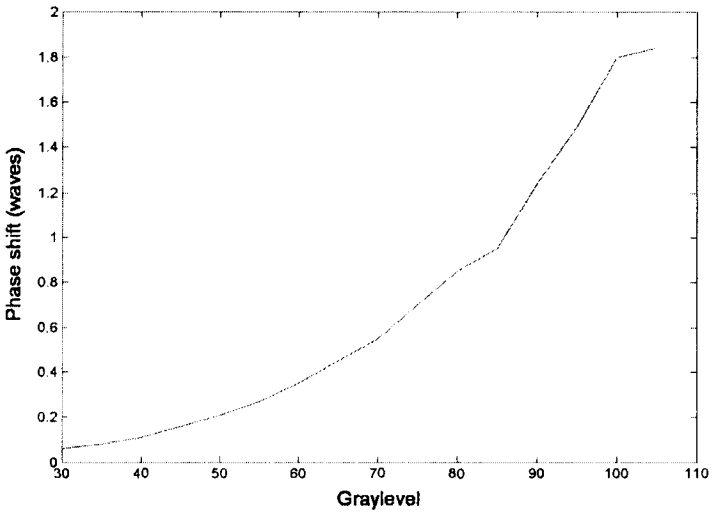

Figure 3.17: Experimental response curve for Nematic liquid crystal processor used in this study

The achievable phase shift from LCs is given by:

$$\varnothing = \frac{2\pi\Delta nd}{\lambda} \tag{3.1}$$

where ϕ is the phase shift, λ is the wavelength, d is the LC cell thickness and Δn is the LC birefringence. In transmissive LC-SLMs, the liquid crystal layer is sandwiched between two transparent electrodes. Application of voltage between the electrodes induces a phase shift in that layer. This is repeated periodically across pixel block with the intent to form a periodic phase profile characteristic of a grating. The operation of a reflective SLM is similar to that of a transmissive SLM however a reflective SLM has one of the electrodes as

a high-reflectivity mirror. The advantage of a reflective SLM is that it can be easily integrated with silicon VLSI circuitry for addressing and driving the LC cells [63,64]. Usually Indium-Tin Oxide (ITO) is used as the transparent electrode and evaporated aluminum is used as reflective electrode. The ITO layer is generally grounded and a voltage is applied at the reflective electrode by the VLSI circuit below the LC layer.

Future optical networks will require optical components that are polarisation insensitive. Therefore the LC-SLM being a key element in dynamic optical networks is expected to meet this requirement. Polarisation insensitive operation for a processor based on Ferroelectric liquid crystal has already been shown [65]. Recent advances in LC materials and layer thickness control have allowed the incorporation of a thin quarter-wave-plate (QWP) layer between the LC and the aluminum mirror to accomplish polarisation-insensitive multi-phase-level LC-SLMs paving they way for use of Nematic liquid crystal based Opto-VLSI processors in various photonic signal processing applications [66].

3.5 Summary

In this chapter we have presented a detailed look at the architecture and operation of an Opto-VLSI processor. We have expounded on dispersive features of an Opto-VLSI processor and how they may be used for optical filtering and channel equalisation. We have examined the various components that make-up an Opto-VLSI processor with a special section devoted to the liquid crystal component used with the VLSI back-plane.

In the following chapter we will examine in detail the processes involved in the creation of phase holograms which are generated by the Opto-VLSI processors and are the key element in modulating optical wavefronts. We will also analyse and derive expressions for the efficiency of the phase holograms using a one and two dimensional Fourier series. We also use a two dimensional model for deriving an efficiency expression taking into consideration the finite number of pixels as well as the phase and spatial quantisation involved in the generation and application of phase holograms using an Opto-VLSI processor.

Chapter 4

Analysis and generation of phase holograms

4.1 Introduction

The word hologram is an amalgam from Greek words meaning "entire recording". This distinguishes a hologram from a photograph in the sense that a photograph only captures the intensity of the incident light from the object being photographed whereas a hologram records both the intensity and phase or direction of propagation of the incident light.

There are various techniques for generation of Computer Generated Holograms (CGH) [67]. Kinoforms or phase only holograms are used in this study. Kinoforms operate only on the phase of an incident wave based on the assumption that for reconstruction of the image of the scattered object only phase information is needed [68].

The pixelated nature of the Opto-VLSI processor where holograms are displayed means that this device acts like a diffraction grating. These pixels act like apertures meaning that as coherent light passes through them spherical wavefronts are produced. However it is worth noting that a pixel will in general emit a truncated plane wavefront. As these wavefronts propagate they interfere with each other. Depending on the nature of these

interference, wavefronts reinforce or destroy each other. Each point of constructive interference gives rise to more spherical wavefronts. This concept is known as Huygens's principle. The result of these interferences are a series of bright and dark spots called a diffraction pattern. At large distances called the far field the spherical wavefronts are approximated as plane waves. This simplifying assumption is known as Fraunhofer diffraction.

Holograms will be used as a reconfigurable tool in an adaptive manner to "process" wavelengths thereby creating for instance a suitable filter response or equalising various WDM channels dynamically. It is worth noting that in addition to beam-steering and multicasting, phase holograms can be used to re-shape an optical wavefront. In appendices B,C and D we have presented the theoretical results confirming the ability of phase holograms to convert a Gaussian beam profile to a profile that is circular.

4.2 Analysis of 2D Phase holograms

A two dimensional phase hologram can be modeled as consisting of N^2 square pixels of width w. We assume that this matrix of square pixels is illuminated with a beam of laser with power P_{in}. Assuming uniform power distribution across the matrix, the intensity can be obtained from:

$$I = \frac{P_{in}}{N^2 w^2} \tag{4.1}$$

The electric field at the surface of the matrix is given by:

$$E = \sqrt{\frac{P_{in} 2z}{N^2 w^2}} \tag{4.2}$$

where $I = \frac{E^2}{2z}$ and 2z is the impedance of the free-space [69]. We can use the scalar diffraction theory to determine the optical field which is generated as a result of the Opto-VLSI

processor being illuminated. From the scalar diffraction theory the optical field at some distance from the processor can be obtained from the Fourier transform of the aperture. Within the Fraunhofer region this field can be expressed as

$$U(x,y) = \frac{\exp(jkz)\exp\left(\frac{jk(x^2+y^2}{2z}\right)}{j\lambda z} FT(A(x,y)) \tag{4.3}$$

Where A(x,y) is the function representing the aperture and FT refers to the Fourier Transform operation.

4.2.1 Basic model

A pixel is the smallest object that makes up the hologram. The hologram consists of an array of pixels equally distributed on the surface of the Opto-VLSI processor. An expression for the far field intensity pattern of the hologram can be obtained from product of the pixel and array contribution. The pixel contribution is the far field pattern from a single pixel. The array contribution is due to the periodic spacing of the pixels (spatial quantisation) and the phase relationship between pixels (phase quantisation). The transmittance of basic cell of pixels forming the hologram can be expressed as [70]:

$$t(x,y) = \sum_{m,n=1}^{m=M,n=N} \exp(j\theta_{nm}) rect\left(\frac{x}{w}\right) rect\left(\frac{y}{w}\right) \tag{4.4}$$

Where $\exp(j\theta_{nm})$ represents the discrete phases associated with pixels.

The diffraction pattern at the replay field is obtained from the Fourier transform of the above expression:

$$T(f_x,f_y) = w^2 sinc(f_x w) sinc(f_y w) \sum_{n,m=1}^{m=M,n=N} \exp(j\theta_{nm}) \exp(2\pi j(mf_x + nf_y)). \tag{4.5}$$

We define the following:

$$f_x = \frac{x}{\lambda z}, f_y = \frac{y}{\lambda z} \tag{4.6}$$

Using the above definition the far field diffraction pattern will be:

$$U(f_x, f_y) = \frac{\exp(jkz)\exp\left(\frac{jk(x^2+y^2)}{2z}\right)}{j\lambda z} w^2 sinc\left(\frac{x}{\lambda z}w\right) sinc\left(\frac{y}{\lambda z}w\right) \sum_{n,m=1}^{m=M,n=N} \exp(i\theta_{nm})\exp\left(2\pi i\left(m\frac{x}{\lambda z} + n\frac{y}{\lambda z}\right)\right) \tag{4.7}$$

The intensity associated with this field is:

$$I(f_x, f_y) = \left(\frac{w^4}{\lambda^2 z^2}\right) sinc^2\left(\frac{wx}{\lambda z}\right) sinc^2\left(\frac{wy}{\lambda z}\right) \times \left[\sum_{n,m=1}^{m=M,n=N} \exp(i\theta_{nm})\exp\left(2\pi i\left(m\frac{x}{\lambda z} + n\frac{y}{\lambda z}\right)\right)\right]^2 \tag{4.8}$$

4.2.2 2D model

In this section we investigate a model proposed by Arrizon et al. [71] and derive an expression for the efficiency of a 2 dimensional phase hologram. Consider a matrix representing a phase hologram consisting of $P \times P$ identical periodic basic cells, each of $M \times M$ pixels of dimensions $s \times s$ with phase levels as illustrated below:

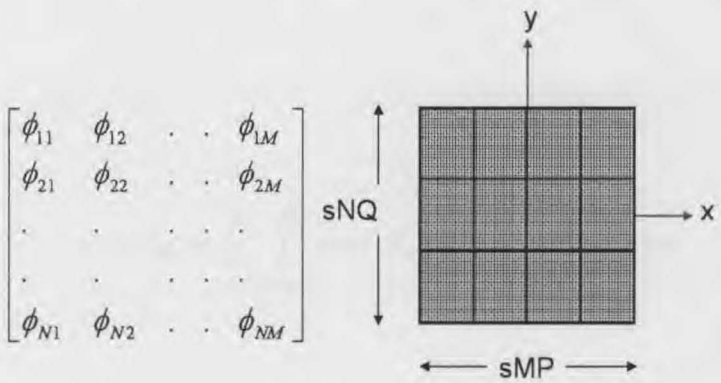

Figure 4.1: 2D phase grid

The amplitude transmittance of the phase hologram can be written as

$$t(x,y) = \left\{ \left[rect\left(\frac{x}{s}\right) rect\left(\frac{y}{s}\right) \otimes \sum_{n=1}^{M}\sum_{m=1}^{M} exp(j\phi_{mn})\delta(x-sn)\delta(y-sm) \right] \right\} \otimes \left\{ comb\left(\frac{x}{sM}\right) comb\left(\frac{y}{sM}\right) \right\} rect\left(\frac{x}{sMP}\right) rect\left(\frac{y}{sMP}\right) \quad (4.9)$$

The diffraction pattern $T(f_x, f_y)$ of the phase hologram is the Fourier Transform of t(x,y) and is given by:

$$T(f_x,f_y) = \left\{ \Im\left[rect\left(\frac{x}{s}\right) rect\left(\frac{y}{s}\right) \right] \times \Im\left[\sum_{n=1}^{M}\sum_{m=1}^{M} exp(j\phi_{nm}\delta(x-sn)\delta(y-sm) \right] \right\} \left\{ \times \Im\left[comb\left(\frac{x}{sM}\right) comb\left(\frac{y}{sM}\right) \right] \right\} \otimes \Im\left[rect\left(\frac{x}{sMP}\right) rect\left(\frac{y}{sMP}\right) \right] \quad (4.10)$$

Therefore we can write:

$$T(f_x,f_y) = \left\{ s^2 sinc(sf_x) sinc(sf_y) \times \sum_{n=1}^{M}\sum_{m=1}^{M} exp(j\phi_{nm}) exp\left[j2\pi(snf_x + smf_y) \right] \right\} \times \left\{ s^2M^2 comb(sMf_x) comb(sMf_y) \right\} \otimes s^2M^2P^2 sinc(sMPf_x) sinc(sMPf_y) \quad (4.11)$$

Another way to express the amplitude transmittance is:

$$t(x,y) = \left[c(x,y) \otimes comb(x,y) \right] s(x,y) \quad (4.12)$$

Where

$$c(x,y) = e(x,y) \otimes \sum_{n=1}^{M}\sum_{M=1}^{M} \exp(j\phi_{nm})\delta(x-ns)\delta(y-ms) \quad (4.13)$$

So we can write the expression for the diffraction pattern as:

$$T(f_x, f_y) = \{C(f_x, f_y)D(f_x, f_y)\} \otimes S(f_x, f_y) \tag{4.14}$$

$$= \sum_{l=-\infty}^{\infty} \sum_{k=-\infty}^{\infty} E\left(\frac{l}{sM}, \frac{k}{sM}\right) W\left(\frac{l}{sM}, \frac{k}{sM}\right) \otimes S(f_x, f_y) \tag{4.15}$$

$$= \sum_{l=-\infty}^{\infty} \sum_{k=-\infty}^{\infty} E\left(\frac{l}{sM}, \frac{k}{sM}\right) W\left(\frac{l}{sM}, \frac{k}{sM}\right) S(f_x - l, f_y - k) \tag{4.16}$$

Where

$$E\left(\frac{l}{sM}, \frac{k}{sM}\right) = s^2 sinc\left(\frac{l}{M}\right) sinc\left(\frac{k}{M}\right) \tag{4.17}$$

$$W\left(\frac{l}{sM}, \frac{k}{sM}\right) = \sum_{n=1}^{M} \sum_{m=1}^{M} \exp(j\phi_{nm}) \exp\left[j2\pi\left(n\frac{l}{M} + m\frac{k}{M}\right)\right] \tag{4.18}$$

$$S(f_x, f_y) = s^2 M^2 P^2 sinc(sMPf_x) sinc(sMPf_y) \tag{4.19}$$

$S(f_x, f_y)$ is a highly compressed sinc function replicated at every diffraction order and the width of its main lobe is $2/sMP$. Therefore if P is large, the spots in the replay field appear isolated and with:

$$\int_{-\infty}^{\infty} S(f_x, f_y)^2 df_x df_y = \int_{-\infty}^{\infty} s^4 M^4 P^4 sinc^2(sMPf_x) sinc^2(sMPf_x) df_x df_y = s^2 M^2 P^2 \tag{4.20}$$

the energy integrated over the spot in the diffraction pattern is

$$e_{l,k} = s^2 M^2 P^2 E^2 \left(\frac{l}{sM}, \frac{k}{sM}\right) \left|W\left(\frac{l}{sM}, \frac{k}{sM}\right)\right|^2 \tag{4.21}$$

The total incident energy is $s^2 M^2 P^2$, therefore the normalised energy for the (l,k) is given as:

$$\bar{e}_{l,k} = E^2 \left(\frac{l}{sM}, \frac{k}{sM}\right) \left|W\left(\frac{l}{sM}, \frac{k}{sM}\right)\right|^2 \tag{4.22}$$

If the output signal is over a range of values such that$(l, k) \in \Omega_s$, the efficiency of the phase hologram can be defined as:

$$\eta_s = \sum_{\Omega_s} \bar{e}_{l,k} = \sum_{\Omega_s} E^2\left(\frac{l}{sM}, \frac{k}{sM}\right)\left|W\left(\frac{l}{sM}, \frac{k}{sM}\right)\right|^2 \tag{4.23}$$

If we take Ω_w to represent the set of all (l,k) values, the desired phase hologram is one that generates normalised spot energies with the following properties:

$$\bar{e}_{l,k} = K\bar{e}_{l,k;opt}(l,k) \in \Omega_s \tag{4.24}$$

$$W(l,k) = 0(l,k) \in (\Omega_w - \Omega_s) \tag{4.25}$$

Where $\bar{e}_{l,k;opt}$ denotes the set of desired normalised energies in the spot array fulfilling the condition:

$\sum_{\Omega_s} \bar{e}_{l,k;opt} = 1$
and K is a constant. But

$$\eta_s = \sum_{\Omega_s} \bar{e}_{l,k} = \sum_{\Omega_s} K\bar{e}_{l,k;opt} = K\sum_{\Omega_s} \bar{e}_{l,k;opt} = K \tag{4.26}$$

Hence $\eta_s = K$

Now

$$\bar{e}_{l,k} = E^2\left(\frac{l}{sM}, \frac{k}{sM}\right)\left|W\left(\frac{l}{sM}, \frac{k}{sM}\right)\right|^2 \tag{4.27}$$

Therefore

$$\left|W\left(\frac{l}{sM}, \frac{k}{sM}\right)\right|^2 = \bar{e}_{l,k}E^{-2}\left(\frac{l}{sM}, \frac{k}{sM}\right) = \bar{e}_{l,k}s^{-4}sinc^{-2}\left(\frac{l}{M}\right)sinc^{-2}\left(\frac{k}{M}\right) \tag{4.28}$$

resulting in

$$\sum_{\Omega_s}\left|W\left(\frac{l}{sM}, \frac{k}{sM}\right)\right|^2 = \sum_{\Omega_s} \bar{e}_{l,k}s^{-4}sinc^{-2}\left(\frac{l}{M}\right)sinc^{-2}\left(\frac{k}{M}\right) \tag{4.29}$$

But from Parsevals theorem we have

$$\sum_{\Omega_s} \left| W\left(\frac{l}{sM}, \frac{k}{sM}\right)\right|^2 = M^4 \tag{4.30}$$

Therefore

$$\sum_{\Omega_s} \bar{e}_{l,k} s^{-4} sinc^{-2}\left(\frac{l}{M}\right) sinc^{-2}\left(\frac{k}{M}\right) = M^4 \tag{4.31}$$

and finally

$$\eta_s = \frac{s^4 M^4}{\sum_{\Omega_s} \bar{e}_{l,k;OPT} sinc^{-2}\left(\frac{l}{M}\right) sinc^{-2}\left(\frac{k}{M}\right)} \tag{4.32}$$

for $\Omega_s = (l, k)$

$$\eta_s = \frac{s^4 M^4 sinc^2\left(\frac{l}{M}\right) sinc^2\left(\frac{k}{M}\right)}{\bar{e}_{l,k;OPT}} \tag{4.33}$$

4.3 One dimensional Fourier Series analysis

In this section we will present an analysis of the phase hologram using a one dimensional Fourier series. This analysis will continue in the next section where, this time we employ a two dimensional Fourier series as an extension to the results achieved in this section.

We start by Fourier Series analysis of one dimensional infinitely long phase Hologram of M phase levels (special case of N=Q=1, $P \rightarrow \infty$) where p is the number of periods. The amplitude transmittance of the Hologram can be expressed as

$t(x) = exp(j\phi)$ for values of $x : mx \leq x \leq (m+1)s$ and for m=1...M

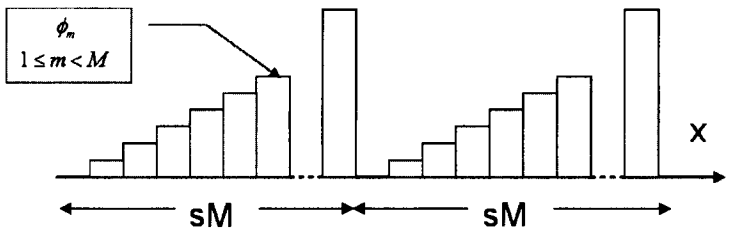

Figure 4.2: A 1 dimensional representation of phase hologram

The diffraction of the phase hologram consists of discrete signals with amplitudes given as:

$$T_l|_{p\to\infty} = \frac{1}{sM}\int_0^{sM} t(x)exp\left(-\frac{j2\pi lx}{sM}\right)dx$$
$$= \frac{1}{sM}\sum_{m=1}^{M}\int_{x=ms}^{(m+1)s} exp(j\phi_m)exp\left(-\frac{j2\pi lx}{sM}\right)dx \quad (4.34)$$

let

$\overline{x} = \frac{x}{s} - m - \frac{1}{2}$ therefore $x = \overline{sx} + ms + \frac{s}{2}$ and $dx = s\overline{dx}$

Hence

$$T_l|_{p\to\infty} = \frac{1}{M}\sum_{m=1}^{M}\int_{-1/2}^{1/2} exp\,(j\phi_m)\,exp\left(-\frac{j\pi l}{M}\right)exp(-\frac{j2\pi lm}{M})exp\left(-\frac{j2\pi l\overline{x}}{M}\right)\overline{dx} \quad (4.35)$$

or

$$T_l|_{p\to\infty} = \frac{1}{M}\sum_{m=1}^{M} exp\,(j\phi_m)\,exp\left(-\frac{j\pi l}{M}\right)exp\left(-\frac{j2\pi lm}{M}\right)\int_{-1/2}^{1/2} exp\left(-\frac{j2\pi l\overline{x}}{M}\right)\overline{dx} \quad (4.36)$$

But

$$\int_{-1/2}^{1/2} exp\left(-\frac{j2\pi l\overline{x}}{M}\right)\overline{dx} = \frac{exp\left(-\frac{j2\pi l\overline{x}}{M}\right)|_{-1/2}^{1/2}}{-\frac{j2\pi l}{M}}$$
$$= \frac{exp\left(\frac{j\pi l}{M}\right) - exp\left(-\frac{j\pi l}{M}\right)}{\frac{j2\pi l}{M}} = \frac{sin\left(\frac{\pi l}{M}\right)}{\frac{\pi l}{M}} \tag{4.37}$$

Hence

$$\int_{-1/2}^{1/2} exp\left(-\frac{j2\pi l\overline{x}}{M}\right)\overline{dx} = \frac{1}{M}\sum_{m=1}^{M} exp(j\phi_m)exp\left(-\frac{j\pi l}{M}\right)exp\left(-\frac{j2\pi lm}{M}\right)sinc\left(\frac{l}{m}\right) \tag{4.38}$$

Where

$sinc(u) = \frac{sin(\pi u)}{\pi u}$

Finally we can write

$$T_l|_{p\to\infty} = \frac{1}{M}sinc\left(\frac{l}{M}\right)exp\left(-\frac{j\pi l}{M}\right)\sum_{m=1}^{M} exp\left[j\left(\phi_m - \frac{2\pi lm}{M}\right)\right] \tag{4.39}$$

The field intensity at each diffraction signal is given by

$$|T_l|^2|_{p\to\infty} = \frac{1}{M^2}sinc^2\left(\frac{l}{M}\right)\left|\sum_{m=1}^{M} exp\left[j\left(\phi_m - \frac{2\pi lm}{M}\right)\right]\right|^2 \tag{4.40}$$

for the special case of $\phi_m = \frac{2\pi m}{M}$

$$|T_l|^2|_{p\to\infty} = \frac{1}{M^2}sinc^2\left(\frac{l}{M}\right)\left|\sum_{m=1}^{M} exp\left[-j\frac{2\pi lm}{M}\right]\right|^2 \tag{4.41}$$

$$|T_l|^2|_{p\to\infty} = \frac{1}{M^2}sinc^2\left(\frac{l}{M}\right)\left|\frac{1 - exp\left[-j2\pi(l-1)\right]}{1 - exp\left[-\frac{j2\pi(l-1)}{M}\right]}\right|^2 \tag{4.42}$$

$$|T_l|^2 |_{p\to\infty} = \frac{1}{M^2} sinc^2\left(\frac{l}{M}\right) \left| \frac{exp\left[j\pi(l-1)\right] - exp\left[-j\pi(l-1)\right]}{exp\left[\frac{j\pi(l-1)}{M}\right] - exp\left[-\frac{j\pi(l-1)}{M}\right]} \right|^2 \tag{4.43}$$

Or

$$|T_l|^2 |_{p\to\infty} = \left[sinc\left(\frac{l}{M}\right)\right]^2 \frac{\left[sin\pi(l-1)\right]^2}{M^2\left[sin\frac{\pi}{M}(l-1)\right]^2} \tag{4.44}$$

But since $sin\pi(l-1)$ is zero for all l, hence $|T_l| \neq 0$ only if l-1 =gM, or l=gM+1 where g is an integer. For these values of l

$$|T_l|^2 |_{p\to\infty} = \left[sinc\left(\frac{l}{M}\right)\right]^2 \tag{4.45}$$

This equation confirms the sinc nature of the results in the replay field.

4.4 Two dimensional Fourier Series analysis

In this case

$$T_{l,k}|_{P,Q\to\infty} = \frac{1}{MN} sinc\left(\frac{l}{M}\right) sinc\left(\frac{k}{N}\right) exp\left(-\frac{j\pi(l+k)}{M}\right) \sum_{m=1}^{M}\sum_{n=1}^{N} exp\left[j\left(\phi_m - \frac{2\pi ml}{M} - \frac{2\pi nl}{N}\right)\right] \tag{4.46}$$

and

$$|T_{l,k}|^2 |_{P,Q\to\infty} = \frac{1}{M^2N^2} sinc^2\left(\frac{l}{M}\right) sinc^2\left(\frac{k}{N}\right) \times \left| \sum_{m=1}^{M}\sum_{n=1}^{N} exp\left[j\left(\phi_m - \frac{2\pi ml}{M} - \frac{2\pi nl}{N}\right)\right] \right|^2 \tag{4.47}$$

For the special case of

$\phi_{mn} = \phi_m + \phi_n$, where $\phi_m = \frac{2\pi m}{M}$ $\phi_n = \frac{2\pi n}{N}$

$$|T_{l,k}|^2 |_{P,Q\to\infty} = \left[sinc\left(\frac{l}{M}\right)\right]^2 \left[sinc\left(\frac{k}{N}\right)\right]^2 \tag{4.48}$$

for values of l=gM+1, k=hN+1 where both h and g are integers.

As in the one dimensional case, the effect of the sinc function can be seen as the main influence in determining the final efficiency.

4.5 Analysis for the general case of finite P and Q

In this case we will consider the realistic situation in which there are a finite number of pixels associated with our phase holograms. In this situation we can express the transmittance as

$$t(x,y) = t(x,y)|_{P,Q\to\infty} \times rect\left(\frac{x}{sMP}\right) rect\left(\frac{y}{sNQ}\right) \tag{4.49}$$

and

$$T_{l,k} = T_{l,k}|_{P,Q\to\infty} \otimes s^2 MNPQsinc(sMPf_x)sinc(sNQf_y) \tag{4.50}$$

When P and Q are sufficiently large, the spacing of the diffracted signals can be assumed to be much larger than the width of the first lobe of both sinc functions. In this case we can assume that the compressed two-dimensional sinc function is in the form of $s^2 MNPQsinc(sMPf_x)sinc(xNQf_y)$ and is replicated at every diffraction order.

Hence the energy integrated over the spot in the (l,k) diffraction order is approximately

$$E_{l,k} = |T_{l,k}|^2 \,|_{P,Q\to\infty} \int_{-\infty}^{\infty} s^4 M^2 N^2 P^2 Q^2 sinc^2(sMPf_x) sinc^2(sNQf_y) df_x df_y$$
$$= s^2 MNPQ \times |T_{l,k}|^2 \,|_{P,Q\to\infty} \quad (4.51)$$

Where we have used the relation

$\int_{-\infty}^{\infty} sinc^2 u du = 1$

Hence finally

$$E_{l,k} = \frac{s^2 PQ}{MN} sinc^2\left(\frac{l}{M}\right) sinc^2\left(\frac{k}{N}\right) \left|\sum_{m=1}^{M}\sum_{n=1}^{N} exp\left[j\left(\phi_{mn} - \frac{2\pi ml}{M} - \frac{2\pi nk}{N}\right)\right]\right|^2 \quad (4.52)$$

Giving the efficiency as

$$\eta_{l,k} = \frac{1}{M^2 N^2} sinc^2\left(\frac{l}{M}\right) sinc^2\left(\frac{k}{N}\right) \left|\sum_{m=1}^{M}\sum_{n=1}^{N} exp\left[j\left(\phi_{mn} - \frac{2\pi ml}{M} - \frac{2\pi nk}{N}\right)\right]\right|^2 \quad (4.53)$$

For the special case of $\phi_m = \frac{2\pi m}{M}$, $\phi_n = \frac{2\pi n}{N}$

$$E_{l,k} == s^2 PQMN \left[sinc\left(\frac{l}{M}\right)\right]^2 \left[sinc\left(\frac{k}{N}\right)\right]^2 \quad (4.54)$$

and

$$\eta_{l,k} = \left[sinc\left(\frac{l}{M}\right)\right]^2 \left[sinc\left(\frac{k}{N}\right)\right]^2 \quad (4.55)$$

Figure 4.3 graphically illustrates the result of using our derived expression and a commonly used expression (please refer to section 4.8 for more details on this expression.) used in case of a phase hologram with 4 phase levels and containing upto 128 pixels. As can be seen there is a close match between the two expressions. The above calculations were performed

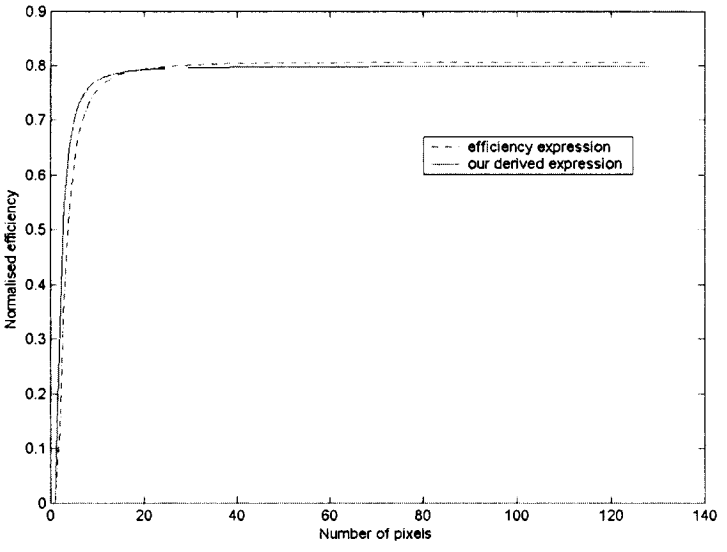

Figure 4.3: Efficiency versus number of pixels

to provide a detailed Fourier based analysis of 2D phase holograms and compare/confirm the results with those obtained by Dammann [72].

4.6 Generation of phase holograms

In the paraxial region (an area in close proximity of the optical axis), the relationship between the phase hologram and its replay field can be described using a scaled Fourier Transform [70].

This means that the hologram can be approximated as the inverse Fourier Transform of its image in the far field. However straight transform of the image only retains amplitude. When Fourier Transform is performed it acts on the intensity which is square of the amplitude. Squaring the complex function in turn drops the phase terms but as we mentioned before we are interested in the phase information. Several methods have been devised to generate transforms which hold the phase information.

Various methods can be used to design and optimise holograms for beam steering purposes [73–83]. Historically majority of these approaches have been iterative and due to

their non-deterministic nature very expensive computationally. Furthermore with these methods as the replay field is typically sampled at the same resolution as that of hologram display device the available resolution will inherently be limited [84]. The last point but just as noteworthy about these approaches is the lack of predictability associated with noise distribution in the replay. This in turn will make the process of optimisation more complex and less optimum. In this section we describe a predictive method for generation of phase hologram as proposed by Tan et al. [85,86] and leave the details associated with some of traditional approaches to the section on algorithms.

Assuming that the locations and relative intensities of diffraction orders within the replay field are entirely caused by phase quantisation and the distribution of these phase elements within a base hologram [85,86], it is possible to design these holograms in a more controlled and predictable manner.

One approach to generate phase holograms is to first generate an array of phase elements using the total number of pixels and the coordinates for the location of the desired first order in the 2D plane of the replay field. These phase elements are then quantised using the total number of phase levels available. Finally, following a Fourier Transform operation the replay field associated with the designed hologram is produced.

Using the above method it is possible to produce phase holograms which will route to desired spots within the replay field. However in order to produce holograms with an efficiency approximately matching the theoretical expectation, optimisation algorithms such as simulated annealing are used. An example of a replay field for a four phase hologram generated using the above mentioned method can be seen in figure 4.4 below. However other orders also appear in the replay field as can be seen in figure 4.5. Depending on the setup of the system, these orders can be a source of crosstalk. One way to reduce the interference from these orders is to introduce a small amount of noise when generating the phase elements. Using this method, after the Fourier Transform operation, there are fewer peaks beside the first order in the replay field and the power associated with those

present is more diffused.

Results of simulations have indicated a two-fold reduction in the noise level whilst paying a small penalty. This trade-off is approximately 10% reduction in the amount of power channeled to desired location.

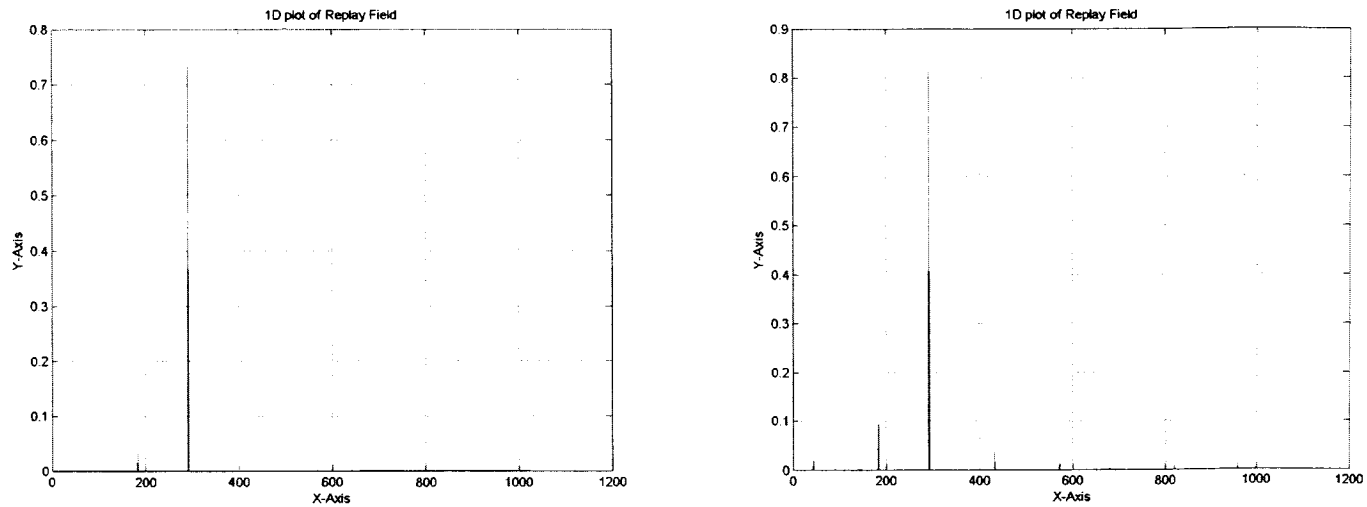

(a) 1D replay field for a hologram generated with scaled noise

(b) 1D replay field for a hologram

Figure 4.4: 1D replay fields with (a) and without (b) use of scaled noise

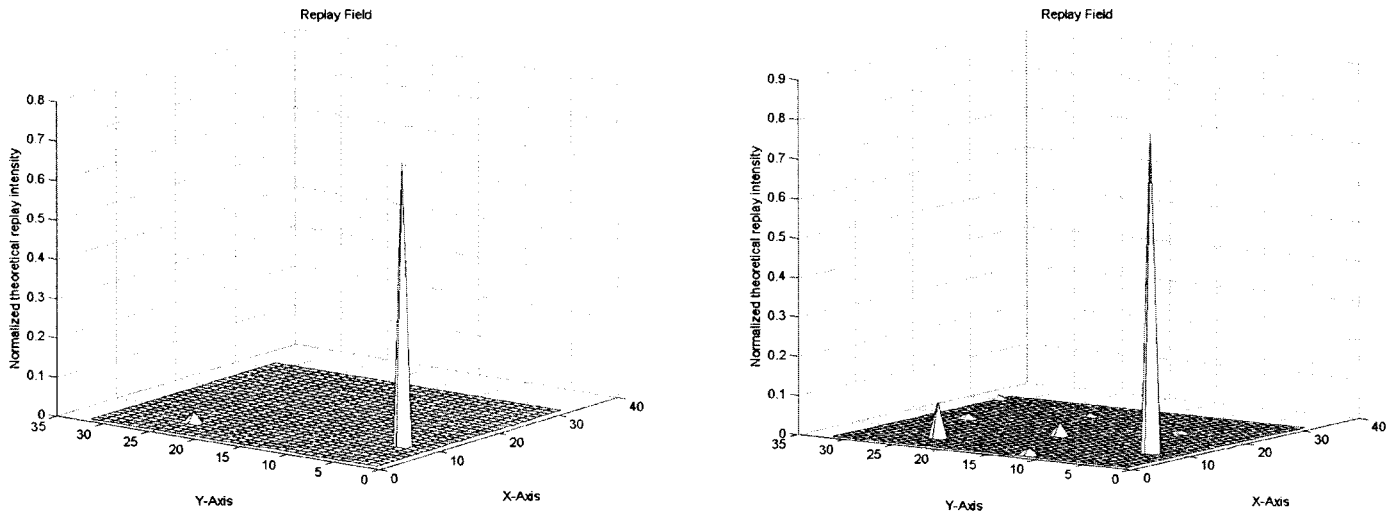

(a) 2D replay field for a hologram generated with scaled noise

(b) 2D replay field for a hologram

Figure 4.5: 2D replay fields with (a) and without (b) use of scaled noise

4.7 Spectral bandwidth

One of challenges for devices used in a DWDM system is wavelength sensitivity. In case of free space beam steering holographic routers it would be important to measure the influence of wavelength variation on the steering angle.

The angle to which light of a different wavelength than the designed wavelength is steered is given (for small angles) by [87]:

$$\theta_\lambda = \theta_0 \frac{\lambda}{\lambda_0} \tag{4.56}$$

where, θ_λ is the steered angle for wavelength λ and θ_0 is the steered angle for the designed wavelength λ_0.

This equation can be rewritten to specify the spectral bandwidth that will allow a desired angular spread in the following manner:

$$\Delta\lambda = \frac{\Delta\theta_\lambda}{\Theta_0}\lambda_0 \tag{4.57}$$

Above equation can be used to estimate the influence of wavelength variation on the deflection angle of the diffractive element.

If we assume a 100 nm bandwidth stretching from 1520 nm to 1620 nm then using the above equation we find that this range of bandwidth will have just over 6% influence on the angular spread. Therefore for say a maximum steering angle of 2^o we can expect 0.127^o of variation as the wavelength changes over the specified range mentioned above. This value appears to be very small and therefore further analysis would be required to actually quantise the impact of this small variation. However some flexibility for maneuvering of the beam of light exists if the surface of the Opto-VLSI processor is furnished with large number of small pixels. In this case it is reasonable to assume that by adjustments made

to the holograms it is possible to counteract majority of undesired effects.

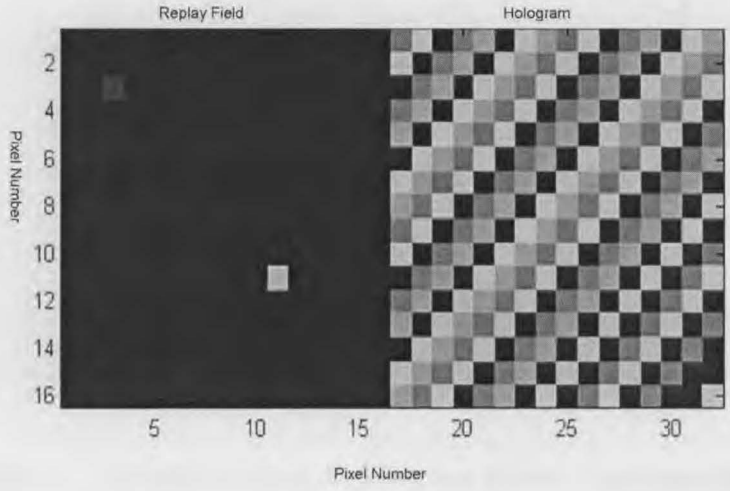

Figure 4.6: A sample hologram and its replay field

Figure 4.6 shows a sample hologram pattern and its replay field. The red dot represents the first order diffraction and the yellow dot an undesired diffraction order. Figure 4.7 shows the replay field for the same hologram.

In order to maximise the diffraction efficiency while minimising noise contributions from unwanted orders various methods can be applied. As was mentioned a simple approach may be to introduce a random noise level before the quantisation process. In some cases this can lead to results comparable to using such optimisation algorithms as simulated annealing [78]. Another approach that requires further investigation, seeks to enhance the previous approach by utilising a shaped noise spectrum. Other possible techniques could be based on error diffusion optimisation where attempt is made to diffuse the energy associated with the noise elements over a region in the replay and thereby minimise the level of noise contribution.

The following figures show some results obtained from analysing the effectiveness of use of random noise for optimisation of the holograms. From these graphs it can be seem that as

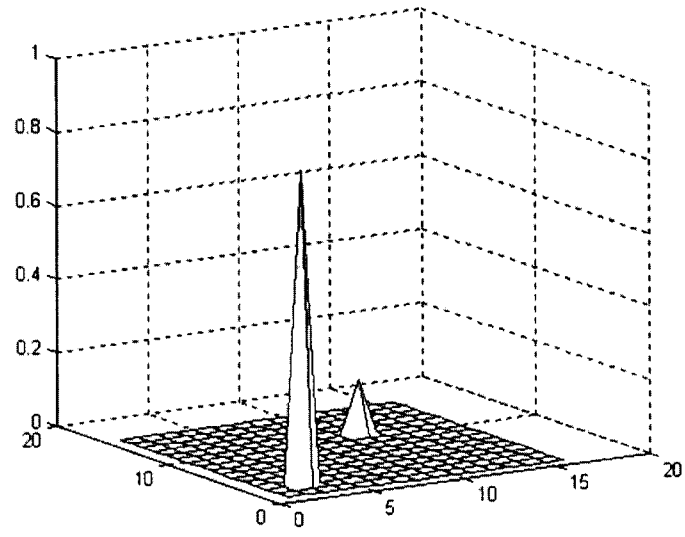

Figure 4.7: 2D replay field of the hologram shown in previous figure

the noise weight is increased there is some reduction in the amount of noise contributing to crosstalk. However at the same time some loss in the optical efficiency of the first diffraction order is also noticed. It is very unlikely that any method could be found to reduce the crosstalk with no degradation in the efficiency. However the challenge remains to find a method of optimisation that offers the least impact on the efficiency whilst reducing crosstalk.

4.8 Effect of number of pixels on crosstalk and power efficiency

In an attempt to investigate the effect of number of pixels on cross-talk and power efficiency a simulation was setup and performed. Below is a brief explanation about the workings of this simulation and the results obtained.

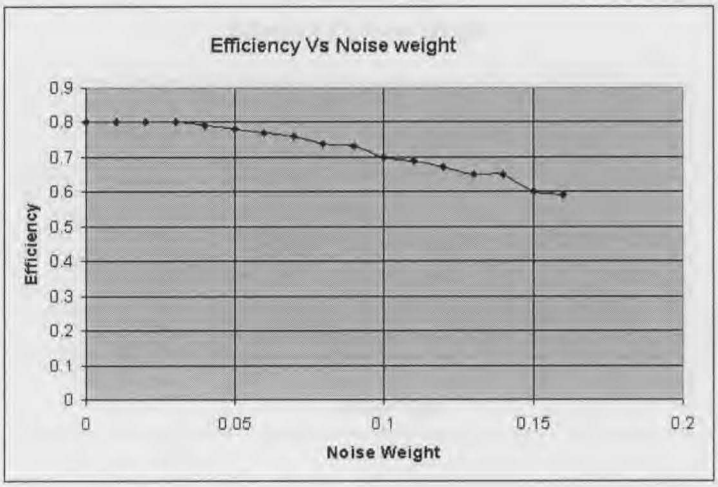

Figure 4.8: Influence of noise weight on efficiency

Based on simulated annealing algorithm a program was developed and was used to generate holograms of various sizes. Different holograms and their relevant replay field covering all the possible fiber arrays were tested. Results were then tabulated and compared. It was noted that as the number of pixels increase there is a drop in the worst cross-talk measured while an increase in minimum power efficiency is observed. In case of cross-talk a steady decrease was noted from a 16 pixel hologram to one containing 100 pixels. From there on the results obtained indicate a plateau behavior as can be seen from figures 4.11 and 4.12.

Similar findings were observed in case of power efficiency. There appears to be a steady increase in minimum power efficiency from a hologram of size 16 to one containing 36 pixels. From there onwards however an almost flat display is noted.

Findings associated with optical power efficiency from above are in agreement with results obtained from the expression proposed by K.L. Tan for measuring the efficiency of a 2-D grating [85, 86]. This expression which is a modification of Dammann's [72] efficiency expression is as follows:

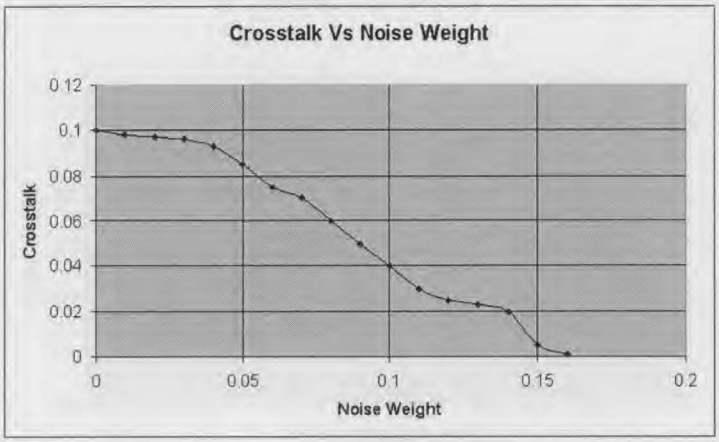

Figure 4.9: Influence of noise weight on crosstalk

$$\eta = \frac{sinc^2\left(\frac{n\pi}{m}\right)}{sinc^2\left(\frac{n\pi}{x_0 y_0}\right)} \tag{4.58}$$

where,

η = optical power efficiency

n = order number

m = number of phase levels

$x_0 y_0$ = number of pixels

Using the above expression for a 4 phase level hologram we can see that once the fundamental limit of efficiency is reached (in this case 81%) very little change is noticed as a result of addition of more pixels. It is worth noting however that this is the ideal case where influence of factors such as pixelation, dead space and phase errors are not considered.

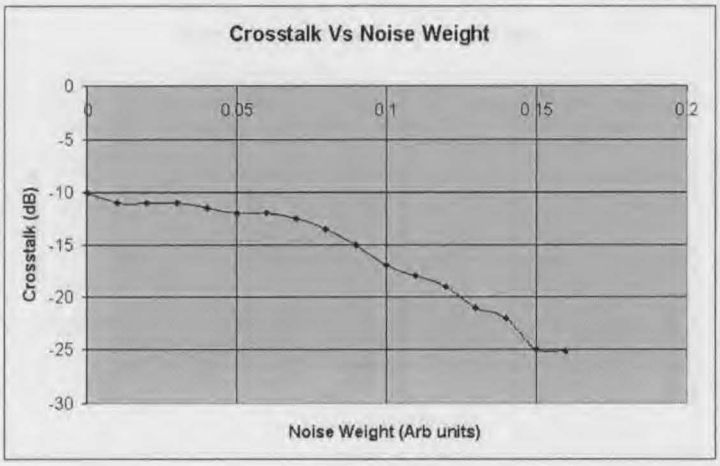

Figure 4.10: Effect of variation of noise weight on crosstalk

4.9 Transient effects associated with switching of holograms

The process of switching a coherent optical beam incident on the surface of an Opto-VLSI processor from one location to another entails reconfiguration of the beam steering element (a computer generated hologram). This process has some similarity to the scrolling technique used to ensure that FLC based processors are DC balanced (refer to appendix A for details). A CGH out of a pre-configured pool could be selected, loaded and further tuned for delivery of maximum amount of intensity for the designated output location. Alternatively a CGH can be calculated in real-time based on necessary information which would include the desired input and output locations. In either case there will be a reconfiguration period while the old CGH is replaced by the new one. As part of this research, we investigated results of possible transient effects experienced by the replay field during this transitory period.

A version of Simulated annealing algorithm was used to generate the holograms. Each hologram was then replaced by a new one gradually and the impact on the replay field was monitored. In this section we will attempt to explain the procedure in its entirety.

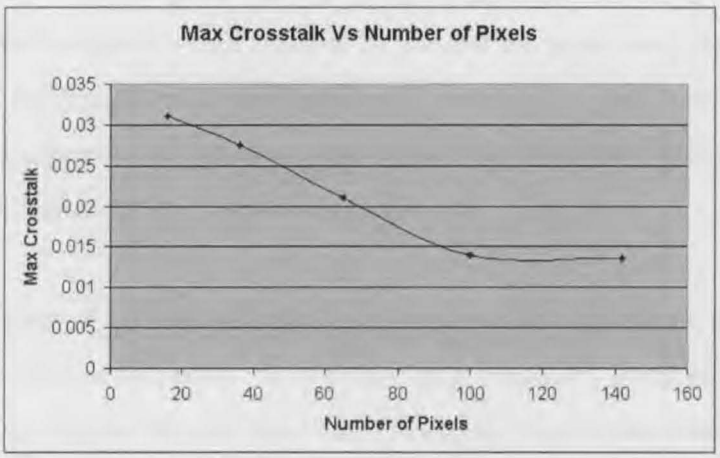

Figure 4.11: Relationship between crosstalk and number of pixels

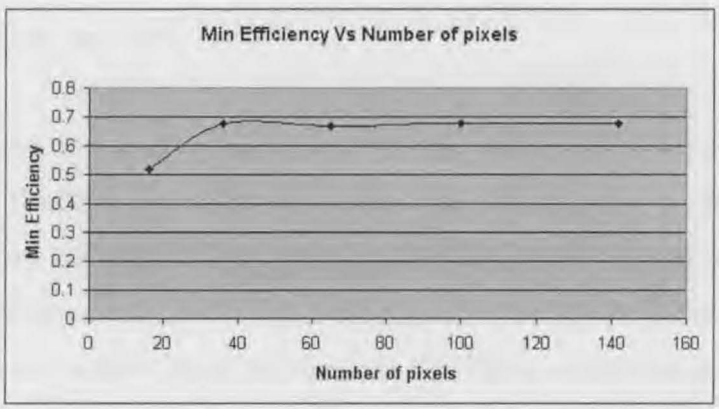

Figure 4.12: Influence of number of pixels on efficiency

The first section of the designed script contains the core of the simulated annealing algorithm used to calculate holograms for steering of light into a given output port. The second section is where one hologram pattern is replaced by another and the replay field is plotted.

The code is originally run once to obtain a hologram that is represented by an array of 32×32 elements. This hologram is used to steer the incoming light into the specified output port. It is worth noting that the first time the code is run it will not contain the section that attempts to replace one hologram by another. A different output port is then specified and the code is executed again. This time however we convert both holograms

(32×32 arrays) into vectors to make the process of replacing one with another more efficient. The second hologram is then replaced by the first hologram one pixels at a time. In general a small number of pixels should be changed at any one time in order to minimise the effect of this operation on the replay field. After each change the replay field produced from the new hologram can be plotted and inspected.

Normally a process of replication is used to strengthen the hologram against possible failure of small number of pixels. In this case each replicated hologram consists of 16 replications of an original 32×32 pixel-based hologram in order to makeup the desired 128×128 resolution as shown in figure 4.20. Due to this replication different schemes were tested in changing the entire hologram to investigate the effects. All of the approaches tested produced very similar results. Therefore for ease of implementation a sequential replacement regime was used.

The results where compared by looking at the replay fields before and after the change and comparing the differences. Figures 4.13,4.14,4.15 and 4.16 show the results obtained. Figure 4.13 shows the intensity plot of the replay field at the begining of the switching process. The hologram used in this case was designed as an 8 phase hologram to generate a single peak in the output. As can be seen from this figure a large percentage of intensity of light is channeled to one particular spot with some unwated spots present in the rest of the replay field.

Figure 4.14 shows the replay field obtained after some of the original hologram has been replaced by the new hologram. As can be seen intensity in the original spot has been reduced by a small amount whilst at the same time more intensity is appearing at the second spot in the replay field where the second hologram is designed for.

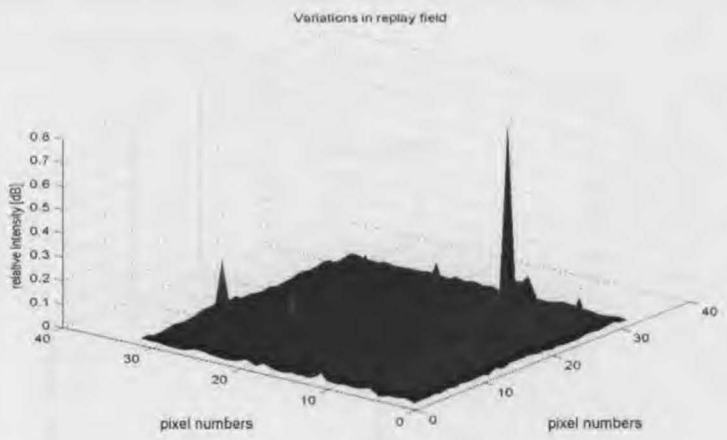

Figure 4.13: Distribution of intensity in replay field - first position

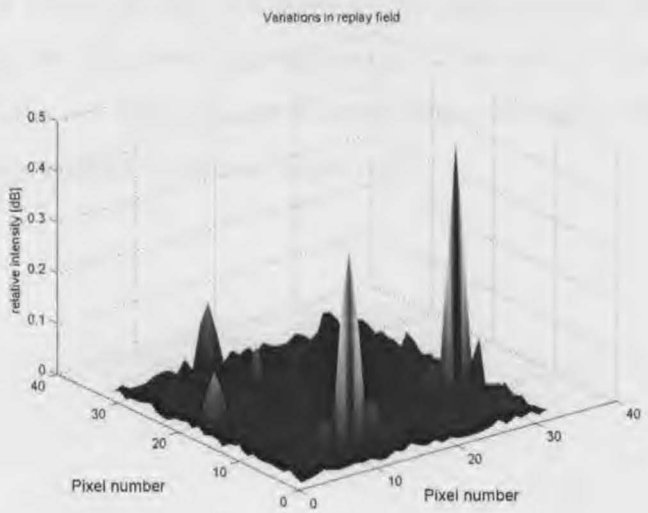

Figure 4.14: Distribution of intensity in replay field - second position

Figure 4.15 shows the replay field after more of the original hologram is replaced by the new hologram. It can be seen that as more of the second hologram replaces the first hologram gradually intensity at the original spot is diminishing and it is being more and more channeled to the second spot.

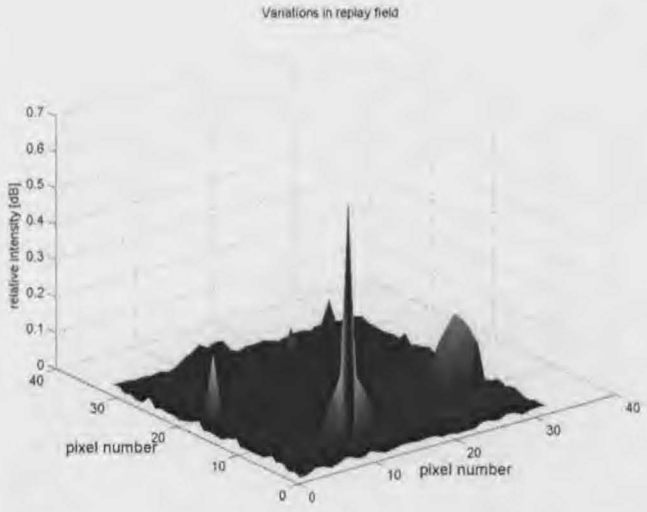

Figure 4.15: Distribution of intensity in replay field - third position

Finally figure 4.16 shows the end of switching from one hologram to another. In this case we can clearly see that now a large percentage of intensity is appearing at the new location for which the new hologram was designed whist once again only a small amount of unwated intensity appears across the replay field.

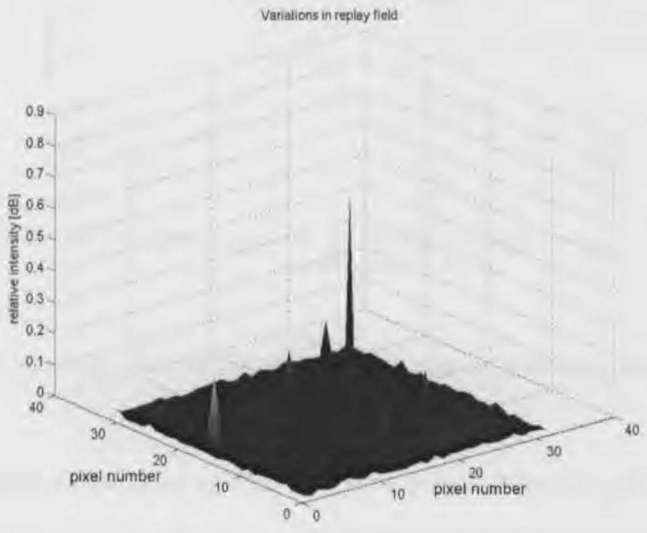

Figure 4.16: Distribution of intensity in replay field - fourth position

Figure 4.17 represents the maximum intesity as it is reduced from one spot and increased at the second location where the light is being channeled using the new hologram. It is worth noting that at about the half way point where about 50% of each hologram is contributing to the steering of the input beam, both locations are receiving approximately equal amount of intensity from the input beam even though this amount is much reduced from the original levels.

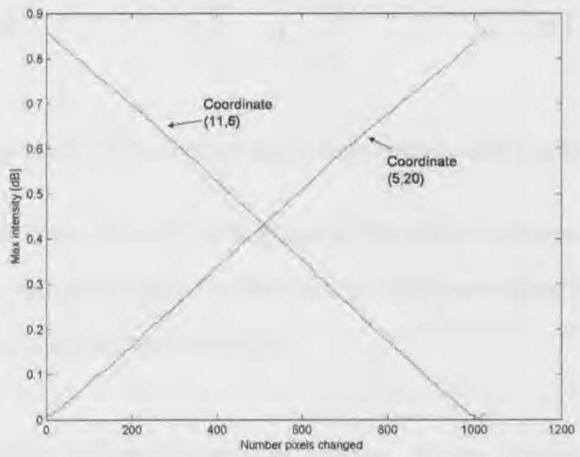

Figure 4.17: Light intensity decreasing at one port and increases at another as the hologram is switched

The impact of transient effects associated with switching a coherent optical beam from one output port to another were investigated. Two holograms were generated using Simulated annealing algorithm and simulation were conducted to emulate the process of switching. The results indicate that the transition period is quite smooth with minimal to no impact on other ports.

4.10 Algorithms

There exists a vast array of problems that due to their complexity can not be solved analytically. When analytical methods fail or if they are not practical, an iterative approach can be used. The problem of synthesising a Fourier transform pair which has desirable properties in both domains is an example of this type of problems. The Error reduction approach a block diagram of which is shown below is one of the approaches for solving this

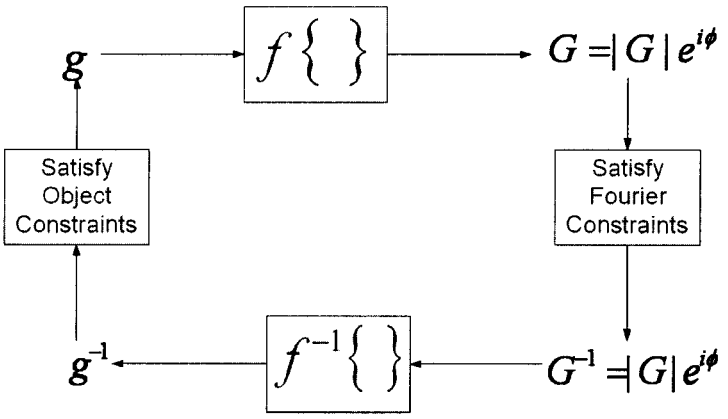

Figure 4.18: Block diagram of error-reduction approach

problem. Gerchberg-Saxton algorithm belongs to the error-reduction class and is one of the algorithms which was investigated in this study. The generalised projection algorithms also follow a somewhat similar approach [88].

The working of this class of algorithms is as follows: given a function represented by an amplitude and phase, one transforms back and forth between the two domains forcing the function to satisfy the constraints in each domain. The first iteration can start in different ways, for example by setting the phase equal to an array of random numbers. The iterations then continues until a Fourier transform pair is found that satisfies all constraints in both domains. A measure of the progress of the iterations and a criterion by which one can determine when a solution has been found is the mean-squared-error.

Genetic algorithms are motivated by the Darwinian principle of "survival of the fittest" [89]. In a typical genetic algorithm members of the next generation are selected based on a probability proportional to their fitness. The expectation is that this process will eventually converge to yield a population dominated with the global maximum of fitness function. The Algorithm typically starts with a pool of randomly generated arrays. It then evaluates the cost function (based on the mean square error) associated with each of these and discards those with worst cost value. It then randomly takes two of the arrays out of the remaining pool and uses them as parents. An offspring is created by randomly

mixing the values from each parent. This offspring is then randomly altered (mutated) and a new cost function is evaluated. The above steps are repeated until no further improvements in the cost function can be detected. Another way to think of it is that the aim of the design is to produce a desired target function $\acute{g}$ at the output plane. The cost function which is a measure of the fitness of the final result can be define as:

$$C = \left\{ |g|^2 - |\acute{g}|^2 \right\} \tag{4.59}$$

Where g is the calculated output and $\acute{g}$ is the desired target function as mentioned above. The aim of optimisation is to minimise the cost function and get as close as possible to the desired target.

Different schemes could be used for the mutation and crossover process and it may be worthwhile to investigate few different possibilities in this area. For instance a straight method of breeding would entail splitting the parents at random points and then splicing them to obtain the offspring. However as *Kirk et al* have reported [90] alternative methods could be used in order to utilise the whole area of parents. Alternative approaches could also be applied to the mutation process. For instance mutations could be random changes each time and for a binary case this would be changing a 1 to -1 or vice versa. Alternatively they can be done based on a probability. As reported by Yang [91] the mutation probability could be set to

$$p = p_0 \left(\frac{1}{k} \right)^r \tag{4.60}$$

Where r and p_0 are parameters which depend on the particular problem and k is the number of iterations. The number of bits to be mutated is determined by mutation probability multiplied by size of the object function:

$$N_{mutation} = P \times N \tag{4.61}$$

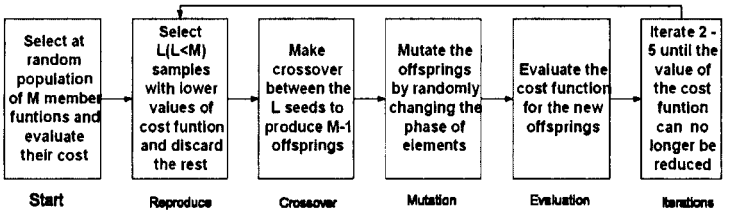

Figure 4.19: Block diagram of a Genetic Algorithm

In practice the bit to be mutated is also chosen randomly. Figure 4.19 shows the above procedure schematically.

Simulated annealing which is an algorithm used in solving many optimisation problems is the third class of approaches which were investigated as a possible candidate for hologram generation [92]. Application of the simulated annealing algorithms to generation of computer generated phase holograms can be considered as an extension to the Direct Binary Search algorithm approach [78]. In the direct binary search we start from a set of pixels representing the initial phase hologram. The process starts by randomly choosing a pixel and flipping its value. In the case of binary phase hologram there are only two possible values to choose from for each pixel. A cost function is normally used to measure the progress of the approach. In this case the mean-squared-error between a desired wavefront and that generated by the present hologram is used as the cost function. If after flipping the value of the pixel the cost function is reduced this value is accepted otherwise the previous value is reassigned. This methods continues until every single pixel is checked at the end of which we should have a hologram which is more optimised than that we started with. The problem with this technique however is that it can produce solutions which fall in the possible sets of local minima. This is particularly relevant as phase holograms are reasonably complex structures with many possible variations. This in turn means that the probability of falling into a local minimum when performing simple search methods such as direct binary search is quite high. The simulated annealing algorithm attempts to overcome this problem by introducing a probabilistic element in its approach to assess

the newly formed hologram at each stage. Over the years this techniques has been used by many researchers investigating applications of computer generated holograms [93–95]. Simulated annealing starts with a similar initialisation step. The value of each pixel is then changed as before and a check is made to see if the mean-squared-error has reduced. If the error has not decreased due to the latest change in pixel value, the algorithms attempts to determine the probability of accepting this change despite the undesired result obtained from the mean-squared-error. Statistically this probability can be written as

$$p = exp[-\Delta E/kT] \tag{4.62}$$

Where p is the probability of change in pixel value being accepted, ΔE is the energy difference between the initial and final states, k is the Boltzmann constant and T is the temperature at which the process takes place. In the context of generating phase holograms, ΔE can be used as the difference in the error function or the mean-squared-error. k can be set to 1 and T is a parameter governing the rate at which changes are accepted. The introduction of a probability of acceptance allows the system to escape from local minima in high temperatures but as T is reduced this probability drops and it may be expected to be zero at the termination of the algorithm. Generally the rate at which T changes should follow a logarithmic scale in relation with number of iterations. However this is very slow and therefore the rate of change can be set to change with the inverse of the iteration [93]. Generally there are two criteria which determine whether the algorithm should end or another iteration should commence. These are that (i)the mean-squared-error becomes zero or (ii) The temperature drops down to zero. Practically none of these condition could be fully satisfied and that is the reason for introducing more realistic limits for both. Basically control values are used to assess how close to an acceptable level the two aforementioned criteria have reached and this will then form the basis for termination or continuation of the process.

Both Gerchberg-Saxton and Genetic algorithm codes were developed in MATLAB, and various variables were modified until a reasonable performance was obtained from each

algorithm. Compared to the Simulated Annealing program, Gerchberg-Saxton was found to be a very fast algorithm, however the holograms generated were not of very good quality, that is the replay field was not highly optimised for power efficiency or crosstalk. On the other hand, Genetic algorithms were very slow to arrive at a solution, however, they gave much better results than Gerchberg-Saxton. If the algorithms are to be mapped into silicon, both algorithms will need to be investigated further. The results obtained indicate that genetic algorithm may be useful in generating diverse and robust results, since there will be a population of good holograms to choose from for a desired target performance.

Two samples of a hologram and its replay field are shown in figure 4.20. The first figure represents a 32×32 pixel-based hologram. The second figure shows the same hologram replicated 16 times in order to produce the desired resolution of 128×128 pixels. Both of these were generated using the Simulated Annealing approach.

There are many issues that need to be considered in selecting an appropriate method for hologram design. The approach chosen should produce holograms that are efficient. This means that they should steer a very high percentage of incoming light to the desired output port. Most of the results presented here are based on binary phase holograms that can only deliver around 40% efficiency. However multiphase holograms can deliver efficiencies greater than 80%. Two of the measures which have been used in assessing the quality of a hologram are power-loss and cross-talk. Preliminary simulations using binary phase holograms have yielded cross-talk and power loss figures better than 20 and 40 dB respectively. In addition to using multiphase holograms, other approaches to enhance the quality of replay field produced by the holograms should be considered. One factor that should be investigated is the effect of dead space on the replay field. O'Brien et al reported [96] that the fill factor or the controllable pixels covering the surface of the hologram should be as large as possible in order to minimise the amount of uncontrollable dead space on the hologram. With finer fabrication VLSI processes currently available an arrangement can be forseen where the surface of the Opto-VLSI processor is covered with large number of small pixels. In this setup there will be a reduction in the space between pixel arrays and

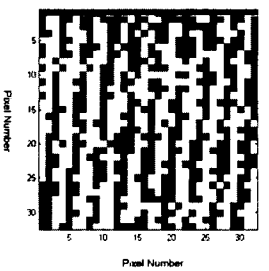

(a) a 32x32 hologram.

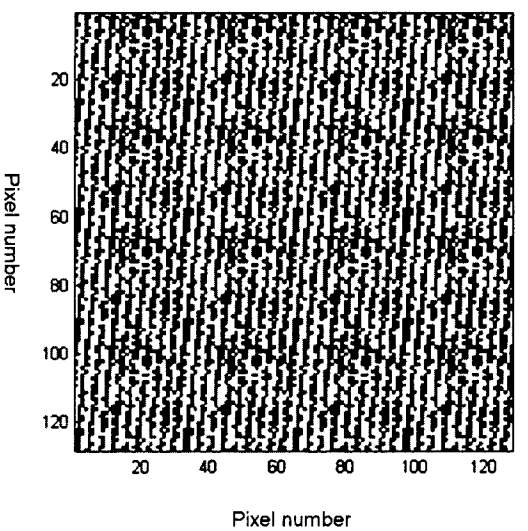

(b) a 128x128 replicated hologram.

Figure 4.20: A 32×32 Hologram and its 128×128 replicated version

this should help to reduce the uncertainty associated with reflections from these areas. Under this scheme what used to be dead-space becomes pixellated areas which could be covered with fixed pattern holograms that push the unwanted light well out of the region containing output ports.

Another aspect of hologram design that needs to be investigated is mappability into the intelligent back-plane. Issues involved in translating various aspects of the algorithm into VHDL (a Hardware Description Language) will be an important part of these investigations.

4.11 Summary

In this chapter we have presented the results of analysis of phase holograms using one and two dimensional Fourier series. We have also presented an expression for the efficiency of phase holograms based on a two dimensional model and taking into consideration the finite number of pixels as well as the phase and spatial quantisation involved in the generation and application of the phase hologram via an Opto-VLSI processor. Furthermore we have presented the results of simulations conducted to investigate the impact of replacing one phase hologram by another as would be the case in many beam-processing applications. We have also shown the results of simulations on the relationship between the number of pixels and the crosstalk as well as power efficiency of a phase hologram. Finally we have examined at some length various methods for generation of phase holograms including some of more commonly used algorithms such as simulated annealing and genetic algorithms and drawn some conclusion about the effectiveness of each method by comparing the results.

In the following chapter we will present our experimental results for the tunable optical filter and dynamic WDM equaliser. We will present the architecture for our device in each case and inspect in detail the experimental results for each individual experiment.

Chapter 5

Tunable optical filtering and equalisation using Opto-VLSI processors

5.1 Basic filter structure

The function of an optical filter is to distinguish one or more optical wavelengths and either pass or reject these. Optical filters may be based on interference, diffraction or absorption effects and could be either fixed or tunable in the way they operate. In this research we are interested in investigating architectures which are based on Opto-VLSI processors and that could be used for tunable optical filtering. Basic requirements for a tunable optical filter are a tuning range of greater than 30 nm, bandwidth of less than 2 nm and uniform loss versus wavelength. Some of the other desirable features of a tunable optical filter are simple control mechanism, small size and low cost. The structure of a basic tunable optical filter is shown in Figure 5.1.

In the following section we will expand on details associated with the experiments we performed to investigate the feasibility of a tunable optical filter based on MicroPhotonic technology.

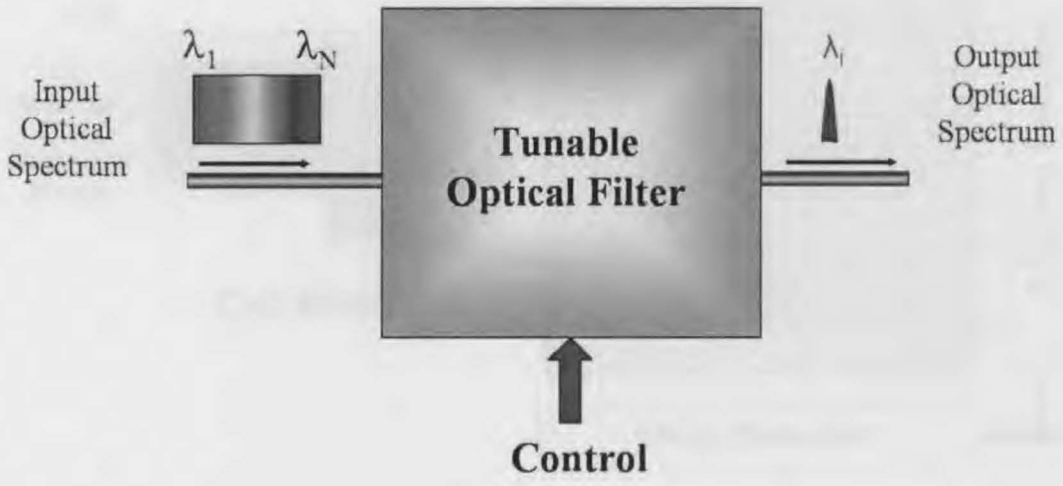

Figure 5.1: Basic tunable optical filter

5.2 Tunable Optical filtering using Opto-VLSI processors

The key element of the tunable optical filter is an Opto-VLSI processor, whose typical layout is shown in Figure 5.2. It consists of an array of liquid crystal (LC) pixels independently addressed by a Very-Large-Scale-Integrated (VLSI) circuit to generate reconfigurable, reflective multiphase holograms capable of steering and/or shaping an optical beam incident on its surface [97].

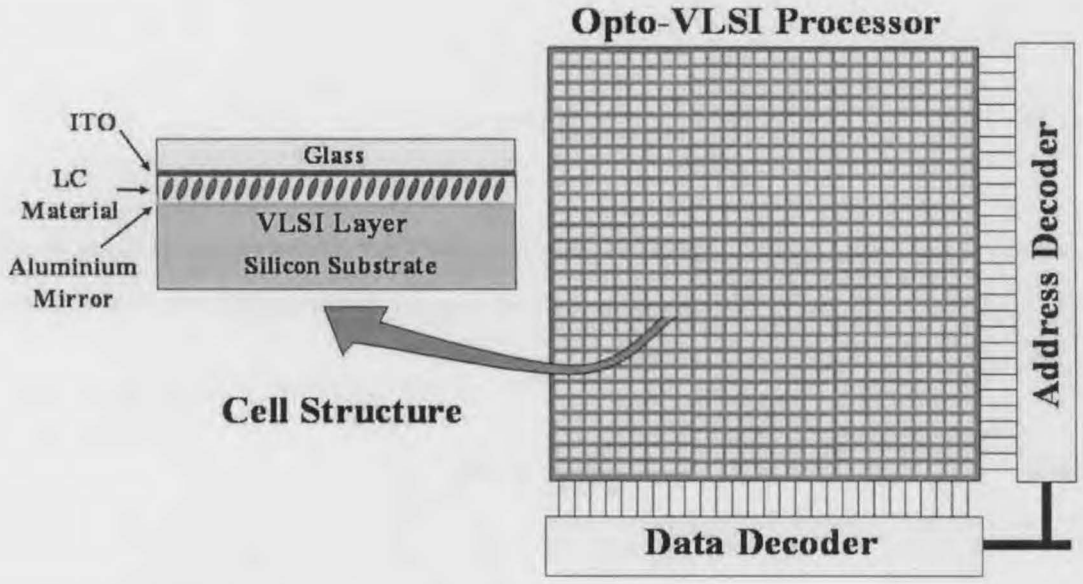

Figure 5.2: A schematic representation of an OptoVLSI processor

The inherent polarisation independence associated with a spatial light modulator using Ferroelectric liquid crystal has already been shown [65]. By incorporating a thin quarter-wave-plate (QWP) layer between the LC and the VLSI backplane, a polarisation-insensitive Opto-VLSI processor can be realised, allowing optical beam steering with low polarisation-dependent loss [66]. In case of a nematic liquid crystal, analogue operation is possible and therefore multiphase phase holograms can be used to enhance the power efficiency. The maximum 1^{st} order diffraction efficiency of an M-phase Opto-VLSI processor operating in a steering mode is given by [98]

$$\eta = sinc^2\left(\frac{\pi}{M}\right) \tag{5.1}$$

For a small incidence angle, the maximum steering range of the Opto-VLSI processor, within which the diffraction efficiency is maximum, is given by

$$\Delta\Theta = \frac{\lambda}{M \times d} \tag{5.2}$$

where d is the pixel pitch, and λ is the wavelength.

5.3 Multiband tunable optical filter

The basic structure of the multiband tunable optical filter is shown in Figure 5.3. It comprises an optical circulator, a fibre collimator, a high-dispersion polarisation-insensitive diffraction grating plate, and an Opto-VLSI processor. The input optical signal is routed, via the optical circulator, to a fibre collimator, and converted into free-space collimated Gaussian optical beam. The high-dispersion diffraction grating plate separates the wavelength components of the free-space optical beam along different directions and maps them onto non-overlapped pixel blocks, as shown in figure 5.3. Each $m \times n$ pixel block is used to generate a multiphase hologram, which either reflects its incident wavelength

component back along the incidence path thus coupling it into the fibre collimator with minimum attenuation or steers the wavelength component so that its power is not coupled back into the fibre collimator, leading to high optical attenuation for that wavelength component. Hence by generating N non-overlapped phase holograms an N-band optical filter is realised. By selecting holograms which provide the required steering and adjusting the hologram position filter passbands can independently be tuned over a wavelength span which is limited by the size of the Opto-VLSI active area and the maximum allowed crosstalk.

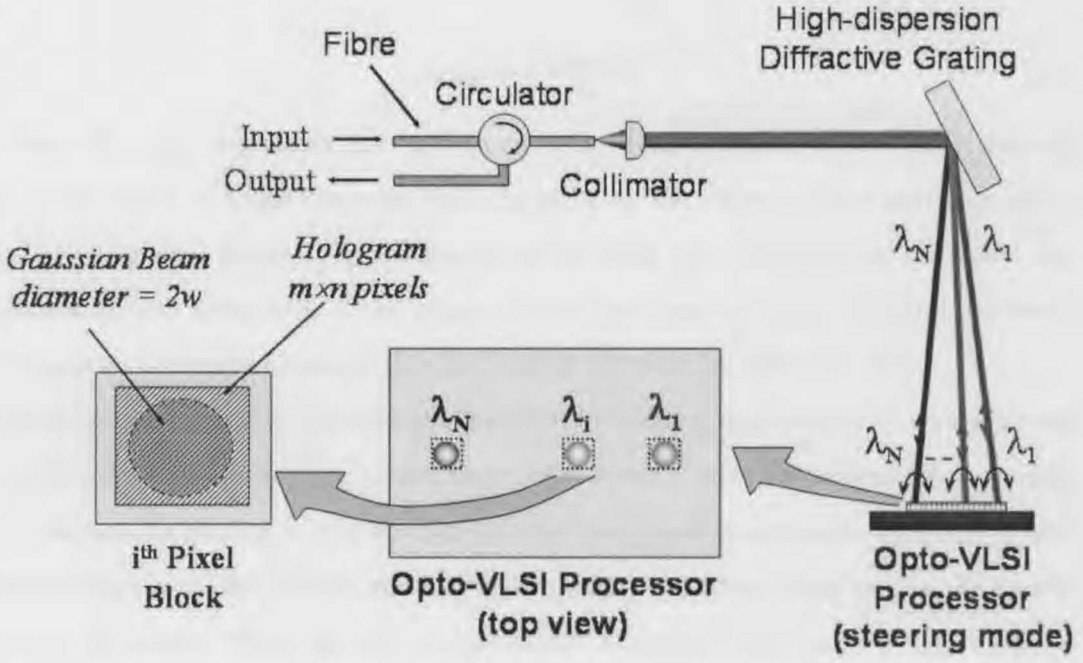

Figure 5.3: Experimental setup for multiband tunable filter

5.4 Theoretical analysis for filtering and equalisation

In this section we will provide some of the theoretical analysis which we have conducted to evaluate the feasibility of an Opto-VLSI processor for filtering and equalisation applications.

5.4.1 Calculation of number of channels and their separation

The total number of channels which can be simultanously equalised or filtered by the processor is determined by taking into consideration the size of the Gaussian beam incident on the surface of the processor and the total active area of this device. Therefore we can write:

$$c_{total} \approx \frac{D_{processor}}{\gamma w} \tag{5.3}$$

Where $D_{processor}$ represents the total active area of the processor in one dimension and w is the width of single Gaussian beam incident on the surface of the processor and γ is the windowing factor. The windowing factor takes into consideration the power loss associated with truncation of the infinite tails of the Gaussian beam by the finite size of holograms. One approximation for this factor is provided by Tan el al. [85].

Before we can determine the minimum distance by which channels will have to be separated by on the processor we have to consider a few points. After the collimated beam falls on the passive grating it will be split into its constituent wavelength components each representing a WDM channel and directed to different physical locations on the surface of the processor. With the use of appropriate hologram each beam is then made to return along its direction of incidence. Using this approach we can then attenuate all or part of each individual beam thereby providing the necessary capability for filtering and equalisation of any given channel. In order to proceed with the calculations we assume that the central beam from the grating is a normal incidence on the processor. Furthermore as was described previously beams need to be a distance of γw apart in order to avoid the overlapping of Gaussian beams onto the wrong hologram as illustrated in figure 5.4. Therefore we can write:

$$tan\theta_1 = \frac{y}{d} \tag{5.4}$$

where $y = D_{processor}/2$ and d is the vertical distance from the grating to the Opto-VLSI processor.

$$tan\theta_2 = \frac{y - \gamma w}{d} \tag{5.5}$$

Therefore from the diffraction equation and assuming small angle we can conclude that:

$$\lambda \approx \frac{\gamma w}{d} d_g \tag{5.6}$$

where λ is the central wavelength and d_g is the period of passive grating.

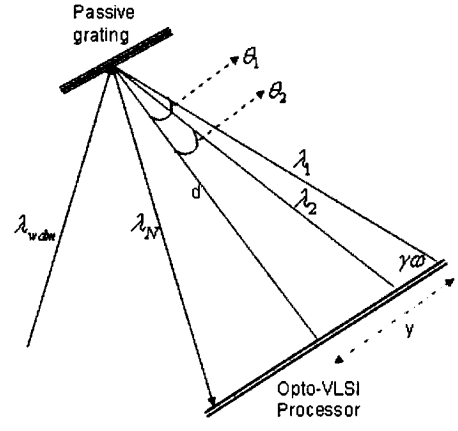

Figure 5.4: Determination of channel spacing

5.4.2 Geometrical considerations

For both applications of filtering and equalisation one of the factors to investigate is the appropriate geometrical locations for the grating and the processor in order to maximise the number of channels that can be filtered or equalised. As can be seen from figure 5.5, the location of the processor should be in such a way that the maximum range of wavelengths from the WDM input can be captured by the surface of the processor. For the arrangement shown in this figure a simple trigonometric calculation provides the answer.

$$tan\theta_1 = \frac{x}{A} \tag{5.7}$$

and

$$tan(\theta_1 + \theta_2) = \frac{y}{A} \tag{5.8}$$

re-arranging these equations we will have

$$\frac{x}{tan\theta_1} = \frac{y}{tan(\theta_1 + \theta_2)} \tag{5.9}$$

We are limited by the size of our processor which we denote as $P_{processor}$

therefore we can write:

$$\frac{x}{tan\theta_1} - \frac{y}{tan(\theta_1 + \theta_2)} < P_{processor} \tag{5.10}$$

This inequality needs to be satisfied for a given distance on the processor. Next we will investigate an alternative arrangement where separate input and output ports are used.

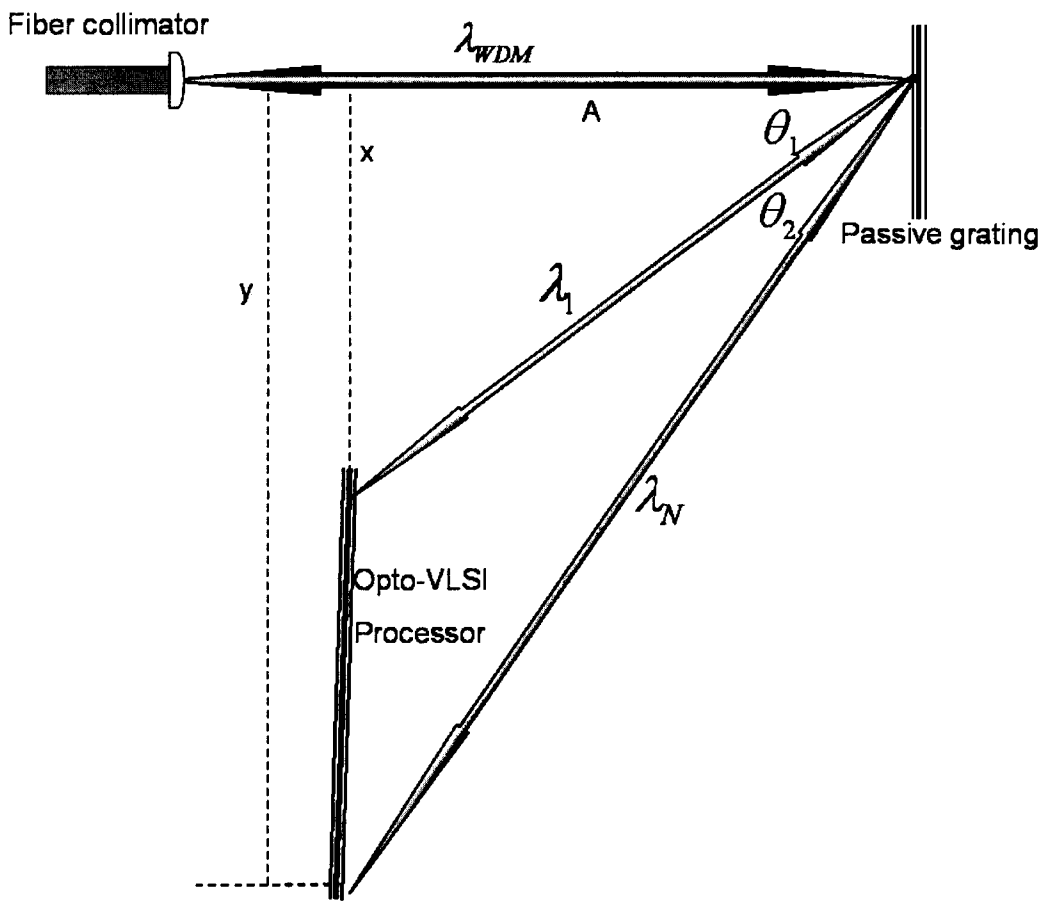

Figure 5.5: A generic arrangement for the passive grating and the Processor

An alternative geometry to investigate is one which utilises separate input and output ports. Figure 5.6 illustrates this arrangement. Here we can use the diffraction law to write:

$$sin\beta = \frac{\lambda}{d_g} + sin\alpha \tag{5.11}$$

$$sin\theta = \frac{\lambda}{d_{processor}} + sin\beta \tag{5.12}$$

$$sin\phi = \frac{\lambda}{d_g} + sin\theta \tag{5.13}$$

Where d_g represents the period of passive grating and $d_{processor}$ the processor's pixel pitch. Therefore re-arranging the above equations we can write:

$$sin\phi = \lambda\left(\frac{2}{d_g} + \frac{1}{d_{processor}}\right) + sin\alpha \tag{5.14}$$

As can be seen from figure 5.6 this relationship applies to the case where separate input and output ports are used.

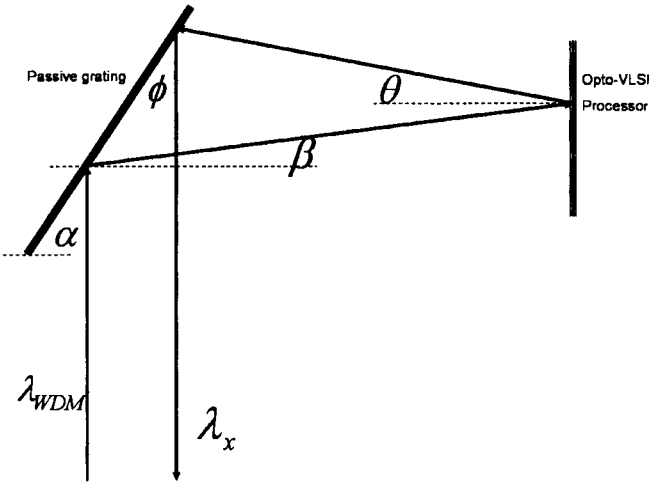

Figure 5.6: An alternative arrangement using separate input and output ports

As can be seen from figure 5.7 for λ_1 we can write:

$$tan\theta_1 = \frac{x}{f} \tag{5.15}$$

and for λ_N we can write:

$$tan\theta_2 = \frac{x+d}{f - dtan\phi} \tag{5.16}$$

combining these equations we will have:

$$tan\theta_2 = \frac{ftan\theta_1}{f - dtan\phi} \tag{5.17}$$

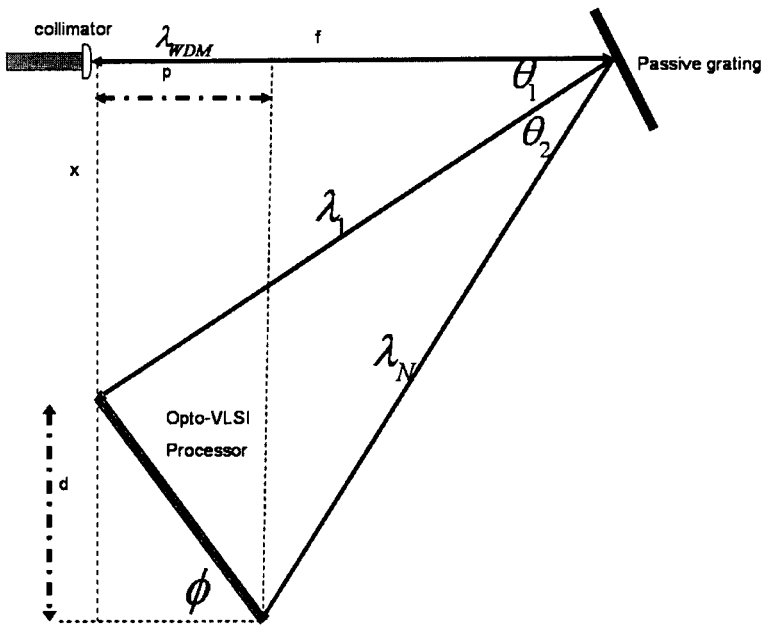

Figure 5.7: Alignment of grating and processor

5.5 General experimental setup

In order to be able to perform many of the experiments in this study we spent some time setting up and automating as much of the procedures as possible to make the process of performing the experiments and collecting the results more efficient. Figure 5.8 shows the schematic representation of the arrangements of various devices in this generic setup which is based on a client-server model. As can be seen from this figure the setup consists of a Personal Computer (PC) which acts as a client in this setup. This computer runs the necessary software to generate and optimise the holograms. Additionally it needs to communicate with the second PC which is our server in this arrangement. The communication between the client and server computers is achieved via the TCP/IP protocol across an ethernet connection which joins both computers. The server PC houses a ISA/PCI card which is used to communicate with the Opto-VLSI processor. It also contains a General Purpose Interface Bus (GPIB) card which is used to communicate with the measurement instruments via the GPIB (IEEE-488) protocol. The server also hosts the main daemon process which is responsible for communication between various components. This process was written in Python and it runs under the Linux platform on the server PC. Next we have the GPIB cables which form the hardware interface between various devices and are used to physically connect the measurement instruments with the server. The measurement instruments used are an optical spectrum analyser, an optical test set (power-meter) and laser sources both fixed and tunable.

The rest of setup consists of the Opto-VLSI processor, a passive diffraction grating, an Infra-red camera, a mirror, an optical circulator/coupler and fibers with collimators. Essentially light from the laser source/s travels down the fiber and is collimated to a Gaussian beam of about 1mm diameter. This collimated light then propagates through free space and falls on the surface of the diffraction grating. The grating simply demultiplexes the beam into its constituent wavelengths and reflects them off to the surface of the Opto-VLSI processor. As different wavelength components fall on different locations on the processor it is possible to manipulate them individually and process them according to desired outputs using appropriate phase holograms. The mirror and IR camera are arranged to

capture the zeroth order reflection from the grating. This is used to adjust the alignment of grating and processor to maximise the amount of intensity captured by the processor. Please refer to Appendix E for details on size of the Opto-VLSI processor.

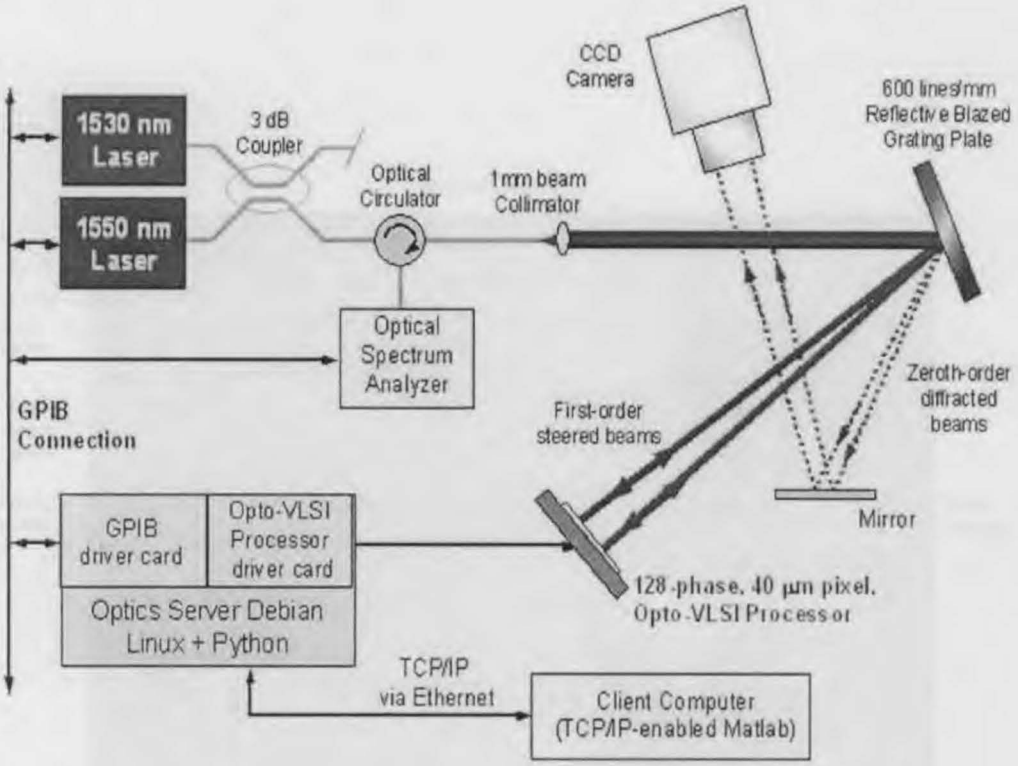

Figure 5.8: Experimental setup

5.6 Experimental results for tunable optical filter

To verify the proof of principle for the multiband tunable optical filter structure described above we used an experimental setup based on Figure 5.3. The in-fibre signal was collimated in free space and its wavelength components were spatially separated using a polarisation-insensitive grating plate having 600 lines per millimeter. The passive diffractive grating is optimised to produce low polarisation loss at 1550nm. The Opto-VLSI processor which is a 128 × 128-pixel, 40-micron-pitch nematic liquid crystal modulator, was properly aligned with respect to the grating plate so that wavelength 1547 nm falls

on the centre of its surface. For the steering capability of our Opto-VLSI processor wavelengths within the 1532-1561 nm range could be coupled back into the fibre collimator using appropriate steering holograms. Figure 5.9 shows a photograph of the setup we used to test our proposed tunable optical filter.

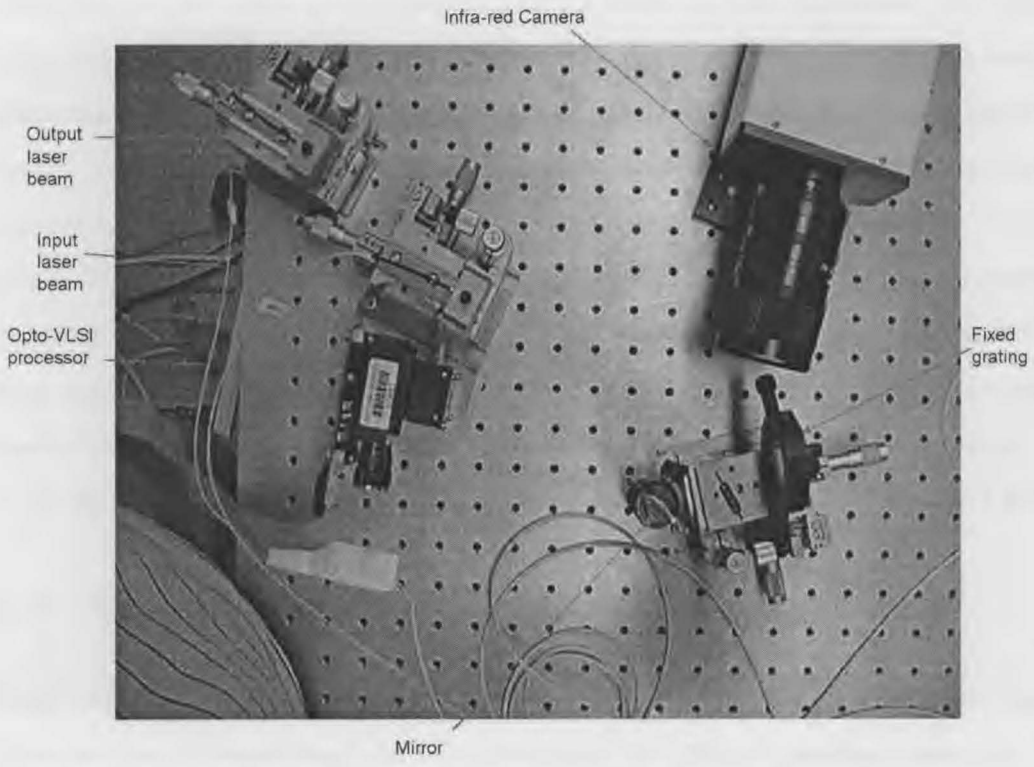

Figure 5.9: Photograph of setup for optical filter

A computer program was developed to efficiently automate the interface with the Opto-VLSI processor and the measuring instruments. The program enables uploading of holograms onto the Opto-VLSI processor, remote control of measuring instruments and processing of measured data, within the same environment.

An algorithm based on annealing method [99] was developed to generate the optimum holograms for a multiband-response target. After measuring the filter response successive modifications were made to the holograms until a target response is attained. An 8-phase hologram of 14 × 14 pixels was found to be adequate for steering a wavelength band at minimum loss. However since the Opto-VLSI processor was operating in a 1-dimensional set-up, 14 × 20 pixel holograms were used in the experiments to eliminate the need to accurately locate the vertical coordinate of the centres of the steering hologram. In addition to filtering it was confirmed that band equalisation can be achieved by appropriately reducing the hologram size. The measured 3 dB bandwidth was 2 nm. The loss of the used high-dispersion grating plate was 2 dB at 1550 nm and the Opto-VLSI processor used in the experiments had low reflectivity and low fill factor resulting in a measured loss of 11 dB for an 8-phase hologram. The two-way fibre coupling losses were around 2dB.

5.7 THREE-BAND band filter results

Figs.5.10(a)-(d) show measured responses of another experimental 3-band tunable optical filter and the corresponding pixel block holograms for different passband scenarios. The holograms were screen captures from a Graphical User Interface (GUI) based user-friendly filter software that has specially been developed to allow non-technical operators to select the centre wavelengths of the filter passbands. Fig.5.10(a) shows the result in passbands at 1533 nm, 1545 nm and 1558.5 nm. In Fig.5.10(b) the holograms were adjusted to produce passbands at 1533 nm, 1547 nm and 1558.5 nm, respectively. In Fig.5.10(c) passbands at 1535 nm, 1547 nm and 1558.5 nm were synthesised. Finally in fig.5.10(d) 1535 nm,1547 nm and 1560.5 nm passbands are represented. It can be seen from these figures that the reconfiguration of the Opto-VLSI processor allows independent tuning of the passbands.

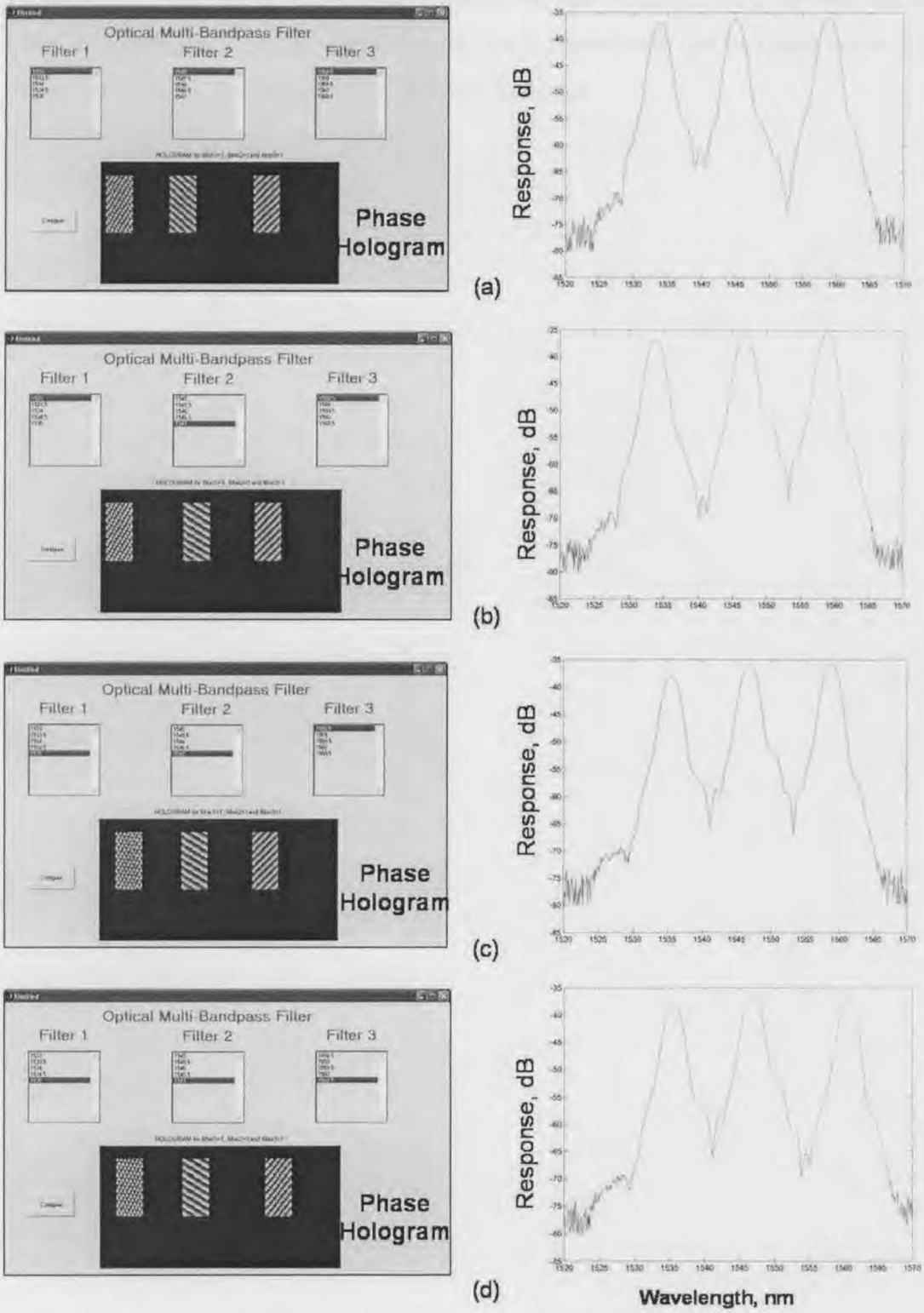

Figure 5.10: Holograms and corresponding measured 3-band filter response for centre wavelengths of (a) 1533, 1545 and 1558.5 nm, (b) 1533, 1547 and 1558.5 nm, (c) 1535, 1547 and 1558.5 nm, and (d) 1535, 1547 and 1560.5 nm.

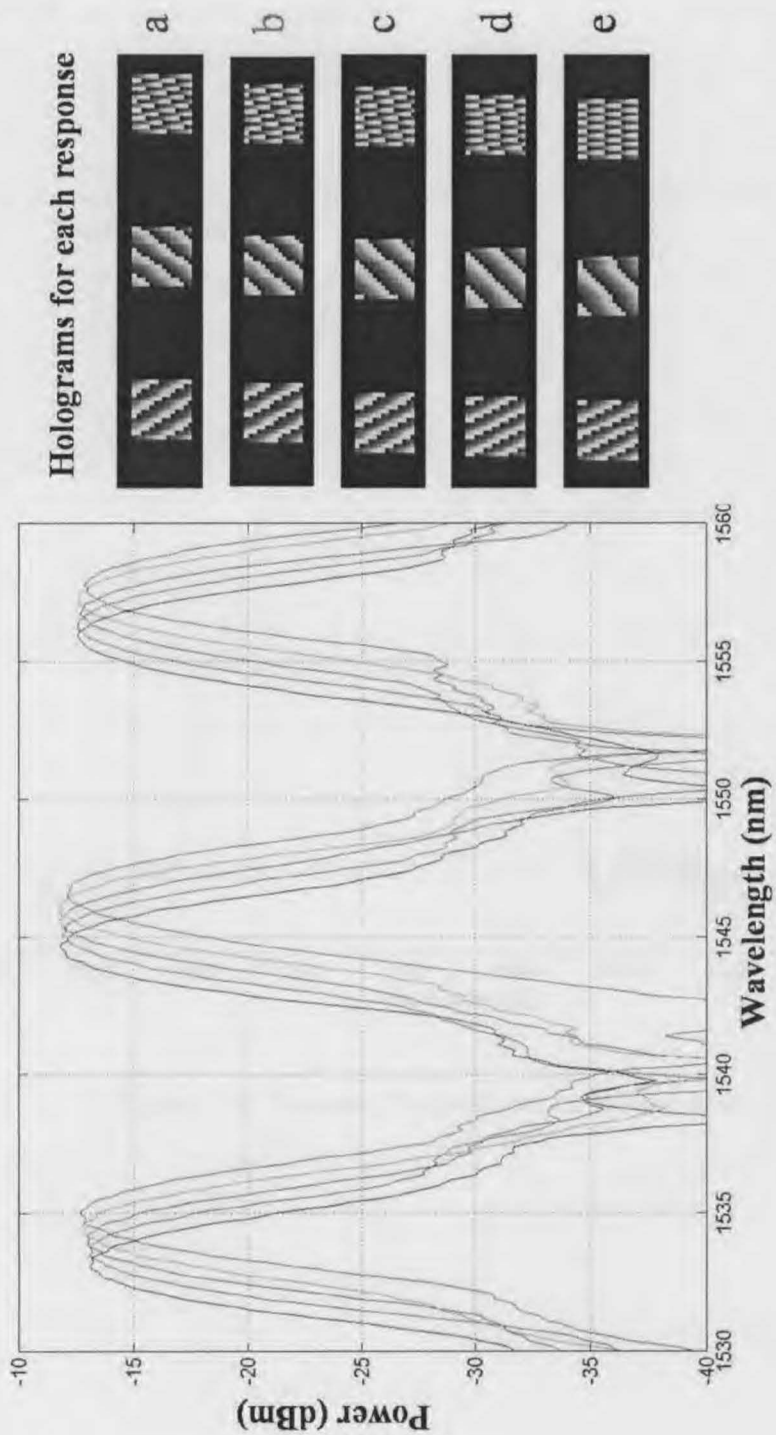

Figure 5.11: THREE BAND filter response

Figure 5.11 illustrates our experimental results for the tuning of the proposed optical filter. In this figure it can be seen that each of the three bands can be tuned across a 2 nm spectrum using the appropriately designed hologram.

Figure 5.12 shows the measured 3dB and 20dB bandwidth associated with our proposed filter. The bandwidth of the filter can be modified by changing the beam width of the Gaussian beam as desribed in equation 5.7.

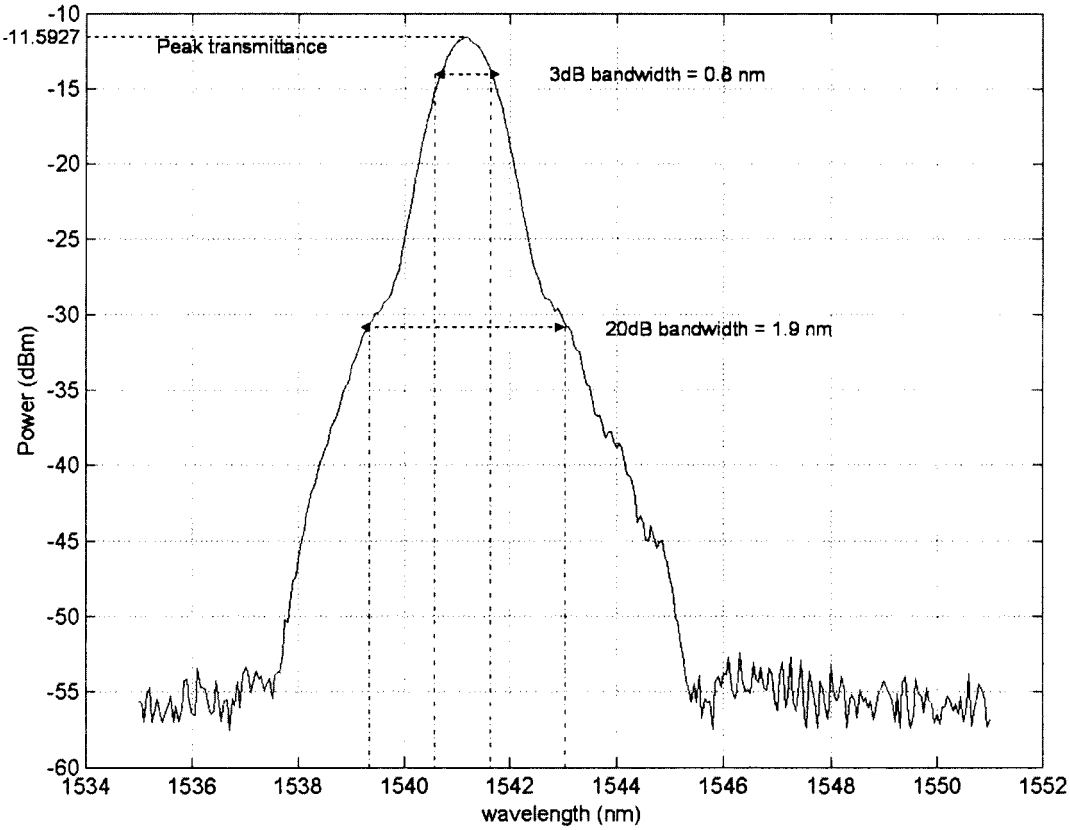

Figure 5.12: Passband for proposed multiband filter

Figure 5.13 shows measured responses of the multiband optical filter for single passbands over the operating wavelength span. Each response corresponds to an optimised hologram that maximises the peak of the response and minimises the skirt rejection of the filter. These are indicated with the 3 different set of colors blue, green and red. In otherwords The first set of 3 band filter has passbands at 1533, 1547 and 1563 nanometers respectively and so on. We have also been able to show the equalisation of peak response of all bands by slightly reducing the size of the steering hologram. This result demonstrates the tuning capability for the multiband tunable optical filter structure.

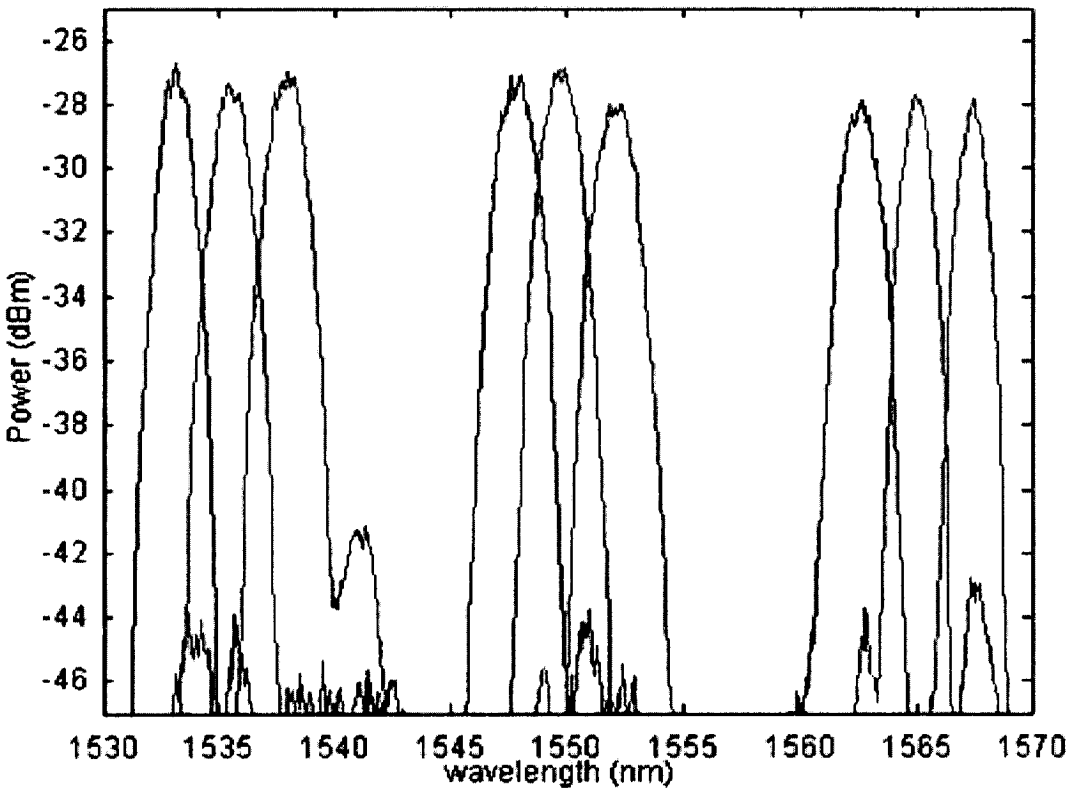

Figure 5.13: Multiband tunable filter response across operating wavelength

5.8 Dynamic WDM equaliser

Dynamic gain equalisers play an important role in WDM networks because of their ability to control the power profile of the wavelength channels, hence maintaining a high quality-of-service and providing more flexibility in transmission management [100]. The key requirements of future dynamic WDM equalisers include low insertion loss, wide bandwidth, fast equalisation speed, small size, and low cost.

Dynamic WDM equaliser structures include micro-opto-mechanical filters [101], Mach-Zehnder interferometer filters [102, 103] acousto-optic filters [104, 105] digital holographic filters [8], and liquid-crystal modulators [106]. These structures utilise few cascaded (or parallel) optical filters whose weights are dynamically optimised to realise smooth spectral equalisation. Since these structures have fewer spectral filters than the number of WDM channels they cannot achieve channel-by-channel equalisation unless the number of optical filters is made equal to the number of WDM channels. Conventional channel-by-channel spectral equalisation requires a demultiplexer, an array of programmable attenuators, and a multiplexer as shown in figure 5.14. Because of the high loss and cost of a demultiplexer-multiplexer pair channel-by-channel spectral equalisation is impractical for WDM networks.

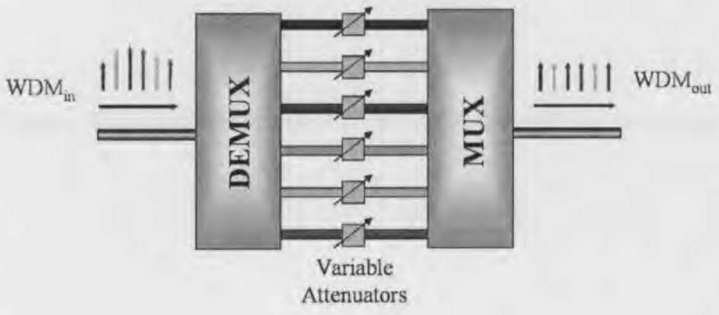

Figure 5.14: Generic Dynamic WDM equaliser

5.9 Experimental configuration for dynamic WDM equaliser

The basic structure of the dynamic WDM equaliser is shown in Figure 5.15. It comprises an optical circulator, a fiber collimator, a high-dispersion polarisation-insensitive diffraction grating plate, and an Opto-VLSI processor.

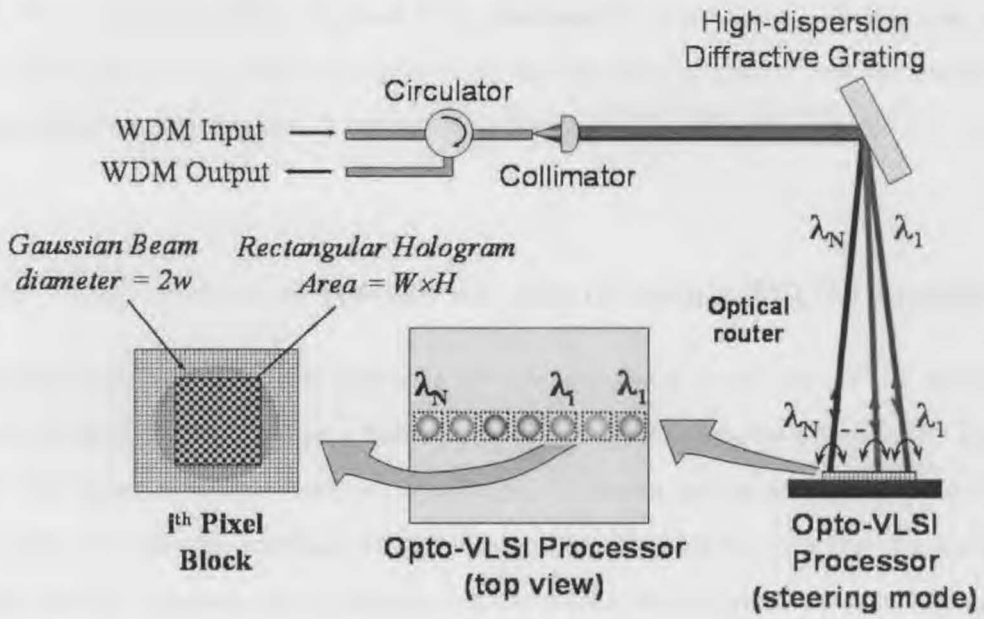

Figure 5.15: Dynamic opto-VLSI WDM equaliser structure

The input WDM signal is routed via the optical circulator to a fiber collimator. The free-space collimated Gaussian optical beam channels are demultiplexed by the high-dispersion diffraction grating along different directions. By adjusting the distance between the grating plate and the Opto-VLSI processor the demultiplexed optical beams can be mapped onto non-overlapped pixel blocks as shown in Figure 5.15. For a large number of WDM channels a lens relay can be used to amplify the angular spacing between the WDM beams. Within each pixel block a holographic diffractive grating is generated to reflect its beam back along the incidence path thus coupling it into the fiber collimator with minimum attenuation. To vary the optical attenuation of a channel a rectangular hologram of area $W \times H$ is generated within the pixel block dedicated to that channel. In this case only the central part of the beam is coupled back into the fiber collimator and the portion of beam falling outside this area is steered away hence significantly attenuated.

5.10 Experimental results for the dynamic WDM equaliser

A preliminary experiment was setup to test the capability of an Opto-VLSI processor based dynamic WDM equaliser. The results of this experiment are presented in Figure 5.16. This figure shows the measured output optical spectra and the associated Opto-VLSI holograms, for different passband attenuation profiles. Note that in this case we used and found circular holograms to be adequate for controlling the Gaussian beam falling on the Opto-VLSI processor. It is obvious from Figures 5.16(b),(d) and (f) that reconfiguring the Opto-VLSI processor allows us to keep the power level of the 1530 nm passband constant while independently varying the attenuation of the 1550 nm passband by more than 30 dB. This demonstrates the proof-of-principle for the novel dynamic WDM equaliser structure. For a VLSI chip fabricated using 0.13 micron process, a 5-micron pixel size and LC area of 16.5 $\times$ 16.5 mm^2 is feasible. For a 64 $\times$ 64-pixel block size, the Opto-VLSI processor can be partitioned into more than 50 independently addressed pixel blocks resulting in a 40 nm tuning band of 0.8 nm resolution. These results confirm the capability of an Opto-VLSI processor to provide dynamic WDM channel equalisation for a dual channel

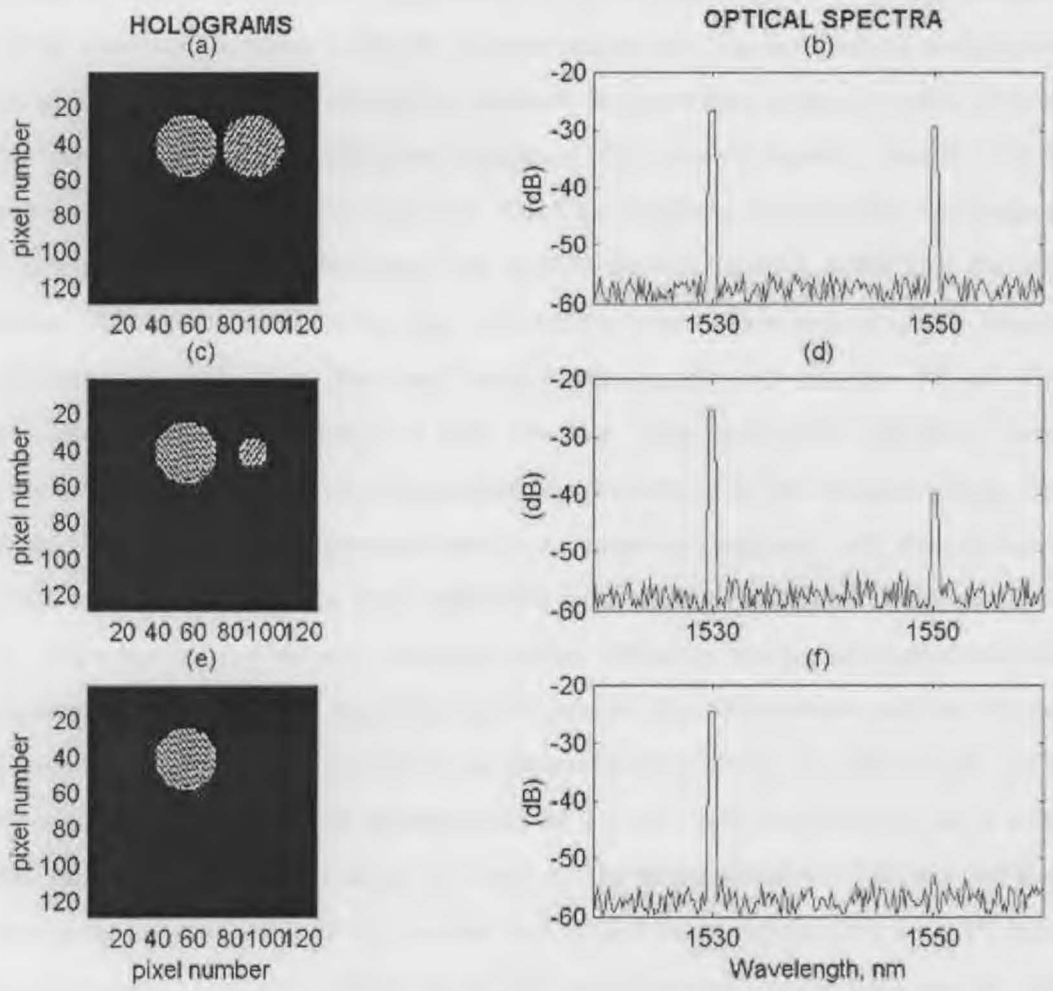

Figure 5.16: Holograms and corresponding output spectra for different channel attenuation profiles. Black and white pixels correspond to phase shifts of zero and, respectively

scenario. This makes the Opto-VLSI technology very attractive for providing reconfigurable optical components for next-generation optical telecommunication networks.

To further test the capability of our proposed WDM equaliser structure we used the architecture illustrated in figure 5.15 in an experimental set up. The experiments were carried out with relatively high-loss components however they provided a demonstration to verify the concepts. Once again a 128-phase, 40-micron pitch nematic liquid crystal Opto-VLSI processor with 128×128 pixels was used. The high-dispersion grating plate was designed to give a low polarisation dependent loss at 1550 nm and consists of 600 lines per millimeter. The optical components were mounted on 5-axis stages and accurately aligned with respect to each other. Two laser beams of wavelengths 1533 nm and 1561 nm were then multiplexed and collimated at 1mm diameter. The zeroth-order diffracted beams reflected back from the Opto-VLSI processor were monitored at the collimator plane. The tilt angle of the Opto-VLSI processor was then continuously adjusted until the monitored zeroth-order diffracted beams were equidistant from the optical axis of the fiber collimator. Following the physical setup a vertical binary diffraction grating was loaded with the minimum pitch possible and the diffracted +1 order of the 1533 nm beam and the -1 order of the 1561 nm beam were observed at the fiber collimator plane. The tilting angle of the Opto-VLSI processor was then adjusted until the +1 order 1533 nm beam and the -1 order 1561 nm beam were overlapped at the centre of the fiber collimator. This ensured that any channel in the 1533-1561 nm window had an incidence angle within the $\pm 1^{st}$ order steering range of the Opto-VLSI processor and could hence be coupled back into the fiber collimator using an appropriate steering hologram.

A computer program was developed to automate and simplify the interface with the Opto-VLSI processor and various measuring instruments. This program operated as a server process and acted as the interface between a PC and the various instruments used. This set-up allowed us to load holograms onto the Opto-VLSI processor and remotely control the measuring instruments and process the measured data within the same environment.

Based on an annealing method [37] an algorithm was developed to generate the optimum hologram for a channel attenuation target. Based on the measured output power level successive modifications were made to the hologram until the target attenuation was attained.

We have found in this case that a hologram consisting of 24 pixels ($\approx 1mm$) is adequate for steering a beam at minimum loss. Channel attenuation was achieved by reducing the hologram size. Figures 5.17(a) and 5.17(b) show the measured input and output optical spectra for a 4-channel WDM equaliser and Figure 5.17(c) shows the phase hologram used for equalisation.

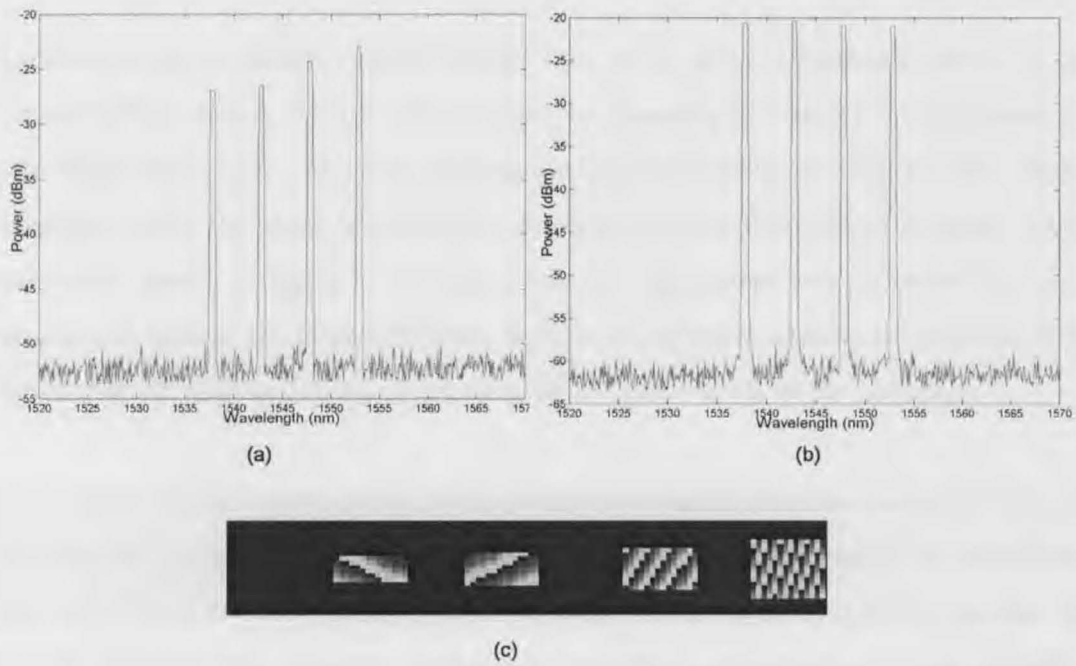

Figure 5.17: Dynamic equaliser response

We have used an input WDM signal that has channel powers ranging from 0dBm to 6dBm and attempted to equalise the measured output WDM signal spectrum. As seen from Figure 5.17(c), by optimising the heights of the pixel block assigned to each channel the output power levels of the 4 wavelength channels were equalised with less than 0.2 dB ripples. We have also been able to vary the attenuation of any channel without affecting the attenuation of other channels. This demonstrated the channel-by-channel WDM equaliser capability of our proposed structure.

Dynamic signal attenuation at the channel level is one of the advantages offered by an Opto-VLSI processor. This is demonstrated by changing the size of the holograms as well their phase range. This was demonstrated experimentally by using a binary phase hologram where the phase is continously decreased thereby decreasing the power of the first-order beam. As figure 5.18 demonstrates this experiment was performed for holograms with radii of 10, 15 and 20 pixels at pixel size of $40\mu m$. As can be seen from this figure, fine attenuation is possible by changing the phase levels of the holograms.

For a VLSI chip fabricated using 130 nm process, a 5-micron pixel size and an LC area of $20 \times 20\ mm^2$ is practical. Theoretically an Opto-VLSI Processor having 32×32 pixel block size and a 16-pixel dead spacing between adjacent blocks, could dynamically equalise 83 WDM channels. This proves the potential of MicroPhotonic technology to offer reconfigurable optical components for future optical networks.

5.11 Other applications

In addition to the two applications which have been the focus of this research program we have been able to successfully demonstrate the capability of an Opto-VLSI processor in other areas. We have experimentally verified the ability of an Opto-VLSI processor to provide add/drop multiplexing and notch filtering. These two applications play very significant roles in the future reconfigurable optical networks. Reconfigurable Add/drop multiplexers are gaining more importance as the channel count in WDM networks increases and the long-haul point-point links without a regenerator grow in length. Tunable optical notch filters can be used in variety of scenarios the most common example of which is flattening of an EDFA gain profile. We have been able to experimentally demonstrate band as well as attenuation tuning for a tunable notch filter. The setup for the notch filter experiment is presented in figure 5.19 and its operation is as follows. The setup consists of an optical circulator, a fiber collimator, a passive diffraction grating with a lens of focal length 200 mm and the Opto-VLSI processor with a lens of focal length 100 mm. The incoming beam will be collimated and sent towards the passive grating where it is reflected based on its angle and wavelength. This time however the lens will focus this beam of light as it traverses towards the Opto-VLSI processor. This beam will be focused by the first lens and then it will begin to diverge as it continues towards the processor. The second lens located before the processor will collimate this beam and sends it towards the processor where it will be received as has been described in the previous experiments. The key point in this arrangement is that various wavelengths are collimated and arrive at the same angle on the surface of the processor and as such by choosing the appropriate hologram we can fully or partially block these wavelength from reflecting back and being coupled into the output fiber. This capability allow us to create notches with various levels of attenuation for specific wavelengths. The preliminary results for the notch filter using the setup as described above is presented as an illustration in figure 5.20.

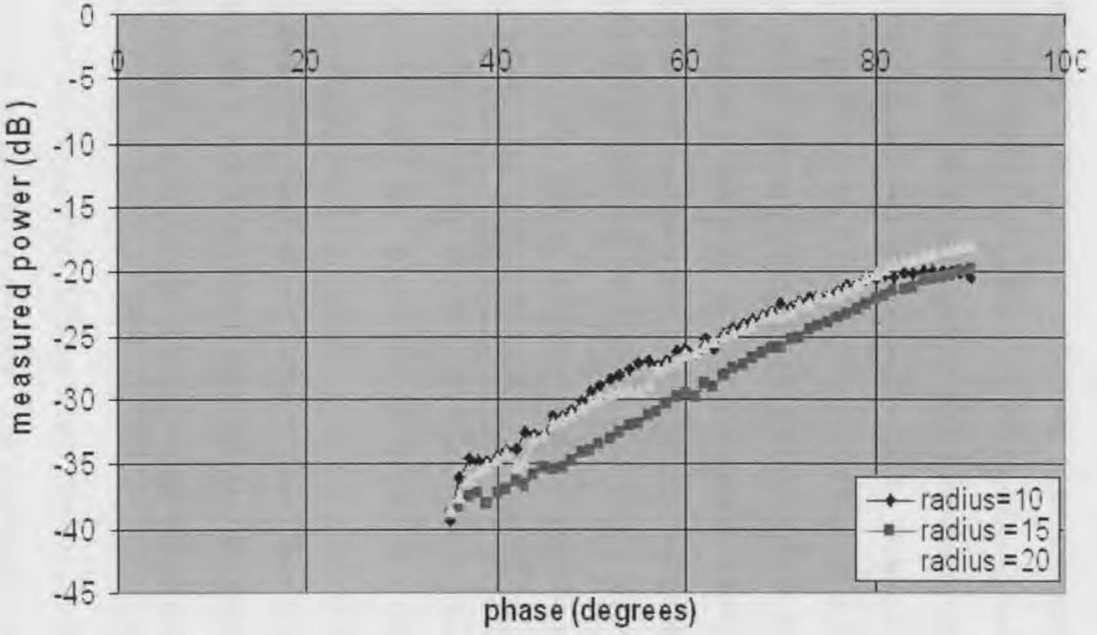

Figure 5.18: Experimental results for change in attentuation by varying the phase levels of three holograms

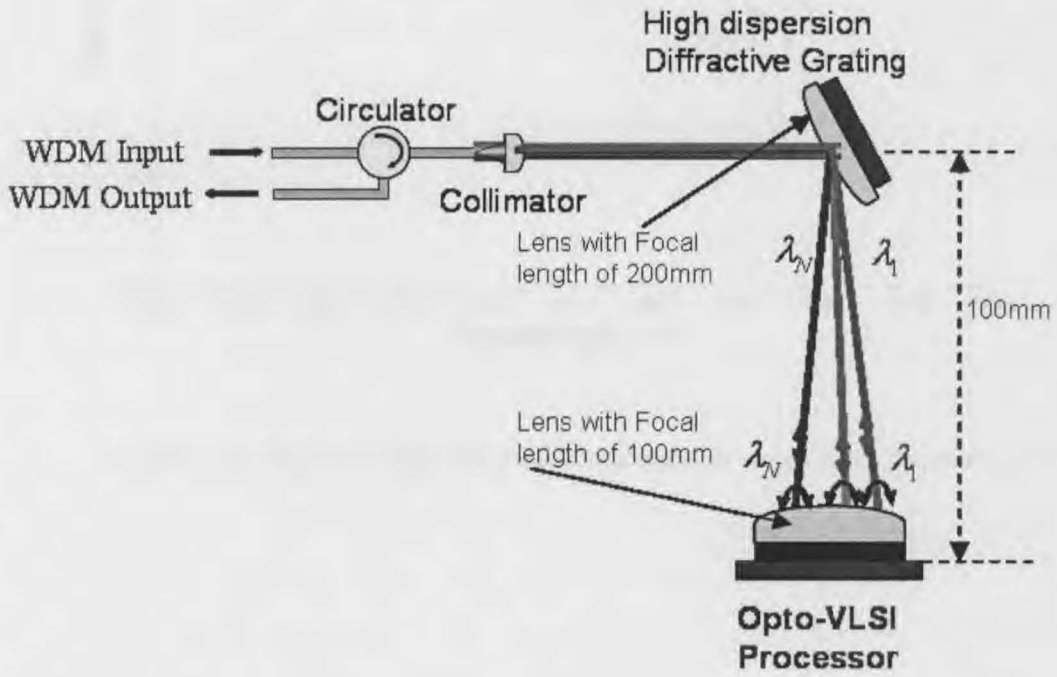

Figure 5.19: Experimental setup for tunable optical notch filter

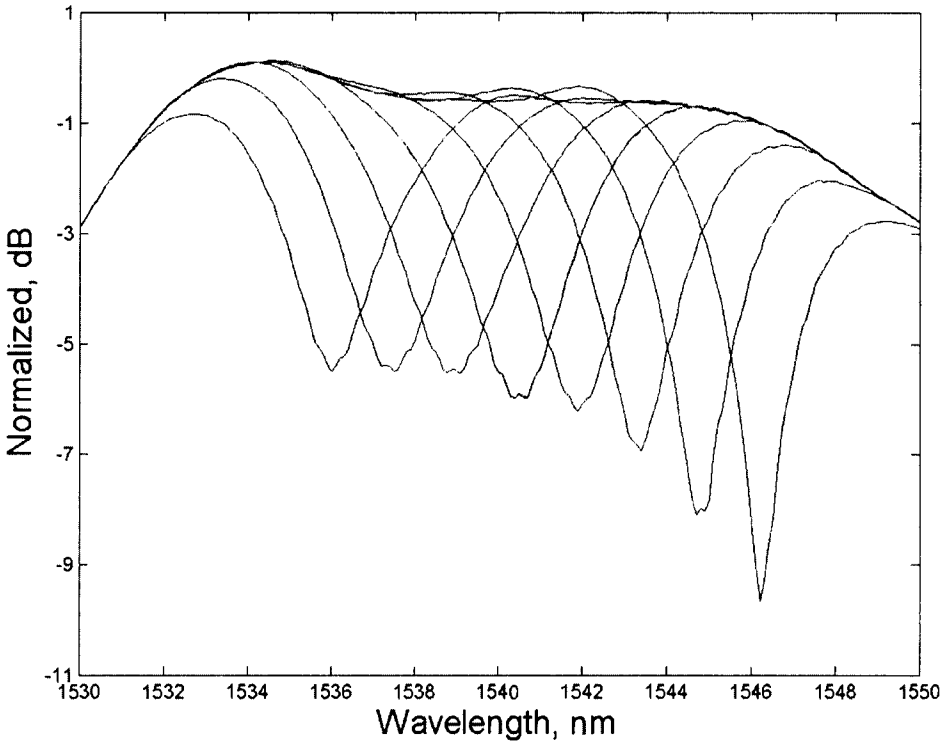

Figure 5.20: Experimental result for reconfigurable notch filter response

5.12 Summary

In this chapter we have reported on a novel tunable multi-band band-pass filter which utilises an opto-VLSI processor to select an arbitrary number of channels. We experimentally demonstrated the proof-of-principle of a 3-band tunable optical filter having 2 nm bandwidth and more than 8 nm tuning range per band over 25nm wavelength span. Therefore we confirm that by generating N non-overlapped phase holograms, an N-band optical filter is realised. By selecting holograms which provide the required steering and adjusting the hologram position, filter passbands can independently be tuned over a wavelength span, which is limited by the size of the Opto-VLSI active area and the maximum allowed crosstalk. ITt is worth noting that wavelength spans closer to 30 nm and beyond are achievable given Opto-VLSI processors with smaller pixel sizes. We provided details on various experimental setups used to test this device and presented the results obtained from these experiments confirming the capability of Opto-VLSI processors in beam processing. We also inspected the results of our research on a novel dynamic WDM channel equaliser. The proof-of-principle of 4-channel WDM equaliser were experimentally demonstrated. These results confirm that independent power control can be accomplished for each channel by varying the radius and/or peak phase of the circular digital hologram dedicated to that channel allowing theoretical realisation of dynamic WDM equalisation for more than 80 channels. Furthermore we have shown how both fine and coarse control of channel gain is possible using the radius and phase of holographic phase elements which are generated by the Opto-VLSI processor. In this case we have used an input WDM signal that has channel powers ranging from 0dBm to 6dBm and attempted to equalise the measured output WDM signal spectrum. Our findings support our assertion and show that by optimising the heights of the pixel block assigned to each channel, the output power levels of the 4 wavelength channels were equalised with less than 0.2 dB ripples. We have also been able to vary the attenuation of any channel without affecting the attenuation of other channels. This demonstrates the channel-by-channel WDM equaliser capability of our proposed structure. Once gain in this case we provided the details associated with various experimental setups used to verify our results. Finally we have alluded to the fact that an Opto-VLSI processor can be used in other significant applications such as

add/drop multiplexing and tunable notch filtering. In this context we have presented the experimental setup we have used to substantiate these assertions and have justified our claims by presenting our experimental results.

In the following chapter we will conclude this study by providing a summary of its findings and suggesting some possible avenues for future extension of this work.

Chapter 6

Conclusion and future work

In this chapter we will provide a summary of findings from this research and point to some potential directions for extension of this study.

6.1 Summary of findings

We began by providing a background to this study thereby building the necessary foundation for the details to follow. We presented reconfigurability as an increasingly pervading approach in dealing with optical networking due to the changing nature of technology and demands being placed upon communications networks. We emphasised the importance of tunable optical filtering and channel equalisation in this new dynamic regime. We then proceeded to present a detailed literature survey on various techniques proposed for tunable optical filtering and channel equalisation. We showed that despite existence of many approaches for performing these functions, there still remains a real need for a truly dynamic/adaptive solution to optical filtering and gain equalisation that meets the ever-growing set of demands placed on communications networks.

The next step was then to introduce the Opto-VLSI processor as an enabling technology for the future reconfigurable optical communications networks. To begin, we reviewed the history of spatial light modulators as devices capable of modifying the phase, intensity or polarisation of an optical beam. In this context we briefly explained the application of

various technologies used for purpose of spatial light modulation. We examined the various components that make-up an Opto-VLSI processor. We described the architecture and dispersive features of an Opto-VLSI processor and how it may be used for optical filtering and channel equalisation.

Having explored the Opto-VLSI processor as a potential candidate for provision of reconfigurable functions in the future optical networks, we moved to provide some details about computer generated phase holograms which are used in conjunction with the Opto-VLSI processor to provide optical beam steering and multicasting capabilities. In this context we presented the results of analysis of phase holograms using one and two dimensional Fourier series. We also derived an expression for the efficiency of phase holograms based on a two dimensional model and taking into consideration the finite number of pixels as well as the phase and spatial quantisation involved in the generation and application of the phase hologram via an Opto-VLSI processor. Furthermore we examined the results of simulations conducted to investigate the impact of replacing one phase hologram by another as well as those testing the effect of number of pixels on crosstalk and power efficiency of a phase hologram. Finally we canvassed in some length various methods for generation of phase holograms including some of more commonly used algorithms such as simulated annealing and genetic algorithms.

Having explored the morphology and operation of an Opto-VLSI processor and probed into the world of phase holograms, we stepped into the the stage where the experimental results in this study were presented. We reported on a novel tunable multi-band bandpass filter which utilises an opto-VLSI processor to select an arbitrary number of channels. We experimentally demonstrated the proof-of-principle of a 3-band tunable optical filter having 2 nm bandwidth and more than 8 nm tuning range per band over 25 nm wavelength span. We provided details on various experimental setups used to test this device and presented the results obtained from these experiments confirming the capability of Opto-VLSI processors in beam processing. We also inspected the results of our research on a novel dynamic WDM channel equaliser. The proof-of-principle of 4-channel WDM

equaliser were experimentally demonstrated. These findings confirm that independent power control can be accomplished for each channel by varying the radius and/or peak phase of the circular digital hologram dedicated to that channel allowing theoretical realisation of dynamic WDM equalisation for more than 80 channels. Furthermore we showed how both fine and coarse control of channel gain is possible using the radius and phase of holographic phase elements which are generated by the Opto-VLSI processor. Once gain in addition to presenting the final results we provided all the details associated with various experimental setups used for verification purposes. In the closing section of chapter five we hinted at the possibility of other applications such as add/drop multiplexing and notch filtering benefiting from the dynamism provided by an Opto-VLSI processor. In this framework, we presented an experimental setup and corresponding results confirming the provision of reconfigurable notch filtering using and Opto-VLSI processor.

6.2 Future directions

6.2.1 Further extension of current capabilities

As an immediate step, this research can continue to investigate Band-pass filtering and channel equalisation capabilities of the Opto-VLSI processor. This could involve examining the possibility of extending the tuning range for the filter and number of pass-bands. Moreover we can investigate the expansion of number of equalised channels in the WDM equaliser. These objectives can be achieved by using an Opto-VLSI processor with a larger reflective surface and in conjunction with use of appropriate optical elements.

6.2.2 A feedback system

One area which requires further investigation is the study and development of a feedback mechanism for generation and optimisation of phase holograms. Current arrangement means that holograms are generated off-line before they are loaded unto the Opto-VLSI processor. This approach has served us well so far but sizable improvements can be achieved if an in-line system is devised to generate the holograms, load them onto the processor and optimise them based on for example power measurements in a feedback

arrangement.

6.2.3 More efficient algorithms

Further research is required to find appropriate algorithms for generation and optimisation of holograms. Most of the existing algorithms suffer from being computationally expensive and in some cases are not able to produce the desired results. In a simplistic scenario, a suitable algorithm should allow the generation of phase holograms which can channel a very high percentage of incoming light into desired locations in the replay field with minimum noise in form of crosstalk present. Moreover this tasks needs to be performed in real-time or as close as possible to it. In addition the selected algorithm should also be easily implementable into the VLSI backplane using a commonly used Hardware Descriptive Language (VHDL).

6.2.4 Other novel applications

The flexibility offered by the Opto-VLSI processor means that there are potentially other applications for which this device can be used very effectively. One of more significant examples is the provision of reconfigurable dispersion compensation. By producing a difference in group delay between different wavelength channels we can provide a variety of dispersion values and slopes. This can possibly be achieved with the use of an Opto-VLSI processor and an optical delay line.

6.2.5 Optical beam shaping

The ability to modify the phase-front of an optical beam has many useful applications in medicine, manufacturing and communications. In this study we have shown analytically that it is possible to change the shape of an optical wavefront using an appropriate phase hologram. It would be very interesting to further explore this capability of the Opto-VLSI processor by devising and conducting the necessary experiments. After experimentally confirming the ability for instance to convert a Gaussian optical beam to a circular beam, specific real-life applications can be looked at where this feature can be used to address existing challenges.

6.2.6 Arbitrary filter response

The tunability of the notch filter in terms of bandwidth as well as attenuation means that we can potentially create a filter where any desired filter profile can be generated by a judicial selection of locations to place the notches. Furthermore the possibility of producing a flat-top profile should also be pursued as this type of profile is eagerly sought after in applications such as channel monitoring, add/drop multiplexers and tunable receivers.

Appendix A

DC balancing for FLC processor

FLC based processors need to be DC balanced to avoid their permanent damage brought about by being exposed to DC voltage for a considerable period. Associated with any procedure to ensure DC balancing of the FLC processors are transient effects manifested on the replay field. In this section we describe different techniques used to simulate and analyse these transient effects.

Two general approaches were tried and the effects on the replay field were analysed. In both methods a hologram is produced using a program based on annealing algorithm. This hologram was then modified in a manner to achieve DC balancing and the impact of this process on the replay field was monitored. The concept of DC balancing as it applies to the FLC is based on the notion of ionic degradation [56]. One way to achieve DC balancing is to ensure that within a specific time frame the liquid crystal only experiences an average of zero volts. This in turn means that each pixel in the hologram should see equal number of both phases in case of a binary hologram. In the following paragraphs we will attempt to explain the procedures that were used for simulation of transient effects in their entirety.

Based on the assumption that all binary holograms produced have equal number of both phases, it follows that if over the available time (a period of 2 minutes was assumed to be adequate in this case) each pixel sees the content of every other pixel then the FLC will remain DC balanced overall.

Given a hologram (an array of $N \times N$ elements) we first convert this array into an equivalent vector to make the scrolling process more efficient. What is followed then is shifting of elements of this vector to emulate the process of scrolling left/right and up/down. Two diagrams below show the scrolling technique visually.

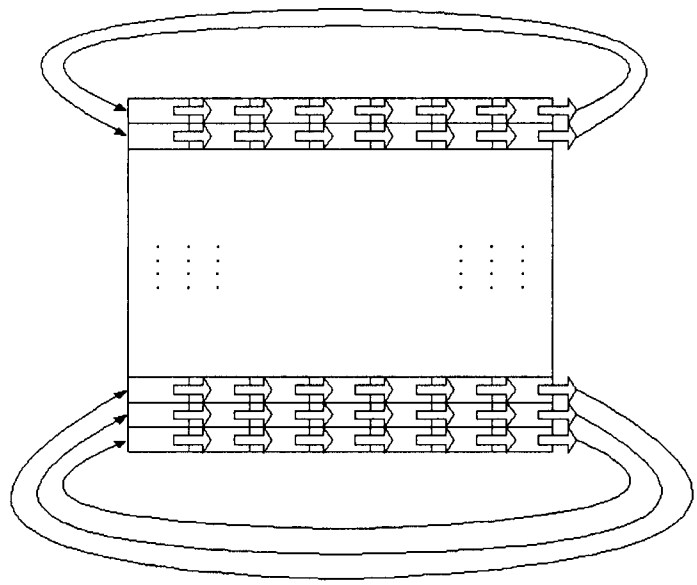

Figure A.1: Scrolling to right

Only a small number of pixels (8 in this case) are shifted at any one time in order to minimise the effects of this operation on the replay field. After each change the replay field produced from the new hologram can be plotted and inspected. After generating the original hologram we extract the coordinates of the point where maximum light intensity resides and keep track of the same coordinates through the simulation. All pixels are shifted first to the right and then they are shifted down. It is found that for any equal dimension matrices, 2N shifts are needed (where N is size of row/column in the matrix)

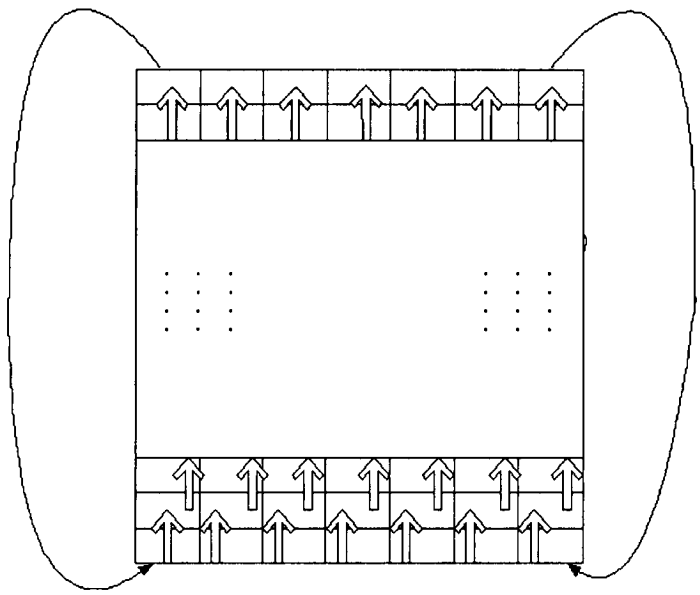

Figure A.2: Scrolling up

to achieve a complete cycle. At any point the vector can be converted back to the corresponding matrix, replay field calculated and displayed for inspection. Figure A.3 shows the results obtained using this procedure for a 32 pixel base hologram.

A subsequent method was also used to achieve the same objectives. This time however we simply inverted the content of each pixel and measured the corresponding impact on the replay field from the new hologram configuration. Once again aside from the usual variation associated with layout of output ports, the overall result obtained were poor and furthermore did not show any degree of improvement over the scrolling technique described earlier. In general results obtained using this method were much poorer than those using the scrolling technique. Diagram A.4 below shows the results obtained for the same original hologram as the one used in the scrolling experiment above.

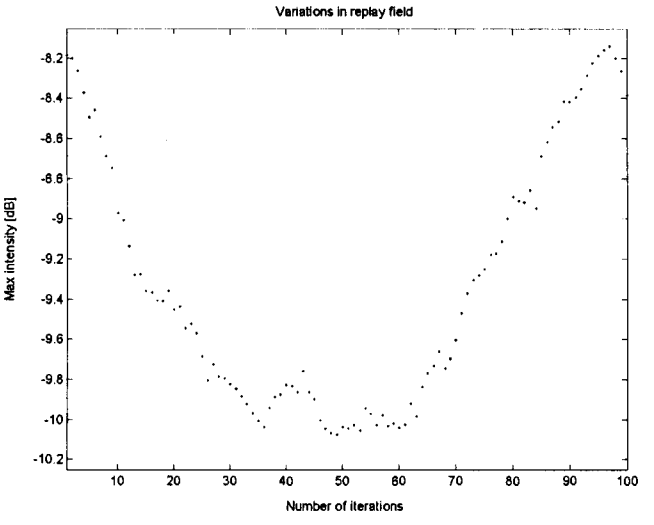

Figure A.3: Simulation results for variations in replay field during scrolling - 32 × 32 hologram

A variation on the inversion technique however resulted in a marked degree of improvement. One of fundamental challenges associated with changing the hologram is that at the point when one half of hologram is different from the other, one can expect to get the largest penalty on the replay field. Based on this mentality an attempt was made to achieve DC balancing whilst avoiding this 50/50 problem. It was decided to try the following approach. A number of pixels in the hologram would be inverted one by one and the variation in the replay field would be monitored as individual pixels are changed. Then we proceed to invert back the content of these pixels while measuring the impact on the replay field as before. We then move to the next set of pixels and apply the same technique. It was found that for a 32 × 32 pixel base hologram 16 to 32 pixels could be changed and the impact proved to be minimal. It is worth noting however that this technique does not produce DC balancing if the FLC is not bi-stable. In other words in this method pixels not being inverted can get exposed to a particular voltage for a duration that is not acceptable. Figure A.5 shows the result of this process.

The final method used was again a straight scrolling method with the difference that this

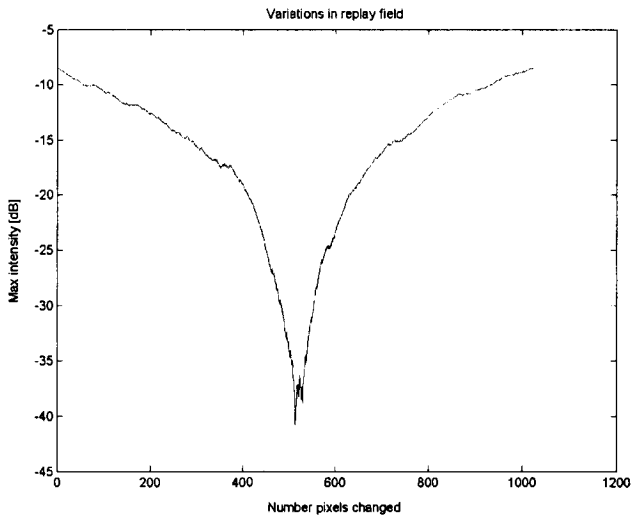

Figure A.4: Simulation results for variations in replay field

time the array representing the hologram was not transposed. Therefore in this case firstly all the last elements in each row were stored in a temporary location. Then each pixel was moved forward (row by row) and once we reached the location of the first pixel in each row we replaced its content with the relevant last element from our storage. This process repeated 32 times (in case of 32 × 32 array) would amount to shifting across of all elements. This is then followed by a shift down. In this case we first store all the last elements in each column. We will then proceed to shift each element down by one until we reach the location of first element in which case we restore the last element. Once again when this is repeated 32 times the entire array would have been shifted down by one position. These twin processes are repeated 2N times as explained earlier to achieve a complete scrolling of the entire hologram. The results obtained from this approach were the best out of all the methods used. For a 32 × 32 hologram, ripples in the replay field as low as 0.6 dB were observed.

The overall findings from the above mentioned simulations indicate that in general the scrolling mechanism devised for DC balancing produces better results (i.e. less impact on the replay field) than the straight inverting technique. It was also found that a variation on

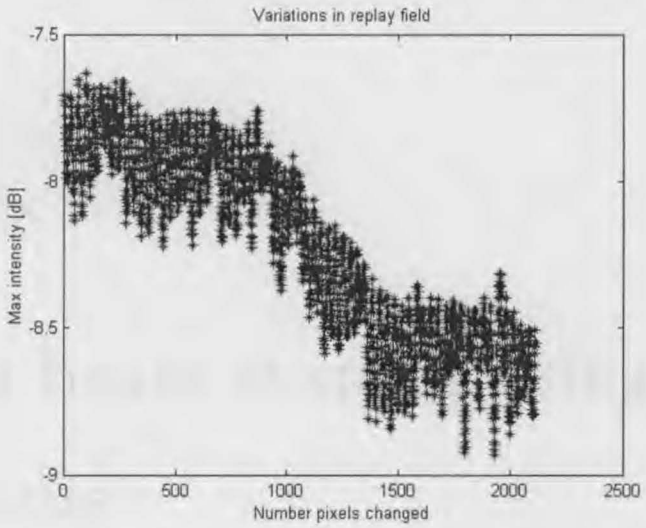

Figure A.5: Variations in replay field

the inverting technique whereby at any time only a limited number of pixels are inverted (and therefore different to those of the original hologram) produced marked improvement. However this approach is clearly not DC balancing. The variations observed for different holograms can be attributed to the difference in hologram pattern. It is also quite possible that layout of output ports contributes to this phenomenon.

Appendix B

Optical beam shaping using phase holograms

In addition to beam-steering and multicasting, phase holograms can be used to modify a wavefront spatially [107–110].

There are two general methods which can be used for optical beam shaping:(i)numerical (ii)analytical. The numerical approach is based on optimisation techniques such as simulated annealing, direct binary search and a myriad of Iterative Fourier transform methodologies. Common to all numerical methods is sampling. The desired reconstruction pattern is regarded as consisting of a finite number of discrete point objects, with the phase of each of them being an independent optimisation parameter. In these methods speckle noise can be introduced, if the inter-depedence of phase of adjacent points is neglected. One way to avoid speckles is to find a smooth function that will translate the incoming beam to the desired output plane. This means that there has to exists a one-to-one relation between the points in the input and output planes.

In this section we present the theoretical results derived for transformation of a Gaussian beam of spot radius w and radius r_o into a uniform circular spot of radius ρ_o. The basic aim here is to calculate a phase-only hologram function that focuses the light coming through an aperture into a given object pattern at a specified focal distance. Before we

begin the derivation for this case, we start by providing some background.

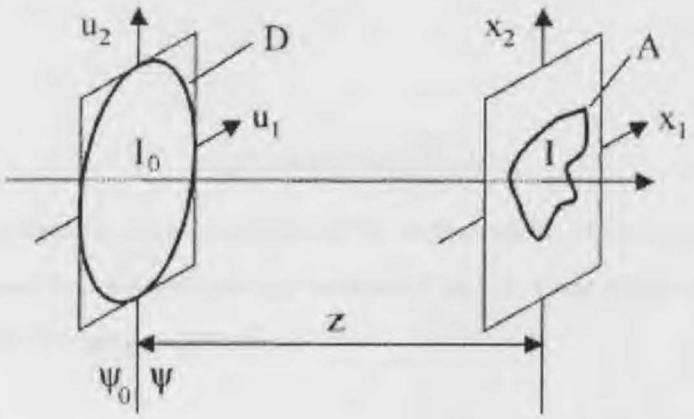

Figure B.1: The reconstruction geometry

We assume that the incident beam has an intensity of $I_o(\vec{u})$ and phase $k\psi_0(\vec{u})$ as illustrated in figure B.1 [108]. The phase of the incident wave passing through the hologram is given as:

$$k\psi(\vec{u}) = k\psi_0(\vec{u}) + \phi(\vec{u}) \tag{B.1}$$

Where $\phi(\vec{u})$ is the phase hologram distribution as illustrated in figure B.2.

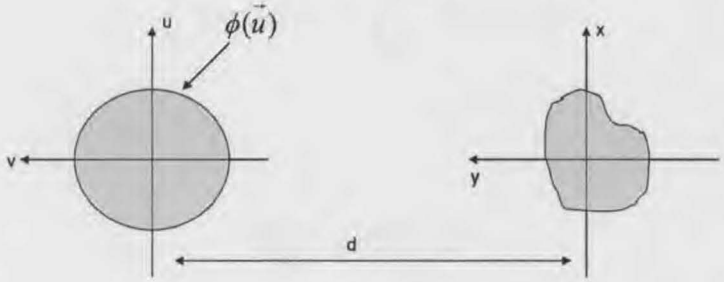

Figure B.2: Simplified optical geometrical reconstruction

We wish to find $\phi(\vec{u})$ for a required output intensity distribution $I(\vec{x})$. It is worth noting that the solution for $\phi(\vec{u})$ is not unique due to the freedom in the output phase $k\psi(\vec{x})$. We assume that the corresponding points $\vec{x} = \vec{x}(\vec{u})$ and $\vec{u} = \vec{u}(\vec{x})$ lie on the same light ray. In this case

$$I_o(\vec{u}) = I(\vec{x}) det\left(\frac{\partial \vec{x}}{\partial \vec{u}}\right) \tag{B.2}$$

We present the derivation of this equation in the next section. In theory, the above equation should provide the required relation between $\vec{u}$ and $\vec{x}$. Once this is shown, $\psi(\vec{u})$ can be found from the following expressions

$$\begin{aligned} \frac{\partial \psi(\vec{u})}{\partial u} &= \frac{x(\vec{u}) - u}{d} \\ \frac{\partial \psi(\vec{v})}{\partial v} &= \frac{y(\vec{v}) - v}{d} \end{aligned} \tag{B.3}$$

and hence $\phi(\vec{u})$.

For a circularly symmetric case we have

$$I_o(r) = I(\rho) det\left(\frac{\partial \rho}{\partial r}\right) \tag{B.4}$$

which can be written in the integral form as

$$\int_0^r 2\pi r I_o(r) dr = \int_{\rho(0)}^{\rho(r)} 2\pi \rho I(\rho) d\rho \tag{B.5}$$

Also we have

$$\frac{\partial \psi(r)}{\partial r} = \frac{\rho(r) - r}{d} \tag{B.6}$$

Hence we can find $\phi(r)$.

We will now look at steps required for transformation of a Gaussian beam into a uniform circular spot.

For a Gaussian beam

$$E_o(r) = \hat{E}_o exp\left[-\left(\frac{r}{w}\right)^2\right] \tag{B.7}$$

or

$$I_o(r) = \hat{I}_o exp\left[-2\left(\frac{r}{w}\right)^2\right] \tag{B.8}$$

giving the total power P_T crossing the area of radius r_o as

$$\begin{aligned} P_T = \int_0^{r_o} 2r\pi I_0(r)dr &= 2\pi\hat{I}_0 \int_0^{r_o} r exp\left[-2\left(\frac{r}{w}\right)^2\right] \\ &= \frac{\pi\omega^2}{2}\left\{1 - exp\left[-2\left(\frac{r_o}{w}\right)^2\right]\right\}\hat{I}_0 \end{aligned} \tag{B.9}$$

Hence

$$\hat{I}_0 = \frac{P_T}{\frac{\pi\sigma^2}{2}\left\{1 - exp\left[-2\left(\frac{r_o}{w}\right)^2\right]\right\}} = \frac{2P_T}{\pi\sigma^2\left[q\left(\frac{r_o}{w}\right)\right]^2} \tag{B.10}$$

Where

$$q(t) = 1 - exp\left[-2t^2\right] \tag{B.11}$$

The total power within the area of radius r_o is then

$$P_T = \int_0^{r_o} 2r\pi I_0(r)dr = 2\pi\hat{I}_0 \int_0^{r_o} rexp\left[-2\left(\frac{r}{w}\right)^2\right]$$
$$= \pi\sigma^2\hat{I}_0\left\{1 - exp\left[-2\left(\frac{r}{r_o}\right)^2\right]\right\} = \frac{P_T\left[q\left(\frac{r}{w}\right)\right]^2}{\left[q\left(\frac{r_o}{w}\right)\right]^2} \tag{B.12}$$

for a circular uniform spot

$$I(\rho) = \hat{I}$$

hence

$$\int_0^{\rho(r)} 2\pi\rho I(\rho)d\rho = 2\pi\hat{I}\int_0^{\rho(r)} \rho d\rho = \pi\hat{I}\rho(r)^2 \tag{B.13}$$

or

$$\pi\hat{I}\rho(r)^2 = \frac{P_T\left[q\left(\frac{r}{w}\right)\right]^2}{\left[q\left(\frac{r_o}{w}\right)\right]^2} \tag{B.14}$$

when $r \rightarrow r_o$, $\rho \rightarrow \rho_o$ and we have

$$\hat{I} = \frac{P_T}{\pi\rho_o^2}$$

substituting we finally have

$$\rho(r) = \frac{\rho_o q\left(\frac{r}{w}\right)}{q\left(\frac{r_o}{w}\right)} \tag{B.15}$$

Appendix C

Derivation of equation for light-flux transformation

As can be seen from figure C.1 the coordinates of point A are u_A and x_A in the u-plane and x-plane respectively.

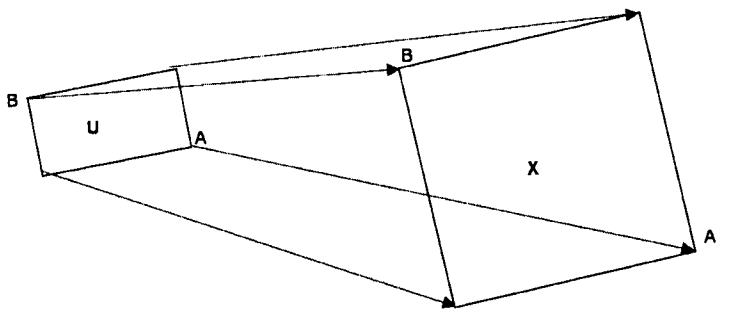

Figure C.1: Coordinates for the transformation

Now

$u_A = du_1 a_{u1}$, $u_B = du_2 a_{u2}$

and

$$x_A = \frac{\partial x_1}{du_1} du_1 a_{x1} + \frac{\partial x_2}{du_1} du_1 a_{x2} \tag{C.1}$$

$$u_B = \frac{\partial x_1}{du_2} du_2 a_{x1} + \frac{\partial x_2}{du_2} du_2 a_{x2} \tag{C.2}$$

The area of the rectangle in the u-plane is $|u_A \times u_B| = du_1 du_2$. The area of the rectangle in the x-plane is

$$\begin{aligned} |u_A \times u_B| &= \left(\frac{\partial x_1}{du_1} du_1 a_{x1} + \frac{\partial x_2}{du_1} du_1 a_{x2}\right) \times \left(\frac{\partial x_1}{du_2} du_2 a_{x1} + \frac{\partial x_2}{du_2} du_2 a_{x2}\right) \\ &= -\frac{\partial x_2}{du_1} du_1 \frac{\partial x_1}{du_2} du_2 + \frac{\partial x_1}{du_1} du_1 \frac{\partial x_2}{du_2} du_2 \\ &= \left(\frac{\partial x_1}{du_1}\frac{\partial x_2}{du_2} - \frac{\partial x_2}{du_1}\frac{\partial x_1}{du_2}\right) du_1 du_2 = det\left(\frac{\partial x}{\partial u}\right) du_1 du_2 \end{aligned} \tag{C.3}$$

But

$I_x dx_1 dx_2 = I_u du_1 du_2$

Hence

$$I_x dx_1 dx_2 = I_x det\left(\frac{\partial x}{\partial u}\right) du_1 du_2 = I_u du_1 du_2 \tag{C.4}$$

and finally

$$I_u = I_x det\left(\frac{\partial x}{\partial u}\right) \tag{C.5}$$

Appendix D

Notes on method of stationary phase

Method of steepest descent and stationary phase are two approaches to finding asymptotic approximations to complex integrals of type $\int g(z)e^{kf(z)}dz$ for large values of k. Both methods depend on choosing a path of integration in such as way that the interand by virtue of its exponential factor contributes negligibly to the integral except in the vicinity of certain critical points which include "'saddle points"' and end points of the path of integration [22].

The problem of transforming a given wavefront of known phase and intensity to another wavefront of given intensity with the help of phase holograms is one that has been investigated by many researchers. One approach in tackling this problem is to first find a purely geometrical distortion which redistributes one intensity to another. Next we try to find this distorion using a phase-only hologram. Method of stationary phase [111] is an effective technique which can be used to redistribute the energy in this process. In the following paragraphs, we provide the basic background to this approach.

Consider first the integral

$$M(k) = \int_a^b f(t)exp(jkt)dt \tag{D.1}$$

For large values of k, the exponential term varies rapidly and $M(k) \rightarrow 0$. We develop an asymptotic series describing the behaviour of the integral as $k \rightarrow \infty$.

It can be seen that the behaviour of k depends on the form of f(t) and its derivative at points a and b. Integrating by parts we have

$$\begin{aligned} M(k) = \int_a^b f(t)exp(jkt)dt &= \int_a^b \frac{f(t)}{jk}\left[exp(jkt)\right] \\ &= \frac{f(t)}{jk}exp(jkt)|_a^b - \frac{1}{jk}\int_a^b \acute{f}(t)exp(jkt)dt \\ &= \frac{f(b)}{jk}exp(jkb) - \frac{f(a)}{jk}exp(jka) - O\left(\frac{1}{k}\right) \end{aligned} \tag{D.2}$$

provided that f(t) is finite at both points a and b.

We now consider the case of $f(t) \rightarrow \infty$ at point a=0. If $a \neq 0$ the integral can be transformed to the particular case of a=0 by a coordinate transformation. The case of $f(t) \rightarrow \infty$ at point b is very similar.

Let

$f(t) = \frac{1}{t^\alpha}\phi(t)$ for $t \rightarrow 0 (0 < \alpha < 1)$

substituting, we have

$$\begin{aligned} M(k) = \int_a^b f(t)exp(jkt)dt &= \int_a^b \frac{1}{t^\alpha}\phi(t)exp(jkt)dt \\ &= \int_0^\epsilon \frac{1}{t^\alpha}\phi(t)exp(jkt)dt + \int_\epsilon^b \frac{1}{t^\alpha}\phi(t)exp(jkt)dt \end{aligned} \tag{D.3}$$

Where ϵ is a positive number. With ϵ close to zero

$$M(k) = \phi(0)\int_0^{\epsilon} \frac{1}{t^{\alpha}} exp(jkt)dt + \int_{\epsilon}^{b} \frac{1}{t^{\alpha}}\phi(t)exp(jkt)dt = \phi(0)\int_0^{\infty} \frac{1}{t^{\alpha}} exp(jkt)dt - \phi(0)$$
$$\int_0^{\infty} \frac{1}{t^{\alpha}} exp(jkt)dt + \phi(0)\int_{\epsilon}^{b} \frac{1}{t^{\alpha}}\phi(t)exp(jkt)dt = \phi(0)\int_0^{\infty} \frac{1}{t^{\alpha}} exp(jkt)dt + O\left(\frac{1}{k}\right) \quad \text{(D.4)}$$

By definition

$\Gamma(z) = \int_0^{\infty} t^{z-1}e^{-t}dt$

or

$$\int_0^{\infty} t^{-\alpha}e^{-jkt}dt = \frac{1}{(jk)^{-1-\alpha)}}\Gamma(1-\alpha) = \frac{1}{(jk)^{-1-\alpha)}}\Gamma(1-\alpha)exp\left[j\pi(1-\alpha)/2\right] \quad \text{(D.5)}$$

Hence finally

$$M(k) = \frac{\phi(0)}{k^{-(1-\alpha)}}\Gamma(1-\alpha)exp\left[j\pi(1-\alpha)/2\right] + O\left(\frac{1}{k}\right) \quad \text{(D.6)}$$

Consider now the integral

$N(k) = \int_a^b f(t)exp[jk\mu(t)]dt$

If

$\frac{d\mu(t)}{dt} \neq 0$ for $a \leq t \leq b$

then integrating by part, we have

$$N(k) = \int_a^b f(t)exp[jk\mu(t)]dt = \int_a^b \frac{f(t)}{jk\acute{\mu}(t)}d\{exp[jk\mu(t)]\} = \frac{f(t)}{jk\acute{\mu}(t)}exp[jk\mu(t)]|_a^b -$$
$$\frac{1}{jk}\int_a^b exp[jk\mu(t)]\frac{d}{dt}\left[\frac{f(t)}{\acute{\mu}(t)}\right]dt = \frac{f(b)}{jk\acute{\mu}(b)}exp[jk\mu(b)] - \frac{f(a)}{jk\acute{\mu}(a)}exp[jk\mu(a)] -$$
$$\frac{1}{jk}\int_a^b exp[jk\mu(t)]\frac{d}{dt}\left[\frac{f(t)}{\acute{\mu}(t)}\right]dt \quad \text{(D.7)}$$

Let $\mu(t) = x$, $\mu'(t)dt = dx$, then for $\mu'(t) \neq 0$

$$\frac{1}{jk}\int_a^b exp[jk\mu(t)]\frac{d}{dt}\left[\frac{f(t)}{\mu'(t)}\right]dt = \frac{1}{jk}\int_{\mu(a)}^{\mu(b)}\frac{1}{\mu'(t)}\frac{d}{dt}\left[\frac{f(t)}{\mu'(t)}\right]exp(jkx)dx = O\left(\frac{1}{k}\right) \quad \text{(D.8)}$$

or

$$N(k) = \frac{f(b)}{jk\mu'(b)}exp[jk\mu(b)] - \frac{f(a)}{jk\mu'(a)}exp[jk\mu(a)] - O\frac{1}{k} \quad \text{(D.9)}$$

If however $\mu'(b) = 0$ at $t = t_0$, the last term in the above expression for N(k) does not hold. In this case, to find the aymptotic expansion for N(k) we assume that $\mu'(t) = \mu^{[1]}(t) = ... = \mu^{[n-1]}(t) = 0, \mu^{[n]}(t) \neq 0$ at $t = t_0 = a = 0$ and $\mu(a) = 0$.

with $\mu^{[n]}(0) \neq 0$, we have

$$\mu(t) = \frac{\mu^{[n]}(0)t^n}{n!},\ t = \left[\frac{\mu(t)n!}{\mu^{[n]}(0)}\right]^{\frac{1}{n}}$$

and

$$\mu'(t) = \frac{\mu^{[n]}(0)t^n - 1}{(n-1)!} = \frac{\mu^{[n]}(0)}{(n-1)!}\left[\frac{\mu(t)n!}{\mu^{[n]}(0)}\right]^{\frac{n-1}{n}} = n\left[\frac{n!}{\mu^{[n]}}(0)\right]^{\frac{-1}{n}}[\mu(t)]^{\frac{n-1}{n}} \quad \text{(D.10)}$$

giving

$$\frac{f(t)}{\mu'(t)} = \frac{f(t)}{n}\left[\frac{n!}{\mu^{[n]}(0)}\right]^{\frac{1}{n}}[\mu(t)]^{\frac{1-n}{n}}$$

Now let $\mu(t) = x$, then

$$\frac{f(t)}{\mu'(t)} = \frac{f(t)}{n}\left[\frac{n!}{\mu^{[n]}(0)}\right]^{\frac{1}{n}}x^{\frac{1-n}{n}} = \frac{1}{x^{\alpha}}\phi(0)|_{t\to 0}$$

where

$$\alpha = \frac{n-1}{n},\ \phi(0) = \frac{f(0)}{n\sqrt[n]{\mu^{[n]}(0)/n!}}$$

Therefore

$$N(k) = \int_a^b f(t)exp[jk\mu(t)]dt = \int_0^{\mu(b)} \frac{f(t)}{\mu'(t)} exp(jkx)dx = \phi(0) \int_0^{\mu(b)} \frac{1}{x^\alpha} exp(jkx)dx \quad \text{(D.11)}$$

or

$$N(k) = \frac{\phi(0)}{k^{-(1-\alpha)}} \Gamma(1-\alpha)exp[j\pi(1-\alpha)/2] + O\left(\frac{1}{k}\right)$$

subtituiting for α and $\phi(0)$ we finally have

$$N(k) = \frac{f(0)\Gamma(1/n)exp[j\pi/2n]}{n\sqrt[n]{\mu^{[n]}(0)/n!}} + O\left(\frac{1}{k}\right)$$

Appendix E

Opto-VLSI processor specifications

The device we used in this study was a 128 × 128 Nematic Liquid Crystal Spatial Light Modulator with the following specifications:

Number of Pixels: 16,384 (128 × 128)

Array Size: $5.12mm \times 5.12mm$

Pixel size: 31 micron

Pixel Pitch: 40 micron

Flat Fill Factor: 60%

Contrast: 200:1

Optical Response (10%- 90%): 0.2-1ms rise and 1-10 ms fall times

Electrical Addressing: 16× 8-bit DACs

Device Configuration: Reflective

Driver Memory: 256 frames of SRAM, randomly selectable

For more information please consult: Boulder Nonlinear Systems (http://www.bnonlinear.com/)
450 Courtney way, #107, Lafayette, CO 80026, USA

Appendix F

Definition of acronyms and abbreviations

AOTF: Acousto-Optic Tunable Filter is an optical filter that can be tuned by altering the refractive index using acoustic waves in the 40- to 68-MHz frequency range.

AWG: Arrayed Waveguide Grating is a device, built with silicon planar lightwave circuits (PLC), that allows multiple wavelengths to be combined and separated in a dense wavelength-division multiplexing (DWDM) system.

BER: Bit Error Rate is the fraction of a message or block of data that is wrong

CGH: Computer Generated Hologram is a phase pattern produced using one of many available techniques to manipulate the phase or intensity of optical beams

CMOS: Complimentary Metal Oxide Silicon is a semiconductor fabrication technology using a combination of n- and p-doped semiconductor material to achieve low power dissipation. Any path through a gate through which current can flow includes both n and p type transistors. Only one type is turned on in any stable state so there is no static power dissipation and current only flows when a gate switches in order to charge the parasitic capacitance.

DMD: Deformable Mirror Device is a spatial light modulator consisting of a metallized polymer film stretched over an array of metal-oxide semiconductor field-effect transistors (MOSFETs). Each mirror element in the film can be independently deformed by means of the charge on the controlling transistor. Thus a laser readout beam can be modulated spatially. Also called a deformable membrane device.

DRAM: Dynamic Random Access Memory is a type of semiconductor memory in which the information is stored in capacitors on a MOS integrated circuit. Typically each bit is stored as an amount of electrical charge in a storage cell consisting of a capacitor and a transistor. Due to leakage the capacitor discharges gradually and the memory cell loses the information. Therefore, to preserve the information, the memory has to be refreshed periodically. Despite this inconvenience, the DRAM is a very popular memory technology because of its high density and consequent low price.

DWDM: Dense Wavelength Division Multiplexing is a fiber-optic transmission technique that employs light wavelengths to transmit data parallel-by-bit or serial-by-character.

EDFA: Erbium Doped Fiber Amplifier is an optical amplifier device that is used to boost the intensity of optical signals being carried through a fiber optic communications system.

FLC: Ferroelectric Liquid Crystals have a layered structure with the molecules at some angle away from the layer normal, and that there is some inherent twist in the structure.

FP: Fabry-Perot interferometer A multiple-beam interferometer, usually consisting of two flat plates, with high reflective ability. The plates are set parallel to one another by spacers so that light waves may bounce back and forth between them several times. The requirements for constructive interference of reflected light waves of a given wavelength can be fulfilled only at particular angles, relative to the normal to the plates. Therefore, Fabry-Perot interferometers can be used as spectrometers with high resolution. Used as

a laser resonator, the Fabry-Perot reinforces only light of specific frequencies traveling perpendicular to the mirror surfaces, and its successive reflections and amplifications form the oscillating mode.

FWHM: Full-width Half Maximum is an expression of the extent of a function, given by the difference between the two extreme values of the independent variable at which the dependent variable is equal to half of its maximum value. For a band-pass filter this is the width of the passband at half of its peak value.

GPIB: General Purpose Interface Bus is an 8-bit parallel bus common on test and measurement instruments. This standard also known as IEEE-488 was developed to connect and control programmable instruments, and to provide a standard interface for communication between instruments from different sources.

ITO: Indium Tin Oxide is a material used in the fabrication of SLMs as an electrode layer.

LC: Liquid Crystal is a liquid exhibiting properties of a crystal that are not shown by ordinary liquids

MEMS: MicroElectroMechanical system is a technology that combines microelectronics with tiny mechanical devices such as sensors, valves, gears, mirrors, and actuators embedded in semiconductor chips.

MZ: Mach-Zehnder interferometer is device derived from the Twyman-Green interferometer. Light passing through a sample region in one direction recombines with a second leg without traversing the sample twice. The instrument is used to study transparent objects and is particularly useful in studying wind tunnel gas dynamics.

NLC: Nematic Liquid Crystal is a transparent or translucent liquid that causes the polarization of light waves to change as the waves pass through the liquid. The extent of the

change in polarization depends on the intensity of an applied electric field. Nematic comes from a Greek prefix nemato meaning threadlike and is used here because the molecules in the liquid align themselves into a threadlike shape.

OSNR: Optical Signal to Noise Ratio is the measure of the ratio of signal power to noise power in an optical instrument for a specified optical bandwidth

QWP: Quarter-Wave Plate is a plate made of a double-refracting crystal having such a density that a phase difference of one-quarter cycle is formed between the ordinary and extraordinary elements of light passing through.

SAW: Surface Acoustic Wave is a sound wave that propagates along the surface of a solid. Also called a Rayleigh wave, it has both longitudinal and transverse (shear) components. Such surface waves are used in hybrid electroacoustic devices for such purposes as signal amplification and recognition, the scanning of visual information and the delaying of fast electrical signals.

SLM: Spatial Light Modulator is a device used to modify the phase or intensity of an optical beam

SRAM: Static Random Access Memory is a Random access memory in which each bit of storage is a bistable flip-flop, commonly consisting of cross-coupled inverters. It is called "static" because it will retain a value as long as power is supplied, unlike dynamic random access memory (DRAM) which must be regularly refreshed. It is however, still volatile, i.e. it will lose its contents when the power is switched off, in contrast to ROM. SRAM is usually faster than DRAM but since each bit requires several transistors (about six) you can get less bits of SRAM in the same area. It usually costs more per bit than DRAM and so is used for the most speed-critical parts of a computer (e.g. cache memory) or other circuit.

TE: Transverse Electric is an electromagnetic mode whose electric field vector is normal

to the direction of propagation.

TM: Transverse Magnetic is an electromagnetic mode whose magnetic field vector is normal to the direction of propagation.

VLSI: Very Large-Scale Integrated circuit is a term describing semiconductor integrated circuits composed of hundreds of thousands of logic elements or memory cells.

WDM: Wavelength Division Multiplexing is a technique for multiplexing several optical carrier signals on a single optical fibre by using different wavelengths (colours) of laser light to carry different signals.

Bibliography

[1] Atul Srivastava, Chien-jen Chen, and Horacio Facca, "The 'smart' money is on network intelligence," *Lightwave*, vol. 18, no. 11, pp. 12–15, 2001.

[2] T.E. Stern and K. Bala, "Multi-wavelength optical networks: A layered approach," pp. 87–89. Addison-Wesley, 1999.

[3] Stamatios V. Kartalopoulos, "Introduction to DWDM technology: Data in a rainbow," pp. 18–20. Wiley-IEEE Press, 2000.

[4] K. O. Hill, F. Fujii, D. C. Johnson, and B. S. Kawasaki, "Photosensitivity on optical fiber waveguides: application to reflection filter fabrication," *Applied Physics Letters*, vol. 32, pp. 123–127, 1978.

[5] A. Locco, H.G. Limberger, and R.P. Salathe, "Bragg grating fast tunable filter," *Electronic Letters*, vol. 33, no. 25, pp. 2147–2148, 1997.

[6] J. S. Patel, M. A. Saifi, D. W. Berreman, C. Lin, N. Andreadakis, and S. D. Lee, "Electrically tunable optical filter for infrared wavelength using liquid crystals in a fabry-perot etalon," *Applied Physics Letters*, vol. 57, no. 17, pp. 1718–1720, 1990.

[7] K. Hirabayashi, H. Tsuda, and T. Kurokawa, "New structure of tunable wavelength-selective filters with a liquid crystal for FDM systems," *IEEE Photonics Technology Letters*, vol. 3, pp. 741–743, 1991.

[8] M. Parker, A. Cohen, and R. J. Mears, "Dynamic digital holographic wavelength filter," *Journal of Lightwave Technology*, vol. 16, pp. 1259–1270, 1998.

[9] S. T. Warr, M. C. Parker, and R. J. Mears, "Optically transparent digitally tunable wavelength filter," *Electronic Letters*, vol. 31, no. 2, pp. 129–130, 1995.

[10] J.Y. Liu and K.M. Johnson, "Analog smectic c* ferroelectric liquid crystal fabry perot optical tunable filter," *IEEE Photonics Technology Letters*, vol. 7, no. 11, pp. 1309–1311, 1995.

[11] Chi Wu, C. Rolland, F. Shepherd, C. Larocque, N. Puetz, K.D. Chik, and J.M. Xu, "InGaAsP/InP vertical directional coupler filter with optimally designed wavelength tunability," *IEEE Photonics Technology Letters*, vol. 4, no. 4, pp. 457–459, 1993.

[12] L. L. Buhl, R. C. Alferness, U. Koren, B. I. Miller, M. G. Young, T. L. Koch, C. A. Burrus, and G. Rayborn, "Grating assisted vertical coupler/filter for extended tuning range," *Electronics Letters*, vol. 29, no. 1, pp. 81–82, 1993.

[13] S.E. Harris and R.W. Wallace, "Acousto-optic tunable filter," *Journal of Optical Society of America*, vol. 59, no. 6, pp. 744–747, 1969.

[14] Dan Sadot and Efraim Boimovich, "Tunable optical filters for dense WDM networks," *IEEE communications magazine*, vol. 36, no. 12, pp. 50–55, 1998.

[15] Kwok-Wai Cheung, "Acousto-optic tunable filters in narrowband WDM networks: System issues and network applications," *IEEE Journal on Selected areas in communications*, vol. 8, no. 6, pp. 1015–1025, 1990.

[16] B. L. Heffner, D. A. Smith, J. E. Baran, A. Yi-Yan, and K. W. Cheung, "Integrated-optic acoustically tunable infra-red optical filter," *Electronic Letters*, vol. 24, no. 25, pp. 1562–1563, 1988.

[17] J. Jackel, M. Goodman, J. Baran, W. Tomlinson, G. Chang, M. Iqbal, G. Song, Bala, C. Brackett, D. Smith, R. Chakravarthy, R. Hobbs, D. Fritz, R. Ade, and K. Kissa, "Acousto-optic tunable filters (AOTF's) for multi-wavelength optical cross-connects: Crosstalk considerations," *Journal of Lightwave Technology*, vol. 14, pp. 1056–1066, 1996.

[18] E. Vail, M. Wu, G. Li, L. Eng, and C. Chang-Hasnain, "GaAs micro-machined widely tunable fabry-perot filters," *Electronic Letters*, vol. 31, no. 3, pp. 228–229, 1995.

[19] D. Hohlfeld, M. Epmeier, and H. Zappe, "Tunable thermo-optic filter for WDM applications," in *The Fifteenth IEEE International Conference on Micro Electro Mechanical Systems*, pp. 564–567. Las Vegas, USA, 2002.

[20] P. Tayebati, P.D. Wang, D. Vakhshoori, and R.N. Sacks, "Widely tunable fabry perot filter using Ga(Al)As-AlOx deformable mirrors," *IEEE Photonics Technology Letters*, vol. 10, no. 3, pp. 394–396, 1998.

[21] Rajiv Ramaswami and Kumar N. Sivarajan, "Optical networks a practical perspective," pp. 101–103. Morgan Kaufmann publishers, second edition, 2002.

[22] Max Born and Emil Wolf, "Principles of optics," pp. 431–435. Cambridge University Press, seventh edition, 1999.

[23] Eugene Hecht, "Optics," pp. 75–81. Addison-Wesley Publishing, fourth edition, 2001.

[24] M. Raisi, S. Ahderom, Kamal E. Alameh, and Kamran Eshraghian, "Opto-VLSI multiband tunable optical filter," *Electronic Letters*, vol. 39, no. 21, pp. 1533–1535, 2003.

[25] B.H. Verbeek, C.H. Henry, N.A. Olsson, K.J. Orlowsky, R.F. Kazarinov, and B.H. Johnson, "Integrated four-channel mach-zehnder multi/demultiplexer fabricated with phosphorous doped SiO2 waveguides on Si," *Journal of Lightwave Technology*, vol. 6, pp. 1011–1015, 1988.

[26] E.L. Wooten, R.L. Stone, E.W. Miles, and E.M. Bradley, "Rapidly tunable narrowband wavelength filter using LiNbO3 unbalanced mach-zehnder interferometers," *Journal of Lightwave Technology*, vol. 14, no. 11, pp. 2530–2536, 1996.

[27] R. Kashyap, R. Wyatt, and P.F. McKee, "Wavelength flattened saturated erbium amplifier using multiple side tap bragg grating," *Electronic Letters*, vol. 29, pp. 1025–1026, 1993.

[28] A. M. Vengsarkar, J. R. Pedrazzani, J. B. Judkins, P. J. Lemaire, N. S. Bergano, and C. R. Davidson, "Long period fiber-grating-based gain equalizers," *Optical Letters*, vol. 21, pp. 336–338, 1996.

[29] Pierre G. Verly, "Design of a robust thin-film interference filter for erbium-doped fiber amplifier gain equalization," *Applied Optics*, vol. 41, no. 16, pp. 3092–3096, 2002.

[30] M. Rochette, M. Guy, S. LaRochelle, J. Lauzon, and F. Trepanier, "Gain equalization of EDFA's with bragg gratings," *IEEE Photonics Technology Letters*, vol. 11, no. 5, pp. 536–538, 1999.

[31] Michael C. Parker, Augustin Yiptong, and Robert J. Mears, "A novel active holographic arrayed-wave-guide grating for WDM subsystems," *Optical fiber communication conference*, vol. 2, pp. 77–79, 2000.

[32] Kirk Flatow, HongTao Hou, and Wayne Sorin, "Overview of dynamic gain-flattening technologies," *Lightwave*, pp. 1–8, 2002.

[33] Seok Hyun Yun, Bong Wan Lee, Hyang Kyun Kim, and Byoung Yoon Kim, "Dynamic erbium-doped fiber amplifier based on active gain flattening with fiber acousto-optic tunable filters," *IEEE Photonics Technology Letters*, vol. 11, no. 10, pp. 1229–1231, 1999.

[34] J. Grinberg, A. Jacobson, W. Bleha, L. Lewis, L. Fraas, D. Boswell, and G. Myer, "A new real-time non-coherent to coherent light image converter: the hybrid field effect liquid crystal light valve," *Optical Engineering*, vol. 14, pp. 217–225, 1975.

[35] Patrick Berthele, Bruno Fracasso, and Jean-Louis de Bougrenet de la Tocnaye, "Design and characterization of a liquid-crystal spatial light modulator for a polarization-insensitive optical space switch," *Applied Optics*, vol. 37, no. 23, pp. 5461–5468, 1998.

[36] N. Collings, W.A. Crossland, P.J. Ayliffe, D.G. Vass, and I. Underwood, "Evolutionary development of advanced liquid crystal spatial light modulators," *Applied Optics*, vol. 28, no. 22, pp. 4740–4747, 1989.

[37] Mark P. Dames, Robert J. Dowling, Paul McKee, and David Wood, "Efficient optical elements to generate intensity weighted spot arrays: design and fabrication," *Applied Optics*, vol. 30, no. 19, pp. 2685–2691, 1991.

[38] R M Matic, "Blazed phase liquid crystal beam steering," *SPIE laser beam propagation and control*, vol. 2120, pp. 194–205, 1994.

[39] R J Mears, M C Parker, and A D Cohen, "WDM channel management using programmable holographic elements," *Proceedings, IEE Colloquium on Multiwavelength Optical Networks: Devices, Systems and Network Implementations*, vol. IEE Colloquium Digest 296, pp. 11/1–11/6, 1998.

[40] R Moignard, Y Defosse, S Kerouedan, J L De Bougrenet de la Tocnaye, P Le Gars, and C Le Moing, "Single mode fiber optical crossbar routing switch with ferroelectric liquid-crystal-vlsi technology and free-space optics," *Applied Optics*, vol. 36, no. 17, pp. 3866–3876, 1997.

[41] D C O'Brien, R J Mears, and W A Crossland, "Optical crossbar switching using dynamic holograms written to ferroelectric liquid crystal spatial light modulators," *IEE colloquium on "optical switching"*, 1993.

[42] Anat Sneh and Christina M. Johnson, "High speed wavelength tunable liquid crystal filter," *IEEE Photonics Technology Letters*, vol. 7, no. 4, pp. 379–381, 1995.

[43] T.D. Wilkinson, D.C. O'Brien, and R.J. Mears, "Dynamic asymmetric binary holograms using a ferroelectric liquid crystal spatial light modulator," *Optics communications*, vol. 109, pp. 222–226, 1994.

[44] E G S Paige, R H Scarbrough, and G G Yang, "Feedback generated holograms," *Electronic Letters*, vol. 30, no. 14, pp. 1174–1175, 1994.

[45] T. H. Barnes, T. Eiju, K. Matsuda, H. Ichikawa, M. R. Taghizadeh, and J. Turunen, "Reconfigurable free-space optical interconnections with a phase-only liquid-crystal spatial light modulator," *Applied Optics*, vol. 31, no. 26, pp. 5527–5535, 1992.

[46] H. Yamazaki and M. Yamaguchi, "4 x 4 free-space optical switching using real-time binary phase-only holograms generated by a liquid-crystal display," *Optical Letters*, vol. 16, pp. 1415–1417, 1991.

[47] N. Konforti, E. Marom, and S.-T. Wu, "Phase-only modulation with twisted nematic liquid-crystal spatial light modulators," *Optics Letters*, vol. 13, no. 3, pp. 252–253, 1988.

[48] Thomas H. Barnes, Tomoaki Eiju, Kiyofumi Matsuda, and Naotake Ooyama, "Phase-only modulation using a twisted nematic liquid crystal television," *Applied Optics*, vol. 28, no. 22, pp. 4845–4852, 1989.

[49] A. Au, C.-S. Wu, S.-T. Wu, and U. Efron, "Ternary phase and amplitude modulations using a twisted nematic liquid crystal spatial light modulator," *Applied Optics*, vol. 34, no. 2, pp. 281–284, 1995.

[50] Victor Arrizon, "Complex modulation with a twisted-nematic liquid-crystal spatial light modulator: double-pixel approach," *Optics Letters*, vol. 28, no. 15, pp. 1359–1361, 2003.

[51] W. E. Ross, D. Psaltis, and R. H. Anderson, "Two dimensional magneto-optic spatial light modulator for signal processing," *Optical Engineering*, vol. 22, no. 4, pp. 485–490, 1983.

[52] D. R. Pape and L. J. Hornbeck, "Characteristics of the deformable mirror device for optical information processing," *Optical Engineering*, vol. 22, no. 6, pp. 675–681, 1983.

[53] Ian Underwood, "Ferroelectric liquid crystal over silicon spatial light modulators - principles, practice and prospects," *Optical Society of America, Trends in Optics and Photonics 1997*, vol. 14, pp. 76–88, 1997.

[54] John A. Neff, Ravindra A. Athale, and Sing H. Lee, "Two-dimensional spatial light modulators: A tutorial," *Proceedings of IEEE*, vol. 78, no. 5, pp. 826–855, 1990.

[55] J.A. Breslin, J.K. Low, and I. Underwood, "Smart pixel with four level amplitude or phase modulation," *Digest of the LEOS Summer Topical Meetings - Smart Pixels*, pp. 33–34, 1998.

[56] K. M. Johnson, D. J. McKnight, and I. Underwood, "Smart spatial light modulators using liquid crystal on silicon," *IEEE Journal of Quantum Electronics*, vol. 29, pp. 699–714, 1993.

[57] H. S. Hinton, "Progress in smart pixel technologies," *IEEE Journal of Selected Topics in Quantum Electronics*, vol. 2, pp. 14–23, 1996.

[58] Ian Underwood, "Vlsi design and fabrication for liquid crystal on silicon," *IEE Seminar on Micro-display and Smart Pixel Technologies Digest no 00/006*, pp. 7/1–7/6, 2000.

[59] Kamal E. Alameh, Kamran Eshraghian, Selam Ahderom, and Mehrdad Raisi, "Opto-VLSI-based reconfigurable photonic RF bandpass filters," in *International Conference on Computer, Communication and Control Technologies*, pp. 49–54. Orlando, Florida, USA, 2003.

[60] J. Cognard, "Alignment of nematic liquid crystals and their mixtures," *Molecular Crystals and Liquid Crystals Supplement series*, vol. 78, no. 1, pp. 1–77, 1982.

[61] Gordon D Love, Janet S Fender, and Sergio R Restaino, "Adaptive wavefront shaping with liquid crystals," *Optics and Photonics news*, vol. 6, no. 10, pp. 16–21, 1995.

[62] Gordon D Love, "Adaptive optical components using liquid crystal devices," *journal of communications research laboratory*, vol. 46, no. 3, pp. 427–430, 1999.

[63] J.N. Lee, "Optical modulators," in *Handbook of Photonics*, M. C. Gupta, Ed., pp. 393–434. Boca Raton: CRC Press, 1997.

[64] P. M. Alt, "Single-crystal silicon for high resolution display," *International Display Research Conference (Society for Information Display*, pp. M–19, 1997.

[65] S. T. Warr and R. J. Mears, "Polarization insensitive operation of ferroelectric liquid crystal devices," *Electronic Letters*, vol. 31, no. 9, pp. 714–716, 1995.

[66] I. Manolis, T. Wilkinson, M. Redmaond, and W.A. Crossland, "Reconfigurable multilevel phase holograms for optical switches," *IEEE Photonics Technology Letters*, vol. 4, pp. 801–803, 2002.

[67] W. H. Lee, "Computer-generated holograms: Techniques and applications," in *Progress in optics*, E. Wolf, Ed., pp. 121–232. Elsevier, Amsterdam, 16 edition, 1978.

[68] L. B. Lesem, P. M. Hirsch, and Jr. J. A. Jordan, "The kinoform: A new wavefront reconstruction device," *IBM Journal of Research and Development*, vol. 13, pp. 150–155, 1969.

[69] B.E.A Saleh and M.C. Teich, "Fundamental of photonics," pp. 231–235. John Wiley and Sons Inc., 1991.

[70] J.W. Goodman, "Introduction to fourier optics," pp. 121–125. McGraw-Hill, second edition, 1996.

[71] V. Arrizon and M. Testorf, "Efficiency limit of spatially quantized fourier array illuminators," *Optics Letters*, vol. 22, no. 4, pp. 197–199, 1997.

[72] H. Dammann, "Blazed synthetic phase-only holograms," *Optik*, vol. 31, pp. 95–104, 1970.

[73] S E Broomfield, M A A Neil, E G S Paige, and G G Yang, "Programmable binary phase-only optical device based on ferroelectric liquid crystal slm," *Electronic Letters*, vol. 28, no. 1, pp. 26–28, 1992.

[74] R. W. Gerchberg and W. O. Saxton, "A practical algorithm for the determination of phase from image and diffraction plane pictures," *Optik*, vol. 35, no. 2, pp. 237–246, 1972.

[75] K Heggarty and R Chevallier, "Signal window minimum average error algorithm for computer-generated holograms," *Journal of Optical Society of America A*, vol. 15, no. 3, pp. 625–635, 1998.

[76] F. Wyrowski, "Diffractive optical elements: iterative calculation of quantized blazed phase structures," *Journal of Optical Society of America A*, vol. 7, no. 6, pp. 961–969, 1990.

[77] Jari Turunen, Antti Vasara, and Jan Westerholm, "Kinoform phase relief synthesis: a stochastic method," *Optical Engineering*, vol. 28, no. 11, pp. 1162–1167, 1989.

[78] Michael A. Seldowitz, Jan P. Allebach, and Donald W. Sweeney, "Synthesis of digital hologram by direct binary search," *Applied Optics*, vol. 26, no. 14, pp. 2788–2798, 1987.

[79] A. W. Lohmann and D. P. Paris, "Binary fraunhofer holograms generated by computer," *Applied Optics*, vol. 6, pp. 1739–1748, 1967.

[80] Juha Fagerholm, Jari Turunen, Antti Vasara, and Jan Westerholm, "computer-generated fourier-transform holograms for optical computing," *SPIE (International Society for optical engineering) Holographic optics II: principles and applications*, vol. 1136, pp. 253–260, 1989.

[81] S E Broomfield, M A A Neil, and E G S Paige, "Four-level, phase-only spatial light modulator," *Electronic Letters*, vol. 29, no. 18, pp. 1661–1663, 1993.

[82] J. R. Fienup, "Iterative method applied to image reconstruction and to computer-generated holograms," *Optical Engineering*, vol. 19, pp. 297–305, 1980.

[83] J. R. Fienup, "Phase retrieval algorithm: a comparison," *Applied Optics*, vol. 21, pp. 2758–2769, 1982.

[84] H. Imam, A.G. Kirk, and T.J. Hall, "Design of multiphase level holograms," *Third international conference on holographic systems, components and applications*, pp. 166–170, 1991.

[85] K. L. Tan, Stephen T. Warr, Ilias G. Manolis, Timothy D. Wilkinson, Maura M. Redmond, William A. Crossland, Robert J. Mears, and Brian Robertson, "Dynamic holography for optical interconnections. i. noise floor of low-crosstalk holographic switches," *Journal of Optical Society of America*, vol. 18, no. 1, pp. 195–204, 2001.

[86] K. L. Tan, Stephen T. Warr, Ilias G. Manolis, Timothy D. Wilkinson, Maura M. Redmond, William A. Crossland, Robert J. Mears, and Brian Robertson, "Dynamic holography for optical interconnections. ii. routing holograms with predictable location and intensity of each diffraction order," *Journal of Optical Society of America*, vol. 18, pp. 205–215, 2001.

[87] Paul F Mcmanamon, Terry A Dorschner, David L Corkum, Larry J Friedman, Douglas S Hobbs, Michael Holz, Sergey Liberman, Huy Q Nguyen, Daniel P Resler, Richard C Sharp, and Edward A Watson, "Optical phased array technology," *Proceedings of IEEE*, vol. 84, no. 2, pp. 268–298, 1996.

[88] Henry Stark, William C. Catino, and Joseph L. LoCicero, "Design of phase gratings by generalized projections," *Journal of Optical Society of America*, vol. 8, no. 3, pp. 566–571, 1991.

[89] John H. Holland, "Adaptation in natural and artificial systems: an introductory analysis with applications to biology, control and artificial intelligence," pp. 64–68. University of Michigan Press, 1975.

[90] A. G. Kirk, R. G. Hoptroff, and T. J. Hall, "Genetic algorithm solution to computer generated holograms," *Applied Optics digest*, pp. 233–234, 1990.

[91] Gouguang Yang, "The performance analysis of the genetic algorithm for the optimum design of diffractive optical elements and its comparison to the simulated annealing," *Optik*, vol. 111, no. 3, pp. 133–137, 2000.

[92] Kirkpatrick, Gelatt, and Vecchi, "Optimization by simulated annealing," *Science*, vol. 220, no. 4598, pp. 671–680, 1983.

[93] A G Kirk, M Ishikawa, S Jamieson, and T J Hall, "The design and fabrication of quasi-periodic computer generated holograms," in *Fourth international conference on holographic systems, components and applications*, pp. 91–95. 1993.

[94] P. McOwan and W.J. Hossack, "Computer generated holograms: Iterative and coordinate transform interconnects," *IEE colloquium on optical interconnects*, pp. 7/1–7/4, 1988.

[95] Jari Turunen, Juha Fagerholm, Antti Vasara, and M. R. Taghizadeh, "Detour-phase kinoform interconnect: The concept and fabrication considerations," *Journal of Optical Society of America A*, vol. 7, no. 7, pp. 1202–1208, 1990.

[96] D C O'Brien and R J Mears, "Real time holograms using ferroelectric liquid crystal spatial light modulators," *IEE colloquium on "Two-Dimensional optoelectronic device arrays"*, pp. 10/1–10/4, 1991.

[97] S. Ahderom, M. Raisi, K. Lo, K.E. Alameh, and R. Mavaddat, "Applications of liquid crystal spatial light modulators in optical communications," in *5th IEEE International Conference on High Speed Networks and Multimedia Communications*, pp. 239–242. South Korea, 2002.

[98] H. Dammann, "Spectral characteristic of stepped-phase gratings," *Optik*, vol. 53, no. 5, pp. 409–417, 1979.

[99] Y. Chen, S. Yamauchi, N. Wang, and Z. Nakao, "A fast kinoform optimization algorithm based on simulated annealing," *IEICE Trans. Fundaments*, vol. E83-A, no. 4, pp. 774–776, 2000.

[100] G. Keiser, "A review of WDM technology and applications," *Optical Fiber Technology*, vol. 5, pp. 3–39, 1999.

[101] J.E. Ford and J.A. Walker, "Dynamic spectral power equalization using micro-opto-mechanics," *IEEE Photonics Technology Letters*, vol. 10, pp. 1440–1442, 1998.

[102] C.R. Doerr, M. Cappuzzo, E. Laskowski, A. Paunescu, L. Gomez, L.W. Stulz, and J. Gates, "Dynamic wavelength equalizer in silica using the single-filtered-arm interferometer," *IEEE Photonics Technology Letters*, vol. 11, pp. 581–583, 1999.

[103] B.J. Offrein, F. Horst, G.L. Bona, R. Germann, H.W.M. Salemink, and R. Beyeler, "Adaptive gain equalizer in high-index-contrast sion technology," *IEEE Photonics Technology Letters*, vol. 12, pp. 504–506, 2000.

[104] S.H. Huang, X.Y. Zou, A.E. Willner, Z. Bao, and D.A. Smith, "Experimental demonstration of dynamic network equalization of three 2.5 Gb/s WDM channels over 1000 km using acousto-optic tunable filters," *IEEE Photonics Technology Letters*, vol. 8, pp. 1243–1245, 1996.

[105] H.S. Kim, H. Y. Seok, K. K. Hyang, P. Namkyoo, and Y. K. Byoung, "Actively gain-flattened erbium-doped fiber amplifier over 35 nm by using all-fiber acousto-optic tunable filters," *IEEE Photonics Technology Letters*, vol. 12, pp. 790–792, 1998.

[106] J. Chiao and T. Huang, "Liquid crystal optical harmonic equalizers," in *IEEE LEOS 2001 Summer Topical Meetings*, Copper Mountain, Colorado, U.S.A., 2001, pp. 403–404.

[107] M.A. Golub, I.N. Sisakyan, and V.A. Soifer, "Infrared radiation focusators," *Optics and lasers in Engineering*, vol. 15, no. 5, pp. 297–309, 1991.

[108] Thomas Dresel, Mathias Beyerlein, and Johannes Schwider, "Design and fabrication of computer-generated beam-shaping holograms," *Applied Optics*, vol. 35, no. 23, pp. 4615–4621, 1996.

[109] Harald Aagedal, Michael Schmid, Sebastian Egner, Jorn Muller-Quade, Thomas Beth, and Frank Wyrowski, "Analytical beam shaping with application to laser diode arrays," *Journal of Optical Society of America*, vol. 14, no. 7, pp. 1549–1553, 1997.

[110] Jorgen Bengtsson, "Kinoform-only gaussian-to-rectangle beam shaper for a semiconductor laser," *Applied Optics*, vol. 35, no. 20, pp. 3807–3814, 1996.

[111] A. Papoulis, "Systems and transforms with applications in optics," pp. 226–241. McGraw Hill, New York, 1968.